General Disclaimer

One or more of the Following Statements may affect this Document

- This document has been reproduced from the best copy furnished by the organizational source. It is being released in the interest of making available as much information as possible.

- This document may contain data, which exceeds the sheet parameters. It was furnished in this condition by the organizational source and is the best copy available.

- This document may contain tone-on-tone or color graphs, charts and/or pictures, which have been reproduced in black and white.

- This document is paginated as submitted by the original source.

- Portions of this document are not fully legible due to the historical nature of some of the material. However, it is the best reproduction available from the original submission.

(NASA-CR-120665) AIRBORNE ELECTRONICALLY
STEERABLE PHASED ARRAY Final Report (Texas
Instruments, Inc.) 88 p HC $4.75   CSCL 17B

N75-28280

Unclas
G3/32 31039

RECEIVED
AUG 1975

TEXAS INSTRUMENTS
INCORPORATED

FINAL REPORT
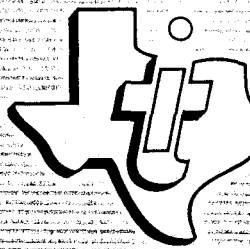
AIRBORNE ELECTRONICALLY

STEERABLE PHASED ARRAY

Prepared for:

National Aeronautics and Space
    Administration
George C. Marshall Space Flight Center
Huntsville, Alabama   35812

Contract No. NAS8-25847

Prepared By:

Robert Coats, Project Engineer
Equipment Group
Texas Instruments Incorporated
P.O. Box 6015
Dallas, Texas   75222

TEXAS INSTRUMENTS
INCORPORATED

DM75-05-10

April 1975

TABLE OF CONTENTS

LIST OF ILLUSTRATIONS

LIST OF TABLES

AESPA Antenna Range

TEXAS INSTRUMENTS INCORPORATED

13500 North Central Expressway

P.O. Box 6015

Dallas, Texas 75222

FINAL REPORT

AIRBORNE ELECTRONICALLY

STEERABLE PHASED ARRAY

SECTION I

INTRODUCTION AND DESCRIPTION OF

CONTRACTUAL WORK REQUIREMENTS

This report contains results of the fifth phase of the Airborne
Electronically Steerable Phased Array (AESPA) program sponsored by the
Astrionics Division of NASA Marshall Space Flight Center under Contract
Number NAS8-25847. The objectives of the AESPA program are:

- To develop a highly reliable solid-state S-band communication
  terminal system applicable to low and high altitude, reusable
  and/or permanently placed satellites

- To provide high-gain electronic beam steering without
  incurring a weight penalty

- To develop a highly efficient modular antenna concept
  applicable to moderate apertures driven by fully duplexed,
  electronic transceiver modules

- To extend these capabilities to Ku-band for high data rate
  payloads (with data rates up to 10^8 bits per second.)

To give the reader a better understanding of the series of tasks
which have been performed on this contract, a description of the phases of
this program which have been completed follows. The first phase of this
program was to perform a preliminary design of a lightweight high-gain,
spaceborne communications array. This array includes simultaneous transmit
and receive (2,282 and 2,101 MHz, respectively), automatic acquisition and
tracking of a signal within a 60-degree cone from the array normal, and
provides for independent forming of the transmit and receive beams.
Application for this array is the space shuttle, space station, or any of
the advanced manned (or unmanned) orbital vehicles under study at MSFC.
Essential parameters in the system design are:

Lightweight - less than 50 pounds

High reliability - 30,000 hours mean time to failure

High efficiency - 60 percent antenna efficiency, 30 percent
transmitter efficiency

High sensitivity - 5 dB noise figure

The first phase of this contract defined the mechanical design concept shown in Figure 1-1, as well as the system block diagram shown in Figure 1-2. The specifications contained in RFQ1-0-40-93877 are summarized in Table 1-1. The concept given in the proposal was verified through analytical and numerical studies in this phase and a final report was issued in April 1971 giving the results of this study.

The results of the study indicated that development of three critical hardware areas was required to further verify the approach. As a result, a second phase (AESPA II) was initiated in April 1971 to design, construct, and test a lightweight, full-scale, 128-element antenna array; develop and test an RF transmit manifold; and develop and test a working electronics module containing diplexer, transmitter, receiver, and phase shifter circuits. The 128-element antenna is shown on the test stand in Figure 1-3. A quarter-section of the RF distribution manifold is shown in Figure 1-4. This distribution manifold is placed on the back of the 128-element array.

During the time frame which saw the development of the critical hardware for the S-band array, it was realized by NASA's cognizant engineer, D.O. Lowrey, that additional development effort was required to allow this technology to be applied to the Ku-Band link to be used with the TDRS. This program fostered the development of the gallium arsenide diode which can be used to generate power at frequencies from C- through K-band. During the fourth contractual phase, a study was conducted to determine the possible configurations for a Ku-band AESPA. The results of this study are contained in a separate report.

The third phase of the AESPA program (AESPA III) began in April 1972 and completed the critical component development undertaken in 1971. This phase included the following line items:

Development of beam-steering logic

Construction of 12 additional modules incorporating phase trim and
lower noise figure and capability of hermetic seal

Development of an RF receive manifold

Development of a dc and logic manifold

Study of a Ku-band electronically steerable antenna system.

The dc and logic manifold is shown in Figure 1-5. The beam-steering logic is contained on two cards. These cards are designed to be suitably packaged in the rear of the array. These cards are shown mounted on the automatic checkout equipment in Figure 1-6. This phase of the AESPA program (AESPA III) was
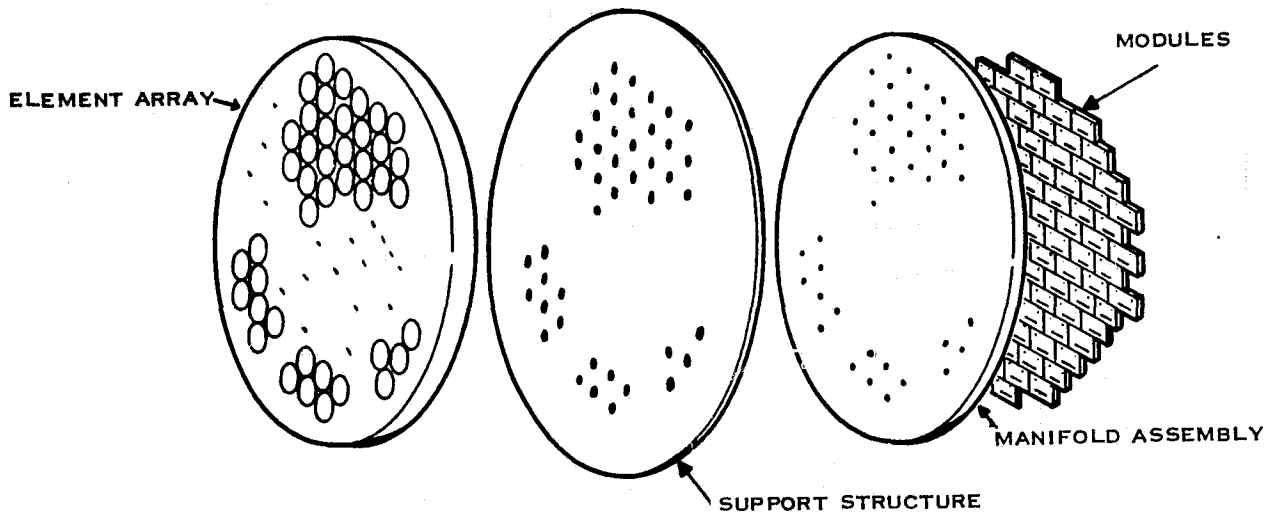
Figure 1-1. Array Assembly
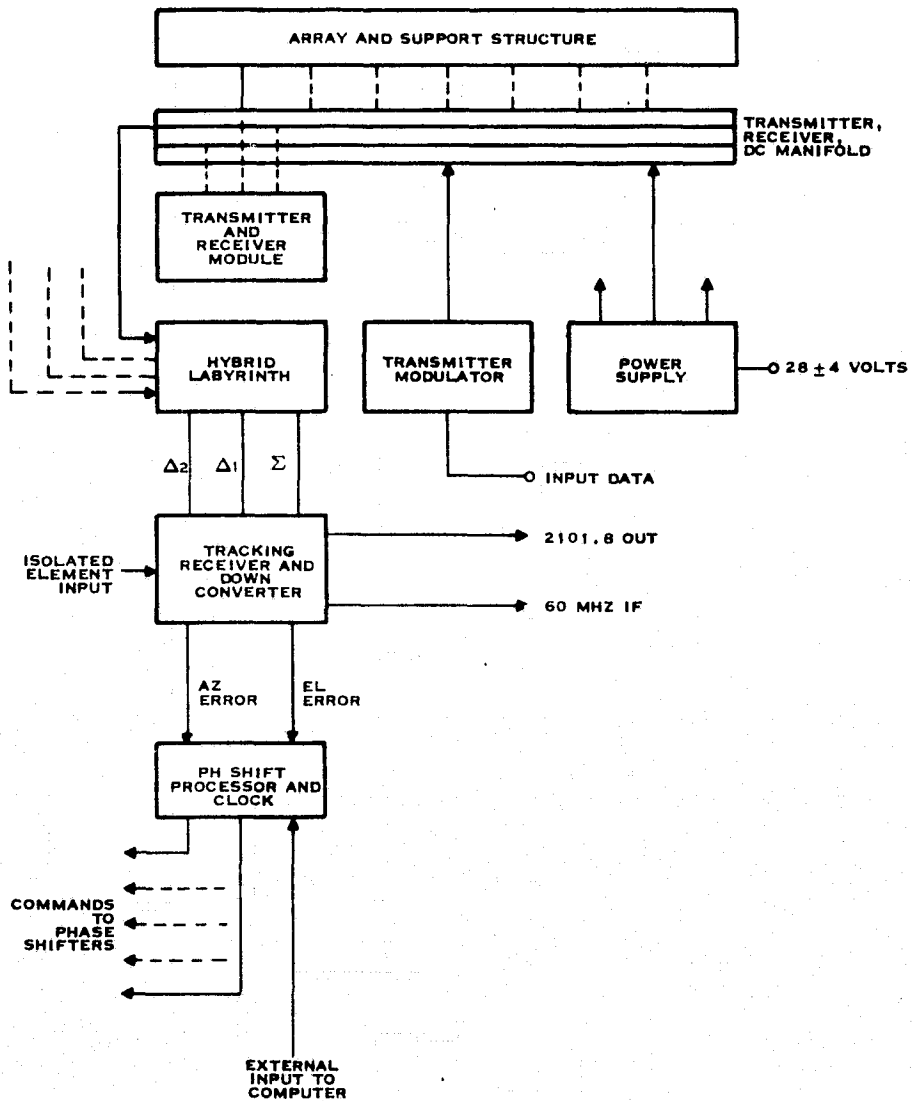
Figure 1-2. System Diagram

Figure 1-4. RF Distribution Manifold

148668 (40-1382)
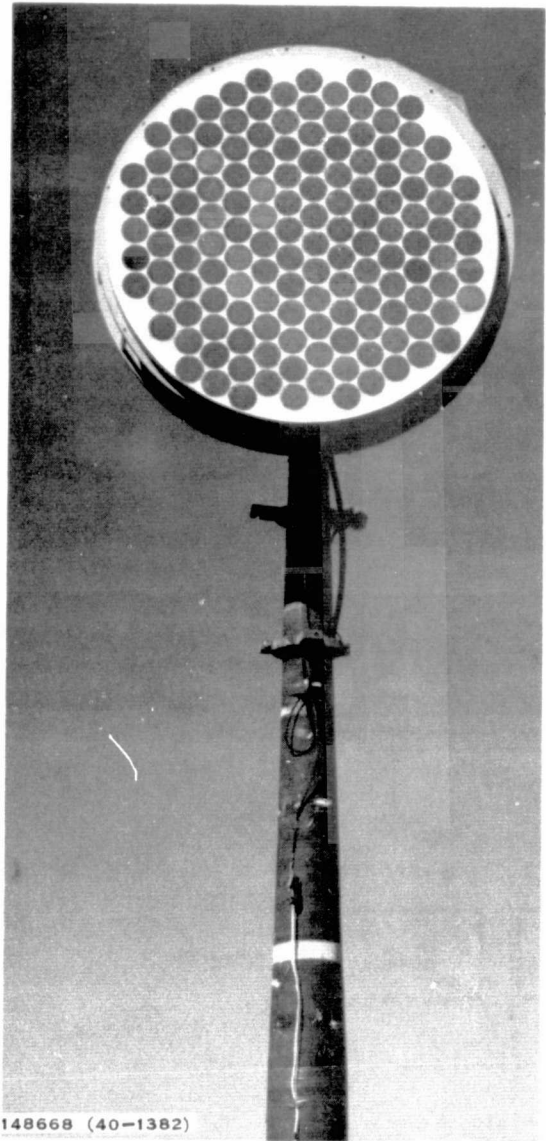
Figure 1-3. 128 Active Element Antenna

155793 (47-228)
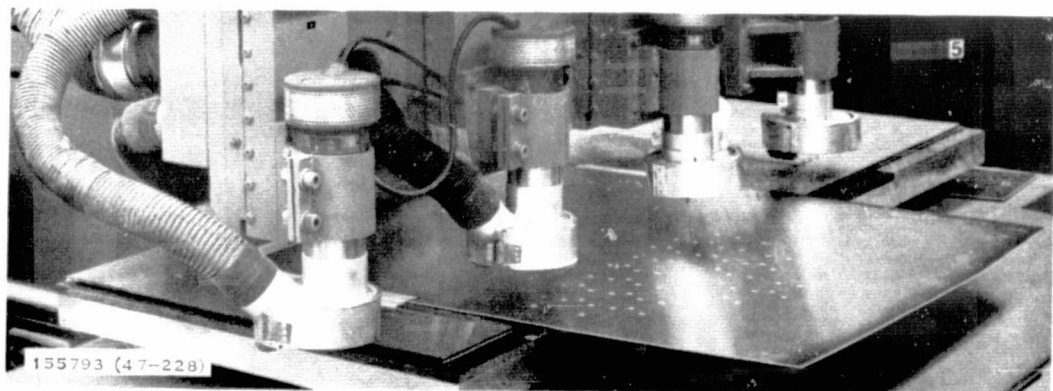
Figure 1-5. DC and Logic Manifold

TABLE 1-1. PERFORMANCE SPECIFICATIONS

Scan angle: 60 degrees from broadside (max)

Scan increments: <2.5 degrees

Transmit frequency: 2282.5 MHz

Transmit gain: 20 dB at max scan

Frequency Stability: ±0.003 percent

Input Impedance: 50 ±3 ohms

Power output: >25 watts at 2282.5 MHz

Polarization: Right-hand circular (RHCP)

Antenna efficiency: 60 percent or greater (at f_T)

Beamwidth: 10 degrees (60 degrees from broadside)

Sidelobes: 12 dB below mainlobe at max scan

Grating lobe: Suppressed below max scan

Bandwidth (XMTR): 30 MHz (min); 60 MHz (max)

VSWR: 1.5 max at any scan angle

Modulation (XMTR): FM

Modulation input impedance: 10,000 Ω (0 < f < 200 kHz)

Modulation distortion: down 35 and 45 dB for

2nd and 3rd harmonics, respectively, at 300 to 500 MHz with peak deviation of 50 kHz

Intermodulation distortion: down 40 dB

Deviation sensitivity: 200 ±10 kHz/rms volt

Deviation linearity: ±1 percent, Δ < 200 kHz; ±percent, Δ < 500 kHz

Carrier deviation: ±500 kHz

Frequency response (XMTR): ±1.5 dB with respect to 50 kHz, 0 < f < 500 kHz

Random motion: 25 g for 5 minutes in each of three orthogonal planes

Acoustical noise: 50M 71810

RFI: MIL-I-6181D

Incidental FM: 8 kHz max

Incidental AM: 5 percent max

Protection: Capable of open circuit, short circuit or ±28 volts applied to modulation input

Receive frequency: 2101.8 MHz

RCVR bandwidth: min 30 MHz, max 60 MHz

Polarization: RHCP

Receive Gain: 25 dB at max scan

Noise figure: 10 dB max

Output frequencies: IF (60 MHz) baseband, 2101.8 MHz

Output impedance: 50 ±3 Ω

Aperture: 225 elements (max)

Operational modes: self-focusing, pointing-logic controlled, hybrid

Prime power source: 28 ±4 volts (Z_0 < 1 Ω)

Conversion efficiency (dc to RF) > 10 percent

Grounding: 10^7 Ω isolation

Polarity reversal (28 ν): no effect

Radius of curvature $\simeq$ 300 cm

Mounting: Flush mount

Covering: Adequate for reentry heating

Size: Thickness not to exceed 6 inches

Weight: Not to exceed 25 pounds

Construction: MIC

TABLE 1-1. PERFORMANCE SPECIFICATIONS (cont'd)

Temperature cycling: -20° to 85°C

Acceleration: 50 g in three orthogonal planes

Shock: Half sinewave, 50 g for 11 ±1 μs

Altitude: 9 months, $p = 10^{-7}$ mm Hg

Moisture resistance: relative humidity 95 percent with $15° < T < 70°C$

Thermal vacuum: 50M 71810

Sinewave vibration: 10 to 2,000 Hz, 20 g peak in three orthogonal planes

Reliability: MTBF, 50,000 hours, 30,000 hours continuous operation

Thermal shock: 20° to 85°C
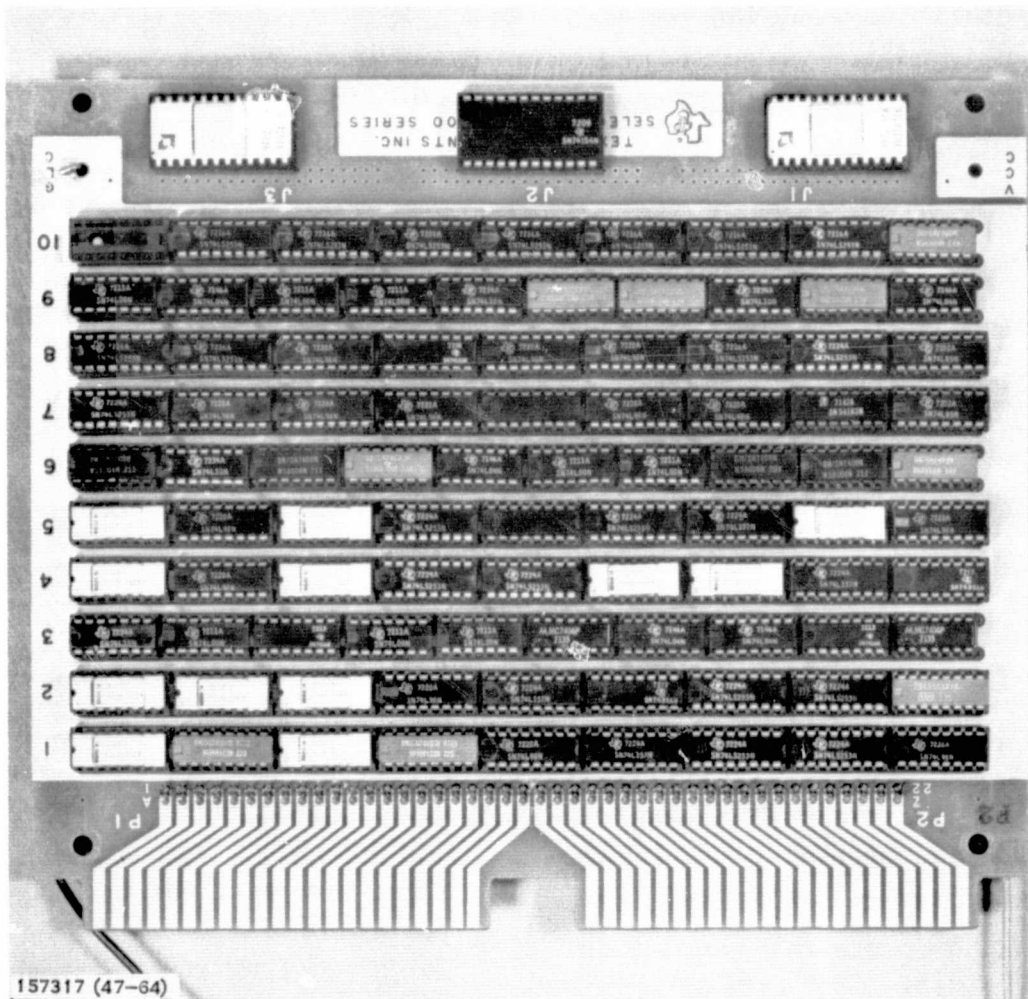
Figure 1-6. Beam-Steering Logic Cards on Automatic Checkout Equipment

completed 3 April 1973, and included a final report for this contractual phase published in June 1973.

With the successful completion of the third phase of the program, several tasks remained to be completed before a brassboard model of the AESPA system could be demonstrated. On 1 December 1972 Texas Instruments submitted a proposal to continue the program through the completion of these tasks. The proposal outlined a program to build a complete 48 element array utilizing brassboard elements that had been developed through Phase III of the program. The AESPA system block diagram of Figure 1-7 depicts elements available from various phases of the program that are required to complete the brassboard system. The remaining items which Texas Instruments proposed to develop in the Phase IV program in order to demonstrate the concept were the Transmit/receive modules, modulator and phase-lock transmitter, and the tracking receiver. The option was provided for NASA to proceed with production of an additional 36 months of the AESPA III type or to adopt a new design approach and produce 48 modules. NASA did not elect to proceed with work on the modulator and phase-lock transmitter, and the tracking receiver. However, modifications number 6 and 7 to Contract NAS8-25847 adopted the new module design.

During the fourth phase of the program, effort was concentrated on construction and evaluation of all hardware elements required to complete assembly of a 48 element active antenna array. Although the RF transmit and dc/logic manifolds had been constructed in earlier phases of the program, they were redesigned and constructed in this phase to accommodate the redesigned T/R module. All elements necessary to complete the array assembly were made available by work accomplished during the fourth phase. The hardware elements completed during this phase were RF transmit manifolds, RF receive manifolds, logic/dc manifolds, and 48 T/R electronics modules. A photograph of the assembled array is shown in the photograph of Figure 1-8.

Table 1-2 summarizes the performance of the 48 modules and RF manifolds.

TABLE 1-2.   AESPA IV PERFORMANCE SUMMARY

	GOAL	MEASURED
Module dc power (Watts)	4.5	4.6
Power output (dBm)	30	29.5
Transmitter gain[1] (dB)	22	15.5
Efficiency[2] (percent)	25	21.1
Transmitter phase error (RMS degrees)	5	4.2
Transmitter phase linearity (degrees)	±5	±11.2
Transmitter frequency (MHz)	2,282 ± 30	2,282 ± 30
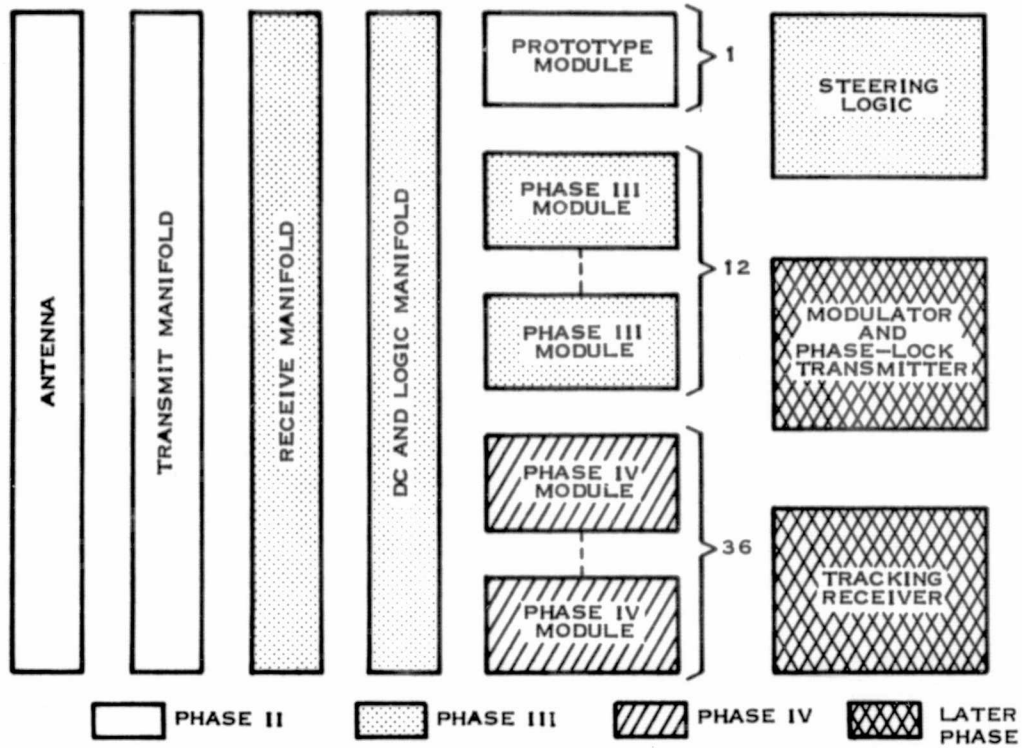
Figure 1-7. AESPA System Block Diagram
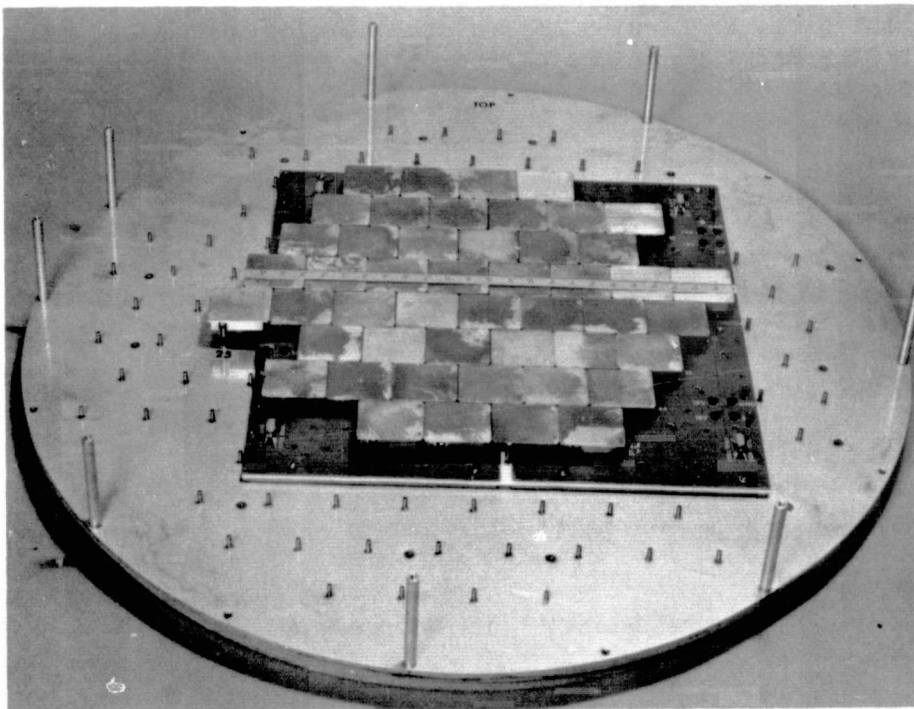
Figure 1-8. Assembled Array

TABLE 1-2. AESPA IV PERFORMANCE SUMMARY (cont'd)

	GOAL	MEASURED
Noise Figure (dB)[3]	4.5	5.6
Transmitter frequency rejection (dB)	40	>33
Receiver gain (dB)	23	17.7
Receiver phase error (RMS degrees)	5	4.3
Receiver linearity (degrees)	±5	±3.7
Receive frequency (MHz)	2,101 ± 30	2,101 ± 30
Transmitter manifold insertion loss (dB)	13	12.3 ± 0.6
Receiver manifold insertion loss (dB)	13	12.0 ± 0.7
Transmitter manifold phase tracking (degrees)	±5	±10.5
Receiver manifold phase tracking (degrees)	±5	±10
Transmitter manifold isolation (dB)	20	>20
Receiver manifold isolation (dB)	20	>20
Transmitter manifold return loss (dB)	14	>12
Receiver manifold return loss (dB)	14	>14
Module weight (ounces)	2.2	2.5
Array weight (pounds)	less than 50	38.5

[1]Transmitter and receiver gain were lowered for budgetary reasons at the beginning of the fourth phase by deletion of one stage from each chain.

[2]Efficiency goal was for power chain. Measured efficiency includes receiver and phasor biases.

[3]Noise figure design goal was stated as 4.5 dB for amplifier. Measured value is for module which includes the diplexer and amplifier.

In the AESPA V Program the brassboard 48 element S-band array was elevated, and a critical component brassboard Ku-band 3-bit phase shifter was developed. This report describes the work performed in the Phase V Program.

SECTION II

SUMMARY OF ACCOMPLISHMENTS

In the AESPA V program tests were performed on the brassboard 48-element S-band array to measure the R.F. performance parameters which define the communications system link margin. The performance parameters measured include effective isotropic radiated power, noise temperature, gain, and dynamic beam steering effects. The measurement techniques employed and results achieved for these tests are discussed in Section III of this report.

Also included in the Phase V program was a study addressed to the investigation, design, fabrication and evaluation of Ku-band phase shifters suitable for use in a phased array space-to-space communications system. Reflection type pin diode 3-bit phase shifters were designed in both strip-line and microstrip transmission line media. The microstrip design was assembled and evaluated, and the comparative performance of the two config-urations was assessed by measuring the "cold" circuit losses of both. These results are also discussed in Section III.

SECTION III

PHASE SHIFTER INVESTIGATION

A.   PRELIMINARY CONSIDERATIONS

        In March 1974 Texas Instruments completed a report summarizing
the results of a study of the feasibility of Ku-band phased-array antennas
for space-to-space communications links. It was recognized in that report
that, regardless of the type of phased array used, a Ku-band phase shifter
was a critical design requirement. The type of phase shifter needed was
seen to be dependent upon the array type. A phase shifter for a diplexed
passive array must have a bandwidth which includes both transmit and receive
bands (approximately 13 percent); while an active diplexed array could use
two phase shifters, each operating over a nominal four percent bandwidth.
The report recommended that a developmental program be undertaken to design
and fabricate a suitable hybrid phasor. This program would concentrate on
a moderate bandwidth component suitable for use in a diplexed active array.
It would be designed for the receive band, i.e., 14.6 to 15.2 GHz, since
demonstration at this frequency would also satisfy (low-to-moderate power)
transmit phasor feasibility requirements. Finally, the report recommended
that prototype phasors be fabricated in both microstrip and stripline in
order to compare the performance and estimate the reproducibility of both
types.

        Modification 8 to contract NAS8-25847 specified that this work be
initiated in August 1974. Preliminary design specifications for the phasor
outlined by the contract modification are given in Table 3-1.

Table 3-1. Preliminary Specifications
for Ku-Band Shifter

|	
Frequency Range	$13.4 \text{ GHz} < f_r < 14.0 \text{ GHz}$
	$14.6 \text{ GHz} < f_t < 15.2 \text{ GHz}$
Loss	3.0 dB Max (passive array)
	5.0 dB Max (active array)
Power Level	0.5 Watt Output Power for Transmit Phasor
Control Power	0.5 Watt max., 0.1 Watt design goal
VSWR	1.3 : 1
Weight	Minimum
Bits	3 (four optional)
Amplitude Tracking	1.0 dB
Phase Track	20 degrees RMS for 3 bits
	10 degrees RMS for 4 bits
DC Drive	Compatible with TTL Logic

The work carried out during this phase of the program is essentially the same as that recommended by the feasibility study outlined previously. The initial task was the choice of the proper phase shifter type. The two types considered for this program are shown schematically in Figures 3-1 and 3-2. Figure 3-1 shows two forms of the switched line type, while Figure 3-2 shows a reflection type employing rat-race directional couplers. The switched line form is the most commonly used in applications at Texas Instruments. A four-bit X-band switched line phasor employing series diodes is shown in Figure 3-3. The design details and loss budget for this unit are shown in Table 3-2. Characteristics of a 3-bit 2.5 - 5.0 GHz switched line phasor developed at Texas Instruments and employing shunt diodes has been described in the literature[1]. A loss budget for the two switched lines forms of a Ku-band phasor (based on both theoretical considerations and experience with the lower frequency components) has been prepared and is shown in Table 3-3. It is seen that the insertion loss of a 3-bit switched-line phase shifter would exceed the specification goals of Table 3-1. The reflection type phase shifter, however, is potentially capable of providing acceptable loss characteristics. This phasor has been shown to be less lossy than the switched-line type when constructed in the same transmission line type[2]. It is also capable of being constructed in stripline transmission line which provides further loss reduction[3,4]. This phasor form was chosen for the AESPA Ku-band development.

B.   PHASE SHIFTER DESIGN

With the phase shifter type chosen, much of the remaining effort on the program was devoted to selection of the transmission line medium. Initial work was done with microstrip using aluminum oxide substrate material. This medium was abandoned because of the inability to find suitable attaching coaxial connectors. The severity of the connector attachment problem was lessened considerably by replacing the aluminum oxide substrate with a lower dielectric constant teflon-fiberglass material manufactured by the Rogers Corporation (Duroid 5880). Performance of microstrip transmission lines employing the two materials is shown in Table 3-4 and 3-5. Table 3-4 is for a .5 inch section of .020 inch thick Al_2O_3 using OSM 14837A connectors and Table 3-5 is for a one inch section of .010 inch thick Duroid 5880 employing OSM 14837A connectors.

1. Robert P. Coats, "An Octave-Band Switched-Line Microstrip 3-B Diode Phase Shifter," IEEE Transactions on Microwave Theory & Techniques," Vol. MTT-21, No. 7, July 1973.
2. Richard W. Burns and Louis Stark, "Pin Diodes Advance High-Power Phase Shifting," Microwaves, Vol.   , No.   , November 1965, pp. 38-48.
3. Joseph F. White, "Phase Shifters for Array Antennas," IEEE Trans. Microwave Theory & Techniques, Vol. MTT-22, pp. 658-674, June 1974.
4. Franklin G. Terrio, Ronald J. Stockton, Wayne D. Sato, "A Low Cost P-I-N Diode Phase Shifter for Airborne Phased-Array Antennas," IEEE Trans. Microwave Theory & Techniques, Vol. MTT-22, pp. 688-692, June 1974.
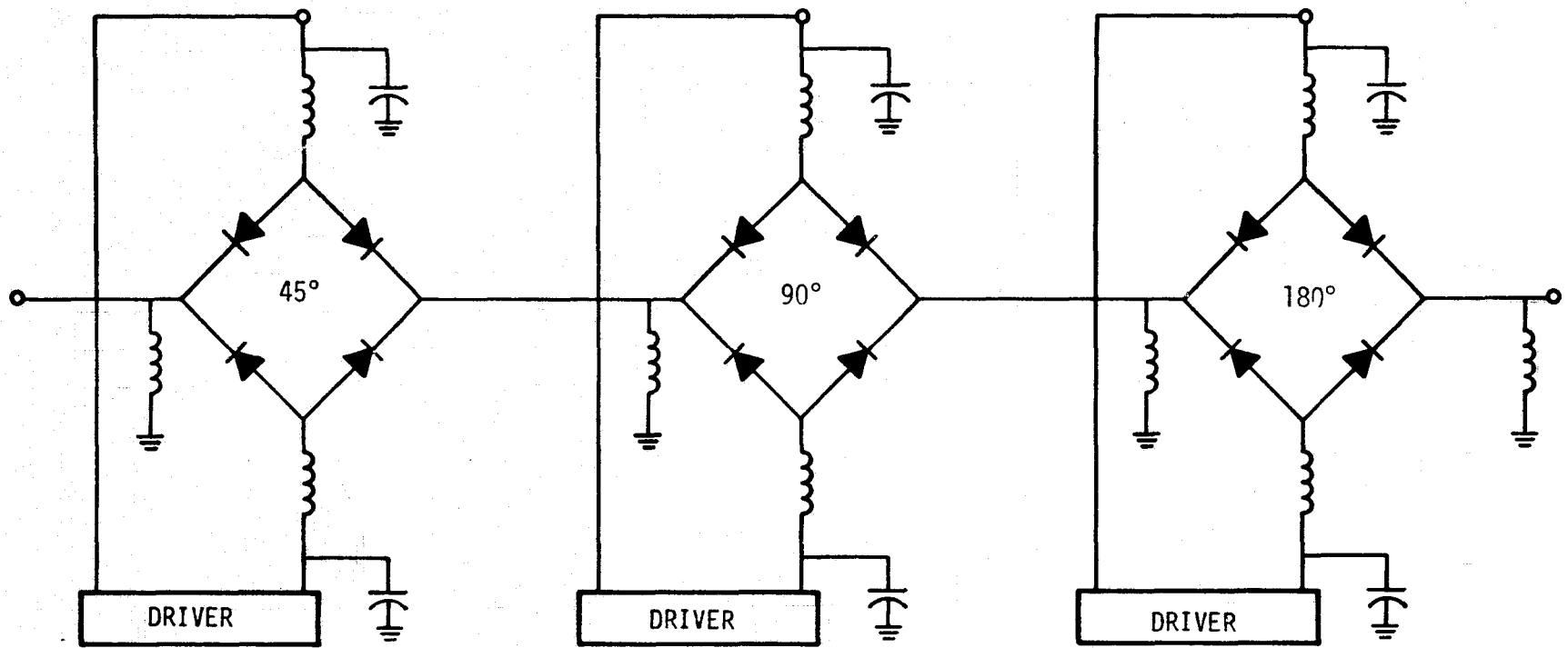
SERIES DIODES
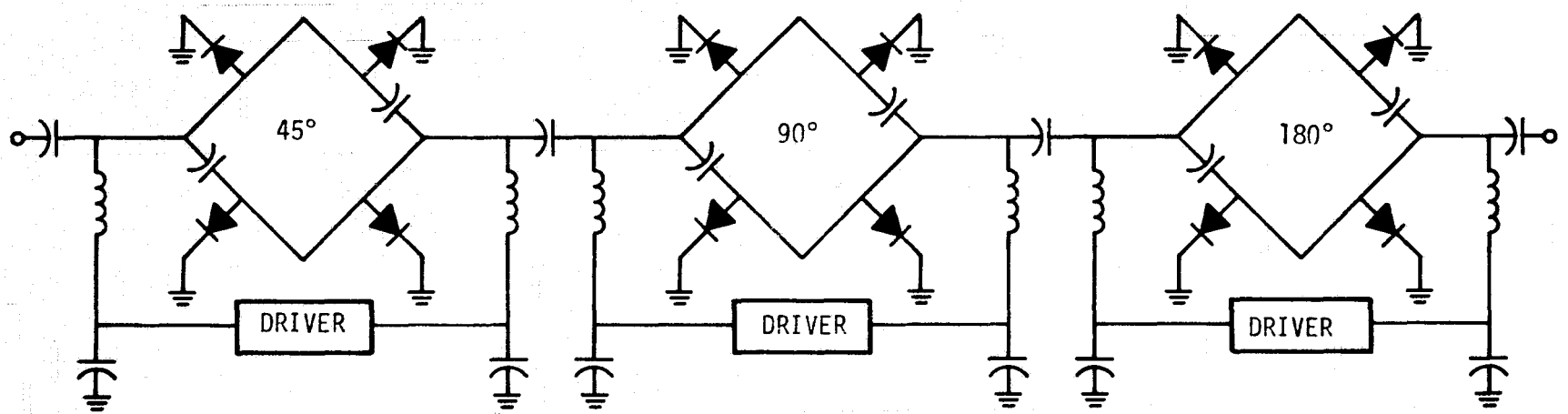
SHUNT DIODES

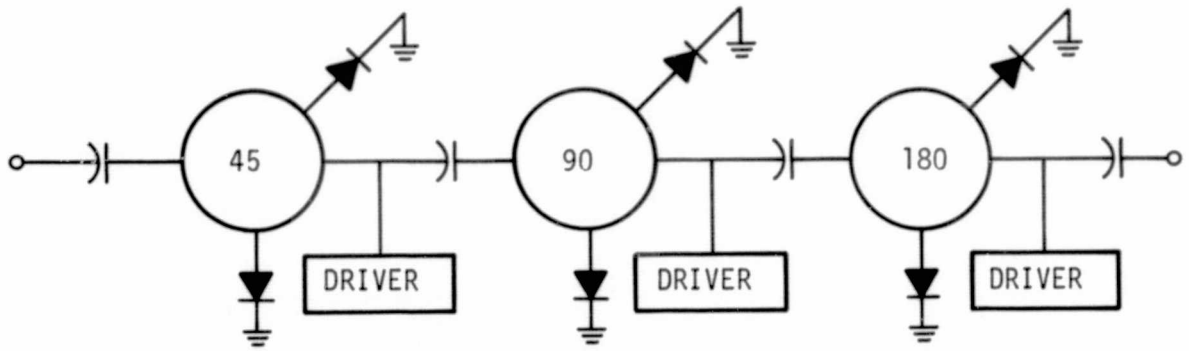Figure 3-1. Switched Line Phase Shifter Configurations

Figure 3-2. Reflection Type Phase Shifter Configuration
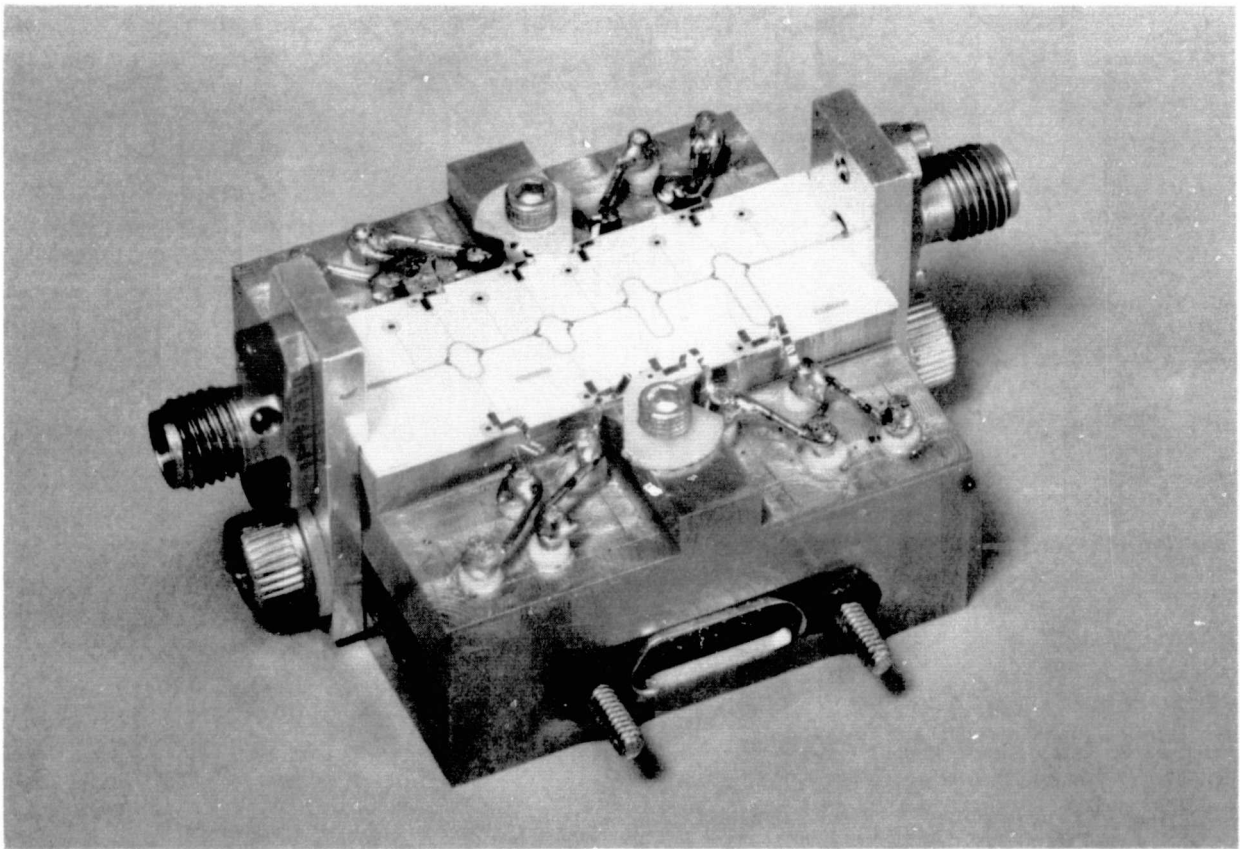

Figure 3-3. Breadboard Phase Shifter

Table 3-2. Loss Characteristics of an
X-band 4-Bit Phase Shifter

Type - Switched Line With Series DIodes (4 bits)

Frequency - 7.25 - 7.45 GHz

Diodes -

	C_T(PF)	$R_s(\Omega)$
(4) T.1 MD 100	.06	4.5
(4) T.1 MD 101	.11	3.5

Transmission Line - 020 THK Al_2O_3 (70Ω Line)

Loss Budget

Circuit Loss	1.50
Diode Loss	2.00
Isolation Loss (MD-101)	.80
Isolation Loss (MD-100)	.40
Predicted Total Loss	4.70 dB
Measured Total Loss	3.0 - 5.2 dB

Table 3-3. AESPA Ku-Band Switched Line
Phase Shifter Theoretical Loss Budget

A.   Series Diode Configuration

Diode Type T.I. MD-090 C_T = 017PF R_s = 7Ω

Circuit Loss	1.50
Diode Loss	3.60
Isolation	.20
	5.30 dB

B.   Shunt Diode Configuration

Diode Type Hewlett-Packard 5082-0001 C_T=.1PF R_s=1.0Ω

Circuit Loss	2.70
Diode Loss	1.20
Isolation Loss	-
	3.90 dB

Table 3-4. Performance of 0.5 Inch Section of 0.020 Inch Thick Al_2O_3

FREQ.	REFL	VSWR	ANGLE	GAIN	PHASE
11400.000	.054	1.135	100.7	- .53	- 29.6
11900.000	.102	1.229	54.5	- .54	- 58.7
12200.000	.114	1.258	33.0	- .51	- 97.7
12900.000	.097	1.215	19.9	- .51	-115.5
13000.000	.091	1.201	21.7	- .39	-144.3
13400.000	.121	1.275	30.2	- .51	-171.7
13900.000	.179	1.437	21.0	- .62	159.6
14200.000	.244	1.647	.5	- .75	129.9
14900.000	.309	1.999	-22.5	-1.64	101.2
15000.000	.358	2.117	-47.5	-1.90	75.1
15400.000	.397	2.919	-73.3	-2.10	47.1
15900.000	.416	2.427	-99.3	-2.17	20.5

Table 3-5. Performance of 1.0 Inch Section 0.010 Inch Thick Duroid (5880)

| FREQ.	REFL	VSWR	ANGLE	GAIN	PHASE
11400.000	.049	1.101	3.2	- .29	94.3
11900.000	.037	1.076	- 3.7	- .39	61.9
12200.000	.021	1.043	9.9	- .49	39.7
12600.000	.035	1.072	30.5	- .39	19.9
13000.000	.046	1.096	13.3	- .49	- 5.9
13400.000	.051	1.109	-14.5	- .53	-27.6
13900.000	.060	1.129	-37.2	- .52	-49.5
14200.000	.055	1.117	-69.9	- .43	-72.5
14600.000	.049	1.102	-94.6	- .59	-95.6
15000.000	.017	1.035	-129.4	- .51	-116.9
15400.000	.016	1.033	96.4	- .41	-140.3
15800.000	.060	1.129	20.9	- .38	-165.3

Prior to completion of these experiments plans had already been made to make use of Duroid for a strip-line phase shifter design. Successful implementation of the material for microstrip transmission line made it possible to utilize it for both proposed phase shifter forms. The strip-line form was expected to provide better performance than the microstrip version. Configuration of the photomasks developed for the two phase shifter types are shown in Figure 3-4. Both types are designed to utilize shunt mounted chip diodes. The microstrip version utilizes rat race directional couplers photoetched on .010 inch thick Duroid 5880 substrate. The stripline version utilizes 8.3 dB tandem connected directional couplers photoetched on three layer stripline composed of three sheets of .010 inch thick Duroid 5880[5].

With the choice of the two transmission line configurations determined, two important tasks remained. The first was development of good quality directional couplers in both transmission medias and the second was characterization and tuning of diodes in both. Directional coupler design was begun in the microstrip medium.

Poor performance achieved with initial rat race couplers evaluated was thought to be due to coupling between rat race terminals of non-TEM radiated energy. The couplers were re-evaluated with metallic walls around all connecting lines and performance was significantly improved. Figure 3-5 shows a comparison of performance achieved with and without shielding walls.

An effort was made to optimize the coupler performance at 14.9 GHz by constructing and evaluating a series of components with different ring diameters. The results achieved with the four units evaluated are shown in Figure 3-6. Ring diameters are .242, .252, .262, and .272 inches. These diameters correspond to calculated center frequencies of 15.9, 15.3, 14.7, and 14.2 GHz, respectively. The predicted performance of rat race couplers has been well documented[6]. The deviation from the performance as presented in Figure 3-6 is thought to be caused by assembly problems. The .262 inch diameter coupler has performance characteristics that most closely agree with the predicted performance, and are adequate for the phasor application. This configuration was chosen for the microstrip phasor design.

5. Joseph A. Mosko, "Theoretical, Experimental, and Tolerance Data for Selected Strip-Line Directional Couplers," Navweps Report 8678, NOTS TP 3732, June 1965.
6. J. Reed and G. J. Wheeler, "A Method of Analysis of Symmetrical Four-Port Networks," IRE Transactions on Microwave Theory and Techniques, Vol. MTT , pp. 246 - 252, October 1956.
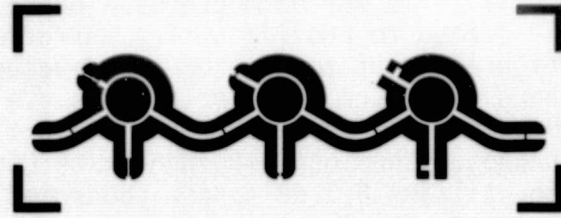
Photomask of Microstrip Phase Shifter
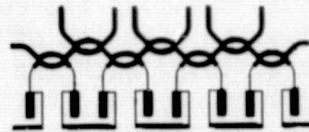
Photomask of Stripline Phase Shifter
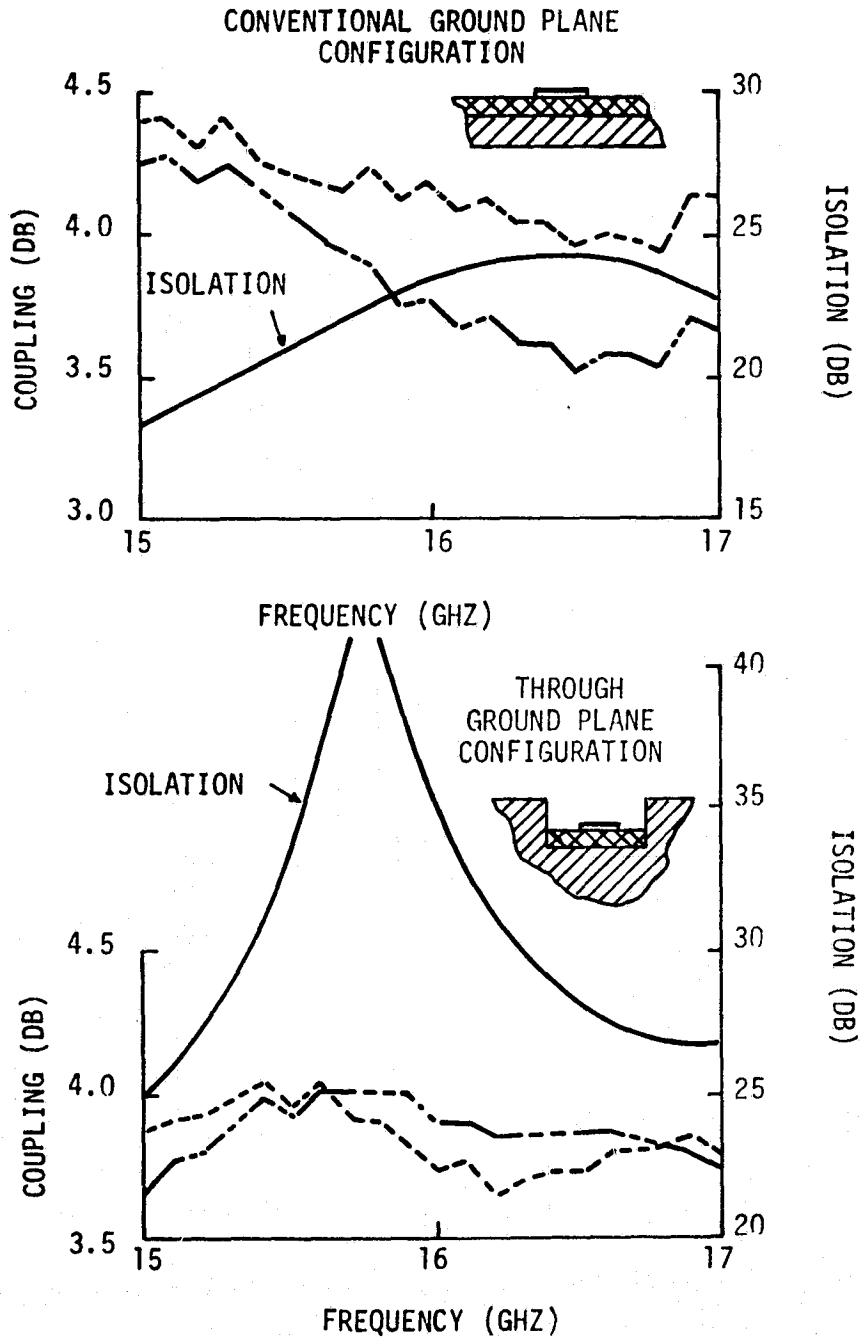
Figure 3-4. Phase Shifter Types

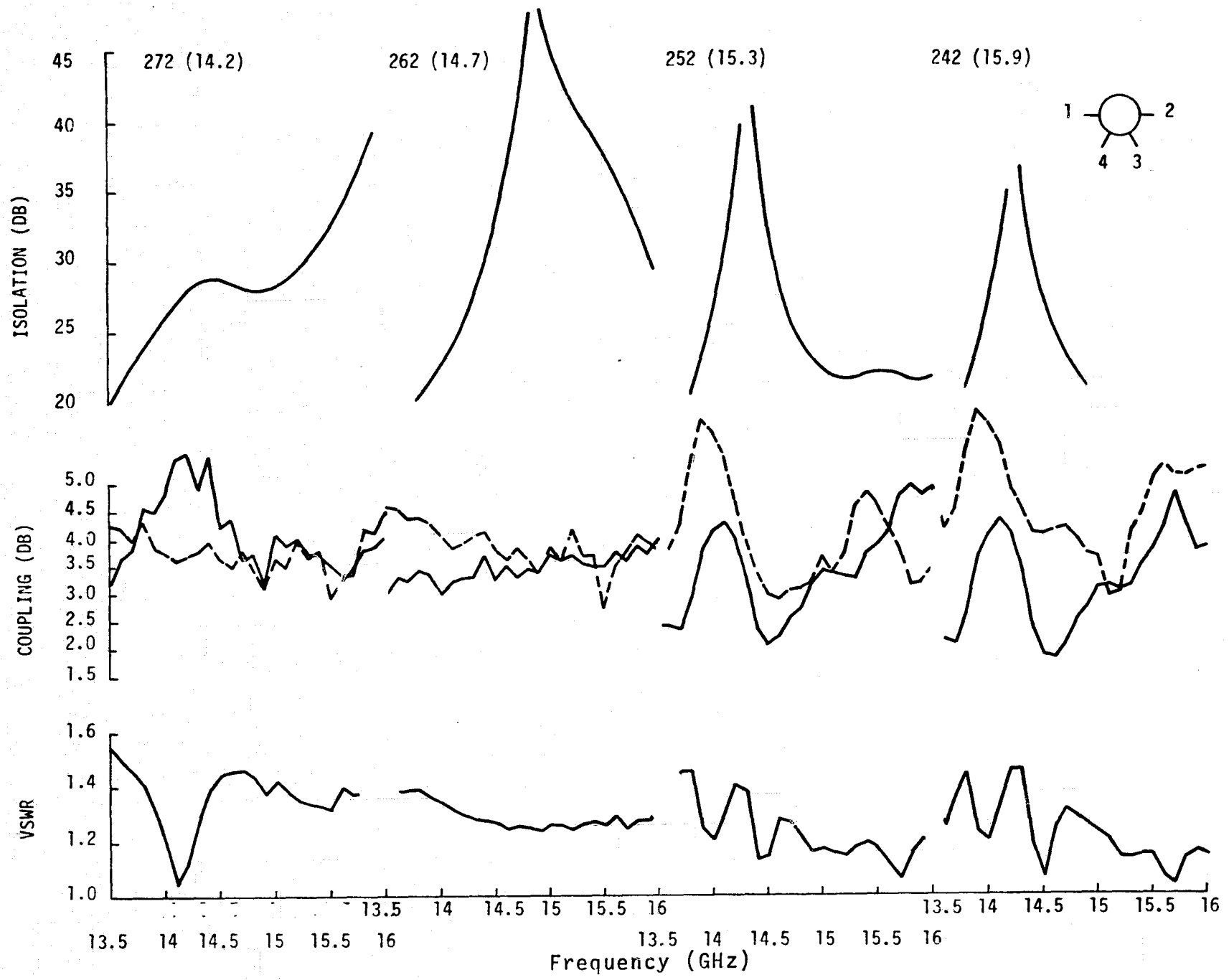Figure 3-5. Performance Characteristics of Ku-Band Rat Race Hybrid Coupler

Figure 3-6. Rat Race Couplers

A 3 dB coupler composed of two tandem connected 8.34 dB couplers photoetched on a stripline composed of 3 layers of .010 inch thick Duroid 5880 was adopted for the stripline phasor configuration. Performance achieved with three initial units evaluated was poor. It was believed that performance degradation for both microstrip and stripline couplers was due largely to attaching coaxial connectors. The microstrip rat race coupler appeared to provide very good performance when connectors were properly attached. Since performance degradation caused by connectors is much less serious for the composite phase shifter than for the coupler, it seemed logical to proceed with the composite phase shifter design if a coupler had been demonstrated to work, even if connector attachment problems were not completely solved. This was done for the microstrip phase shifter configuration. This could not be done for the stripline version, however, because it had not exhibited adequate performance in any of the three units assembled. One method of obtaining a more accurate evaluation of the coupler was to scale it to lower frequencies where connector attachment is not a problem. This was done by photo-reducing the ten-times-size coupler layout to two, three, and four times actual size; and photo-etching the coupler on duroid 5880 boards of .020 inches, .030 inches, and .040 inches thickness. The photo-etched boards were then assembled to produce couplers of exactly the same configuration as the 15 GHz coupler, but with center frequencies of 7.5 GHz, 5 GHz, and 3.75 GHz. Evaluation of these couplers determines the adequacy of the design and provides an indication of how it performs over a frequency range where connector attachment is not a problem. Figure 3-7 shows the results of this evaluation. These results show that the basic design is good and that although some degradation occurs with increasing frequency, that operation thru Ku-band should be possible with proper connector attachment.

Diode characterization and tuning work was carried out using a Hewlett-Packard 5082-0001 diode chip alloyed to ground at the end of a 50Ω microstrip transmission line. The diode was bonded to the transmission line with two 1-mil wires. The impedance of the diode at both 10 mA forward bias and 5 Volts reverse bias over the 13.4 - 15.2 GHz band is shown in Figure 3-8.

As hybrid coupled phase bits were to be utilized, it was desired to alter the diode characterization with suitable transmission line elements to achieve the proper difference in reflection coefficient arguments existing in the two bias states. This difference represents the differential phase shift provided by the diode bit.

The diode characterization was first altered by use of an open stub .132λ long located .090λ in front of the diode to produce a 180° bit. The theoretical effects of this stub on the characterization at 15 GHz are shown in Figure 3-9. Measurements performed using this tuning scheme revealed that better results could be achieved using a .110λ stub located .110λ in front of the diode. Measured results for these stub parameters are shown for the complete frequency band in Figure 3-10. The difference in reflection coefficient arguments is shown in Figure 3-11. This figure indicates that the 180° bit is capable of operating over both required bands with a phase error of less than $\pm10^{\circ}$
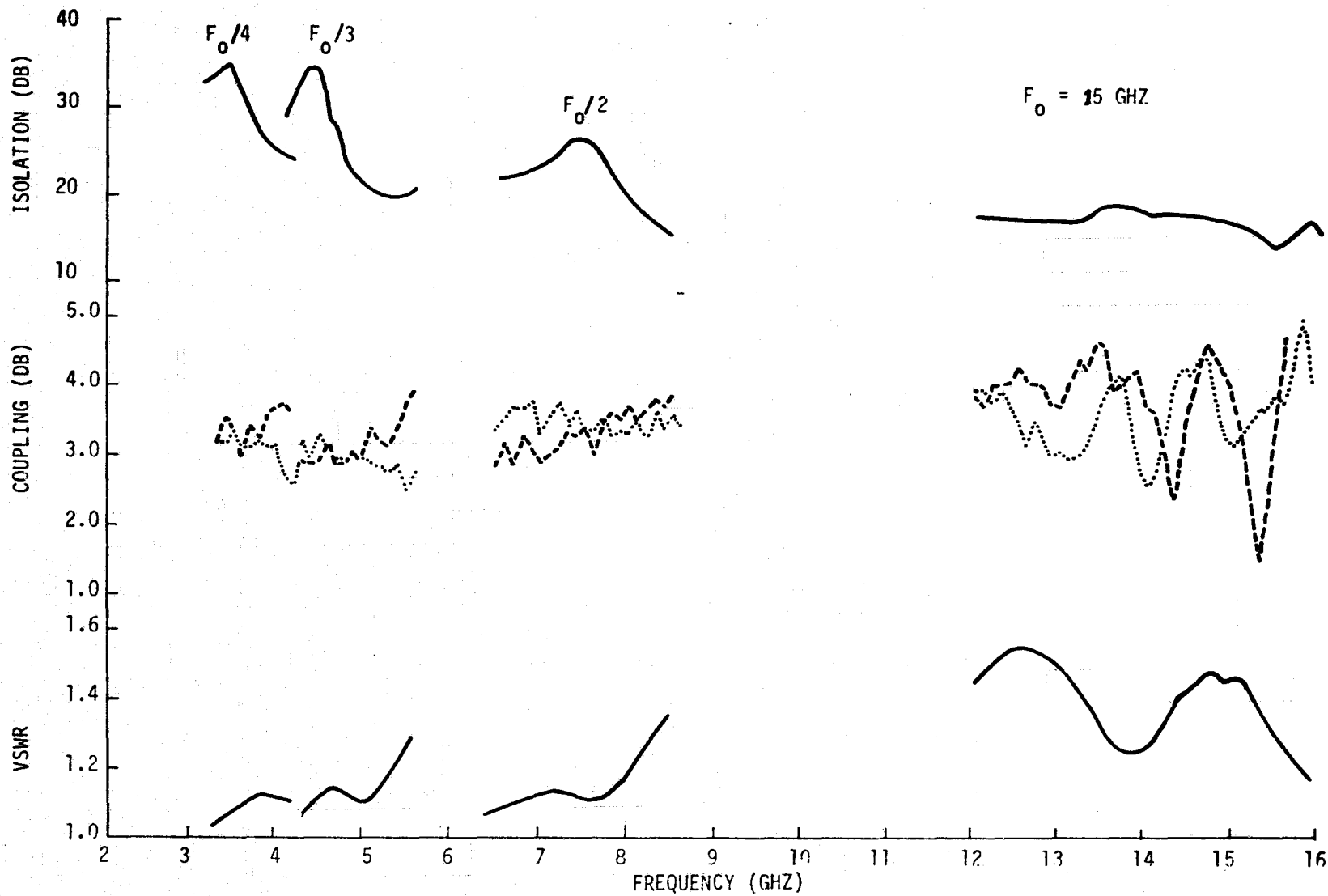
Figure 3-7. Performance Characteristics of the Ku-Band Stripline,
3 dB Tandem Connected Directional Coupler and Its
Scaled Versions

IMPEDANCE OR ADMITTANCE COORDINATES

DUROID 5880 MICROSTRIP
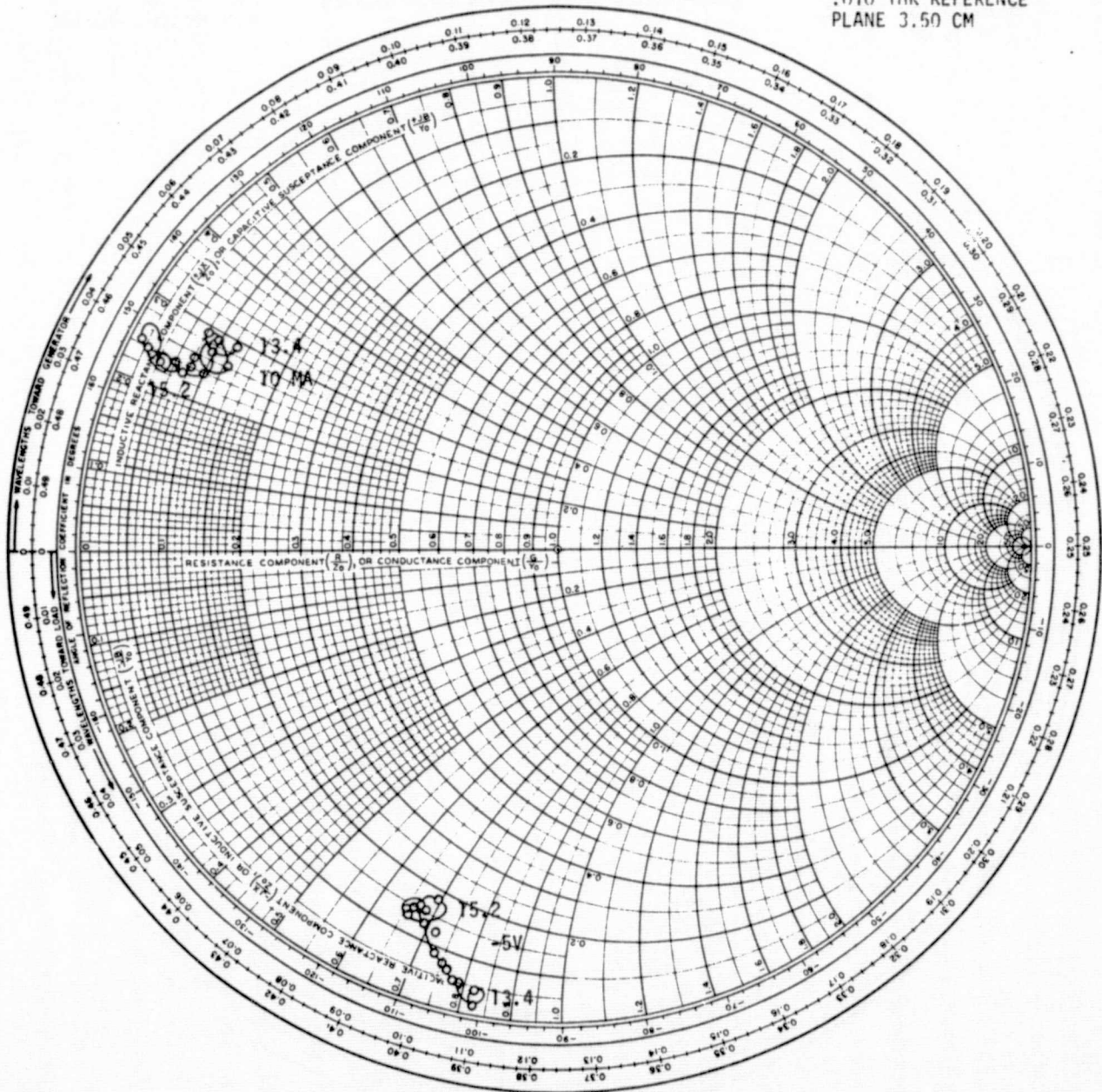.010 THK REFERENCE
PLANE 3.50 CM

Figure 3-8.   Measured Diode Impedance Characteristics

THEORETICAL STUB TUNING
CONFIGURATION FOR 180°
BIT AT 15 GHZ

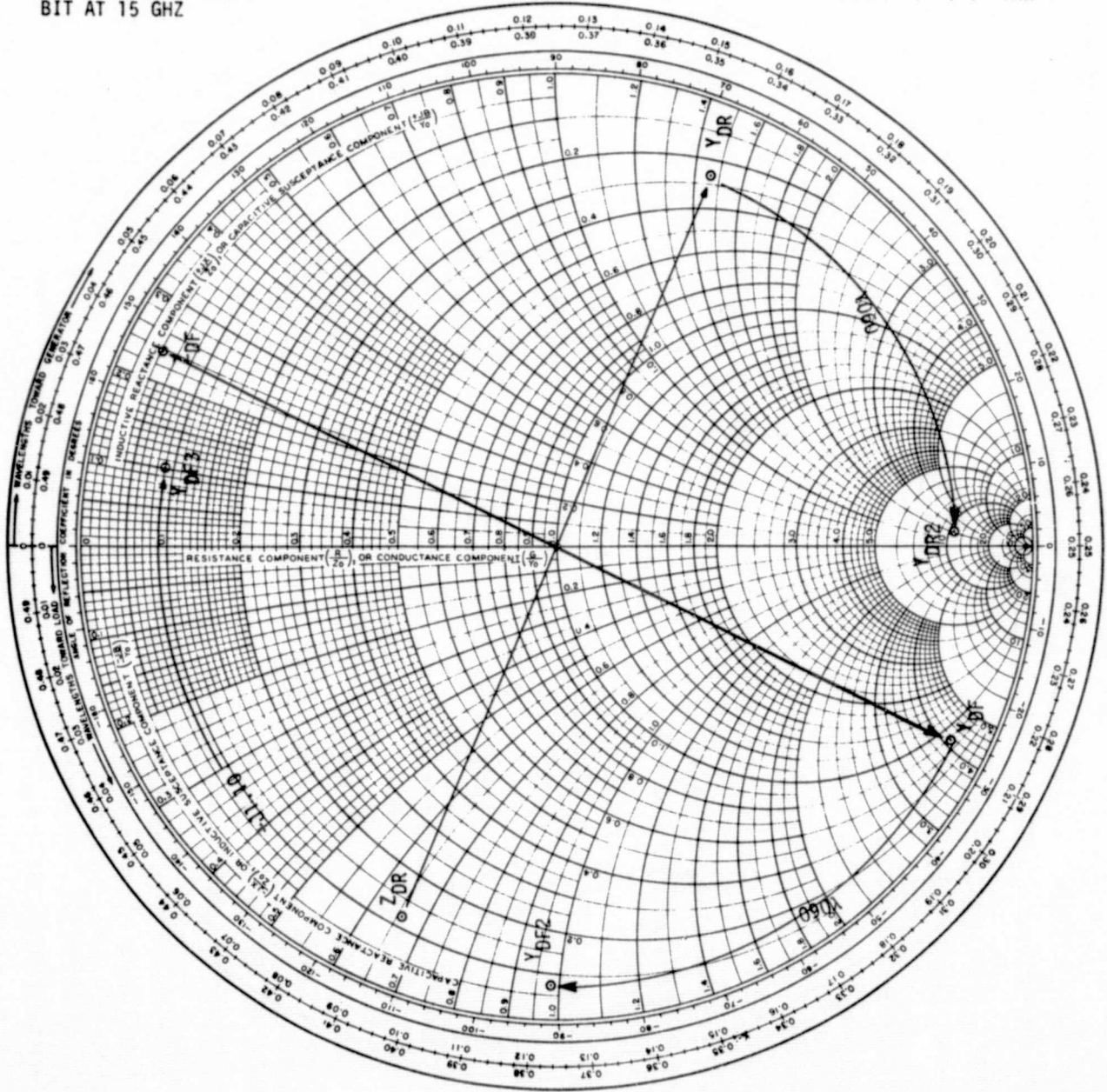IMPEDANCE OR ADMITTANCE COORDINATES

DUROID 5880
MICROSTRIP .010 THK

Figure 3-9. Graphical Determination of Diode Impedance for 180° Bit
Employing Shunt Tuning Stub

IMPEDANCE OR ADMITTANCE COORDINATES
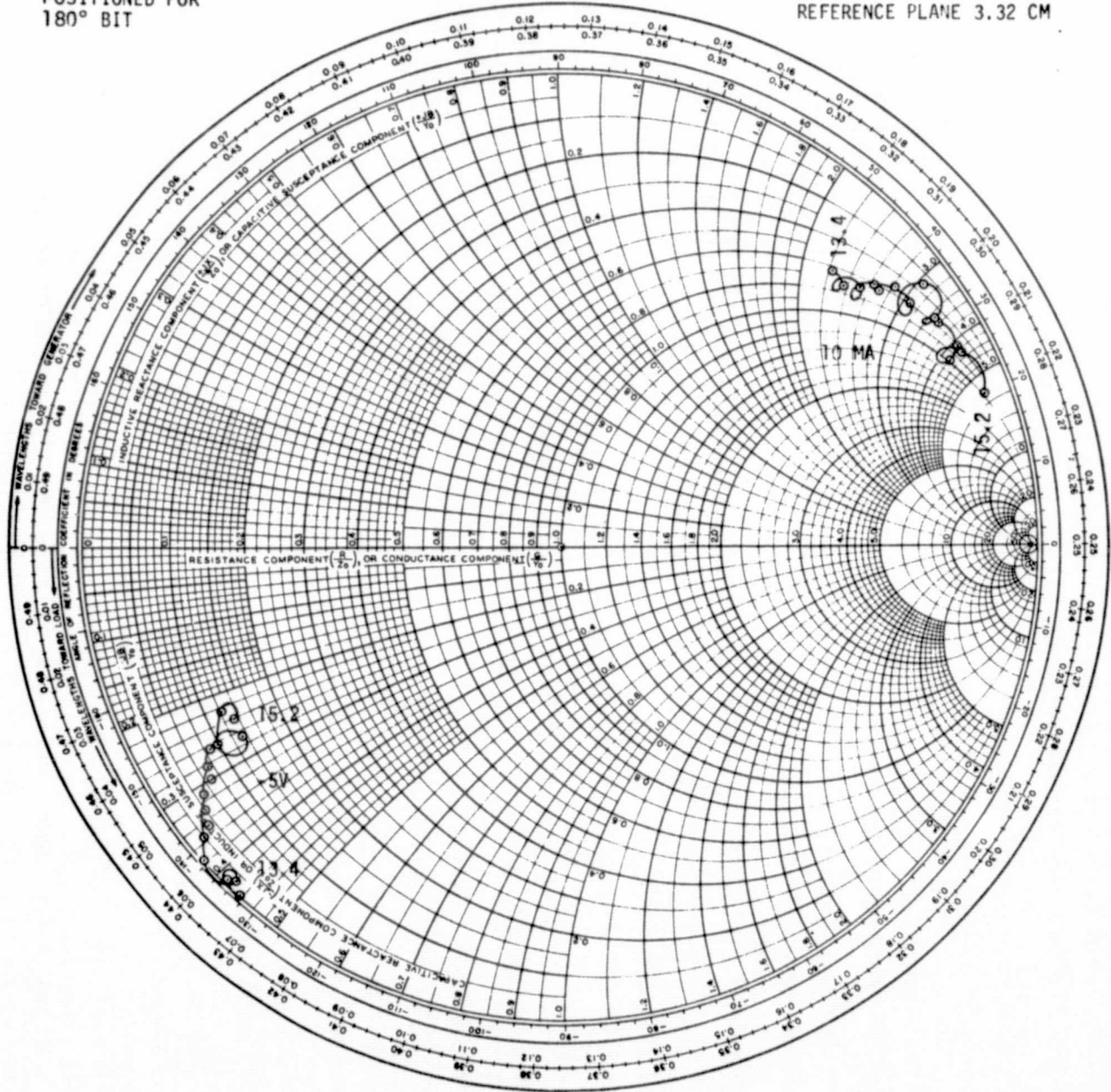
DUROID 5880
MICROSTRIP .010 THK
REFERENCE PLANE 3.32 CM

Figure 3-10. Measured Diode Impedance for 180° Bit Employing
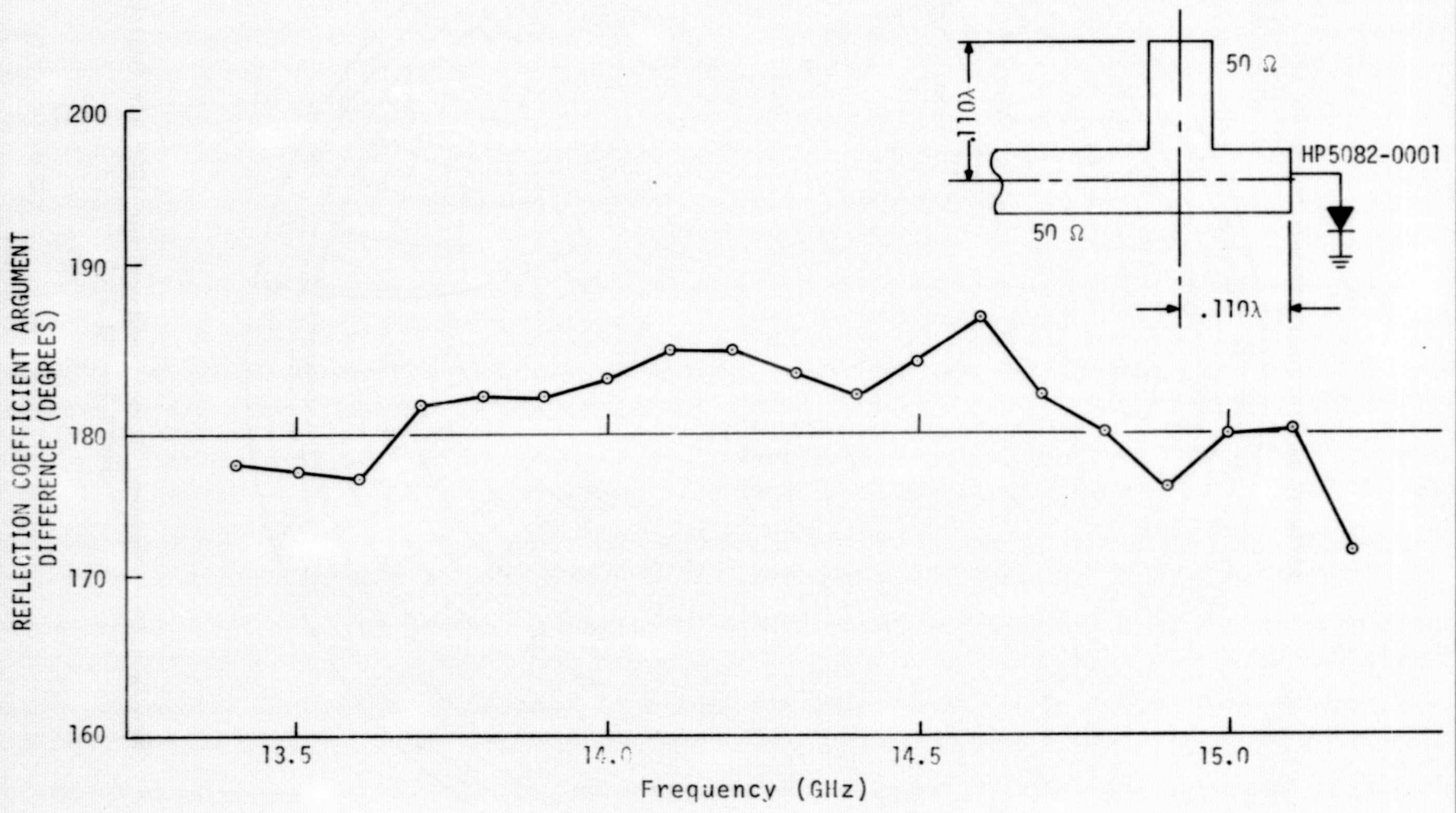Shunt Tuning Stub

Figure 3-11. Shunt Diode Characterization With Diode Tuned For Operation
As 180° Bit With Shunt Stub

The diode characterization was next modified by use of a 100Ω impedance transformer .090λ long located .029λ in front of the diode. The theoretical effects of this stub on the characterization at 15 GHz are shown in Figure 3-12. This matching scheme provides a theoretical reflection coefficient argument difference of 45°. Measurements revealed that better performance was achieved when the 100Ω line length was changed to .178λ. These results are shown in Figure 3-13 and the reflection coefficient argument difference is shown in Figure 3-14. Although not optimized, the data of Figure 3-14 indicates that a 45° bit can be realized over one band with an error of approximately ± 2 degrees.

The two tuning techniques utilized proved to be satisfactory for increasing or decreasing the reflection coefficient argument difference. The angular difference between the two states of the diode, as originally characterized, was approximately 100°. A 90° angular difference is achievable by use of a 100Ω impedance transformer .030λ long located .029λ in front of the diode. Use of these techniques is also applicable to the stripline phasor. Characterization of a diode of the same type mounted in stripline was started, but had to be terminated because of reassignment of personnel to the S-band array evaluation.

Layout work on both 3-bit phase shifter configurations was begun when coupler designs were completed. Diode tuning was added to the microstrip layout when completed and photomasks of both configurations were prepared. The photoetched 3-bit microstrip phase shifter substrate is shown in Figure 3-15 and the assembled unit is shown in Figure 3-16. Measured performance achieved with this phase shifter is shown in Figures 3-17 and 3-18. No attempt was made to improve phasor performance; instead, assembly of a second unit was started and tests were conducted after each assembly step to determine the source of losses. The results of these tests are shown in Figure 3-19.

The stripline phase shifter design was not completed because of the need for additional diode characterization data. In order to obtain a basis for comparing the two phase shifter types, "cold circuit" loss and VSWR were measured on both. The second of the microstrip phasors was used for this experiment. The results of this test are shown in Figures 3-20 and 3-21.

The stripline configuration is found to provide better loss characteristics than the microstrip configuration, as had been anticipated. It appears that the passive array phase shifter performance goals may be achievable with the stripline unit. It is recommended that work on this configuration be continued in the next program phase.

THEORETICAL TRANSFORMER
TUNING CONFIGURATION
FOR 45° BIT AT 15 GHZ

IMPEDANCE OR ADMITTANCE COORDINATES

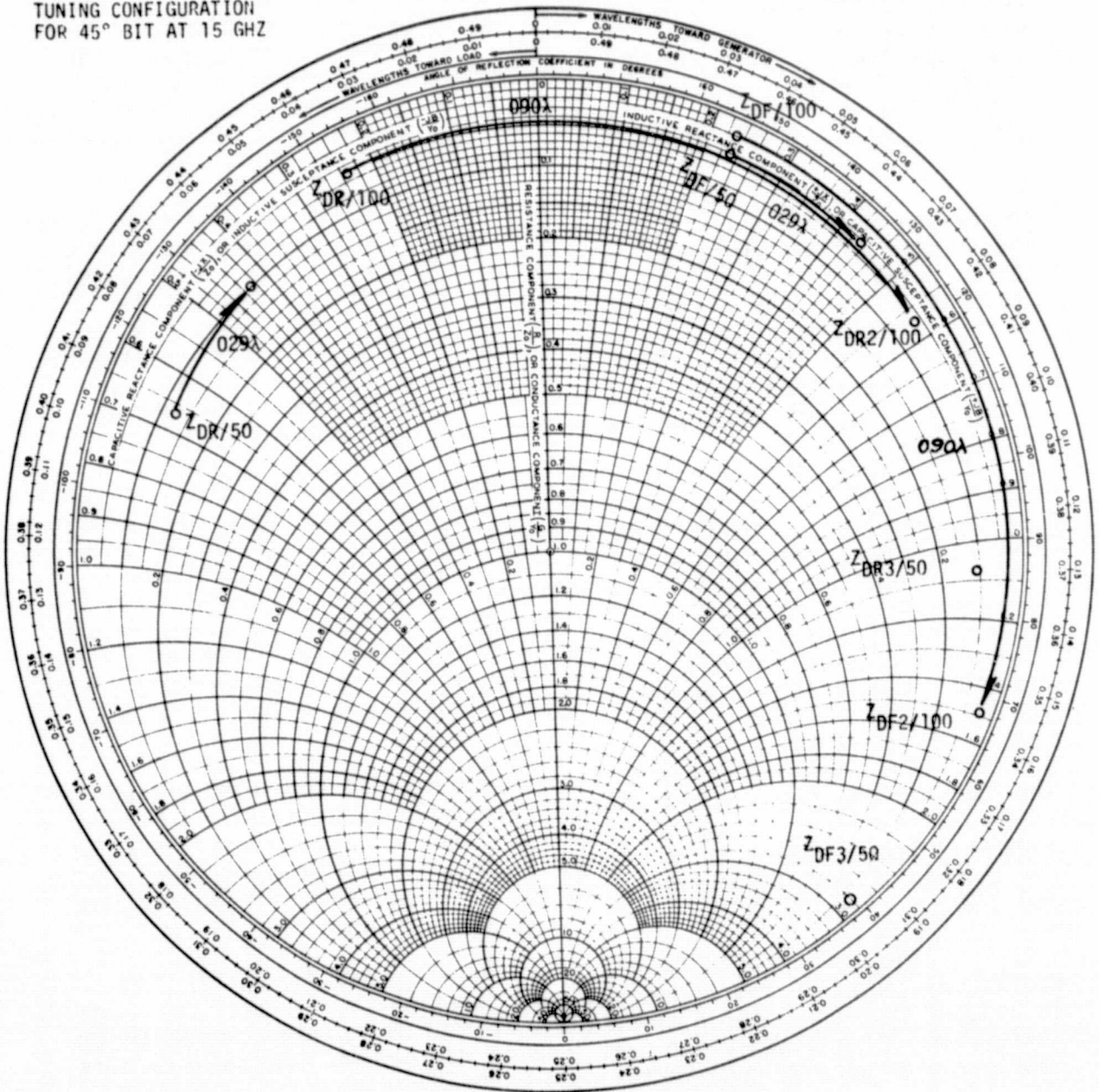DUROID 5880
MICROSTRIP .010 THK

Figure 3-12. Graphical Determination of Diode Impedance for 45° Bit
Employing 100Ω Impedance Transformer .090 Inches Long

FREQUENCY
13.4-15.2 GHZ

IMPEDANCE OR ADMITTANCE COORDINATES

DUROID 5880
MICROSTRIP .010 THK
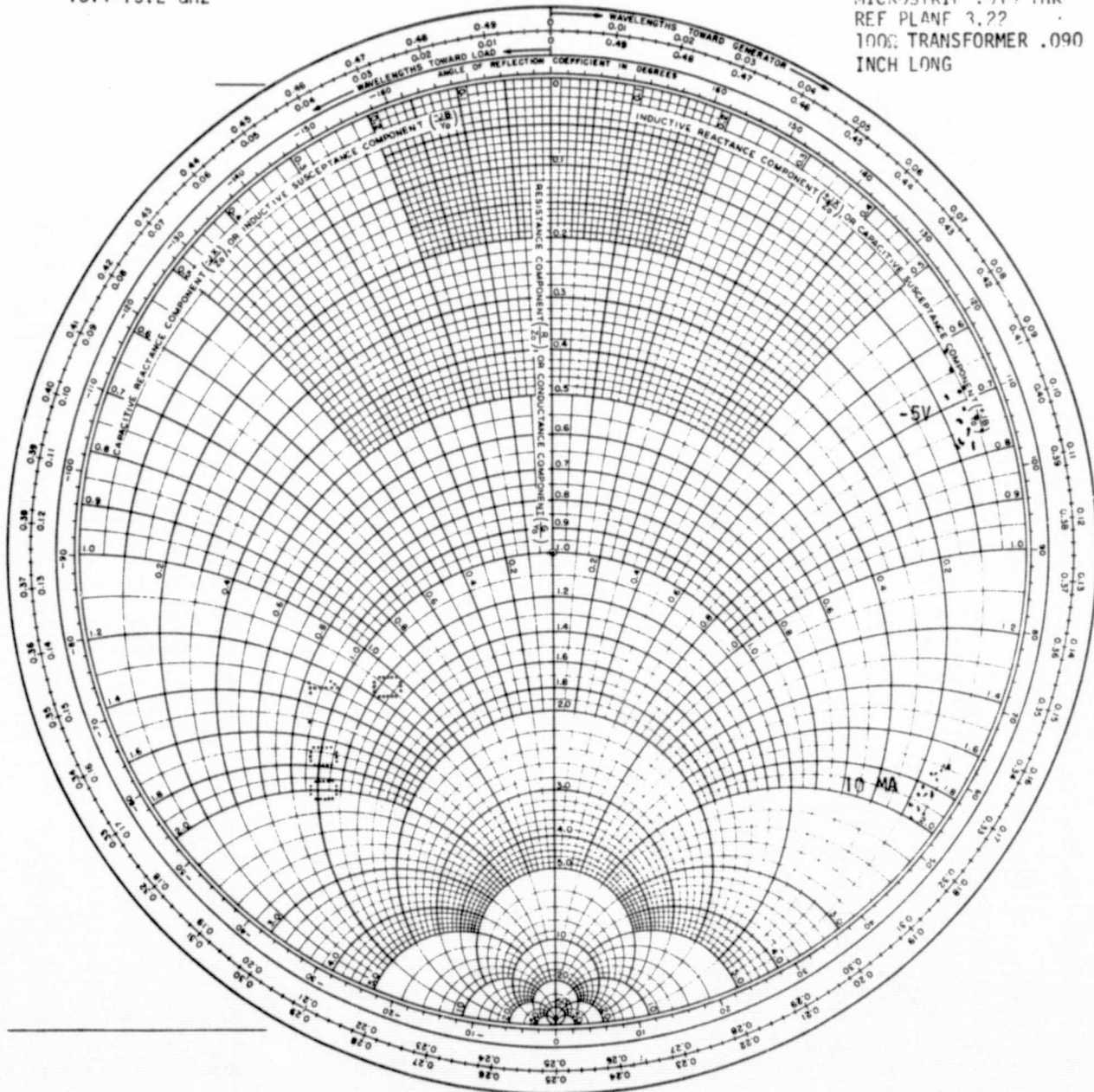REF PLANE 3.22
100Ω TRANSFORMER .090
INCH LONG

Figure 3-13.   Measured Diode Impedance for
45° Bit Employing 100Ω Impedance
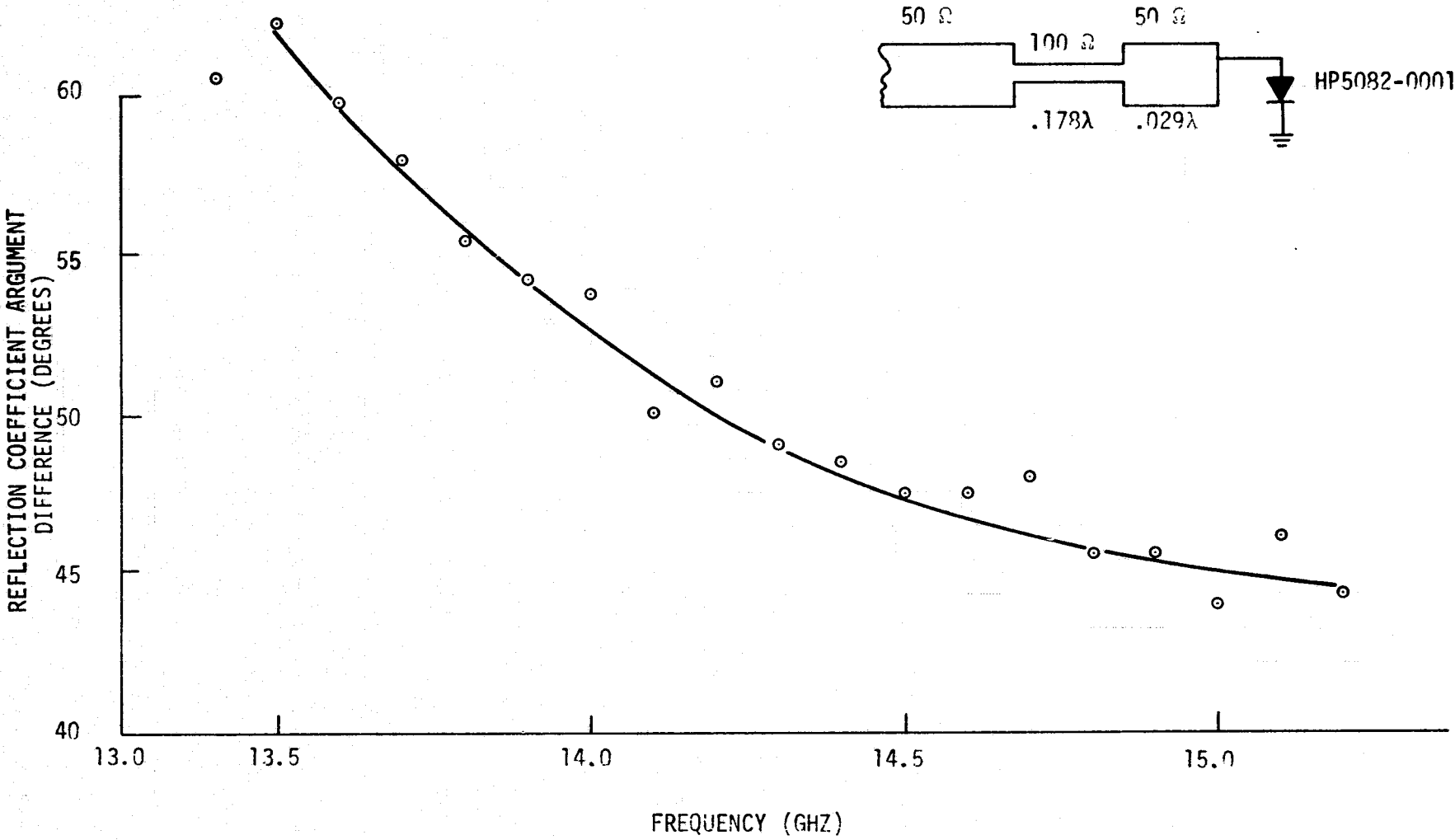Transformer .090 Inches Long.
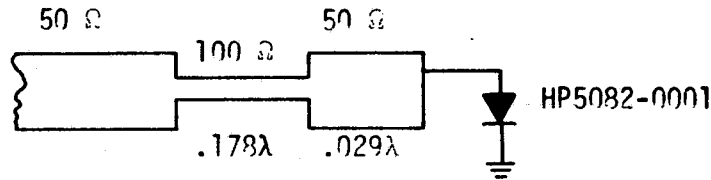
Figure 3-14. Shunt Diode Characterization With Diode
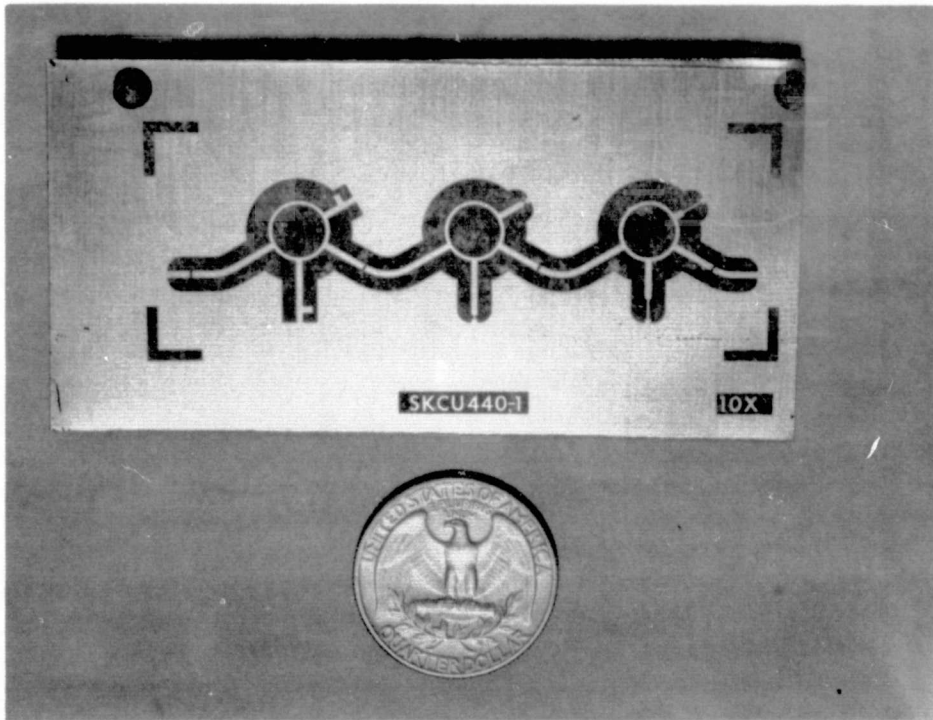Tuned for Operation As 45° Bit With
Impedance Transformer.

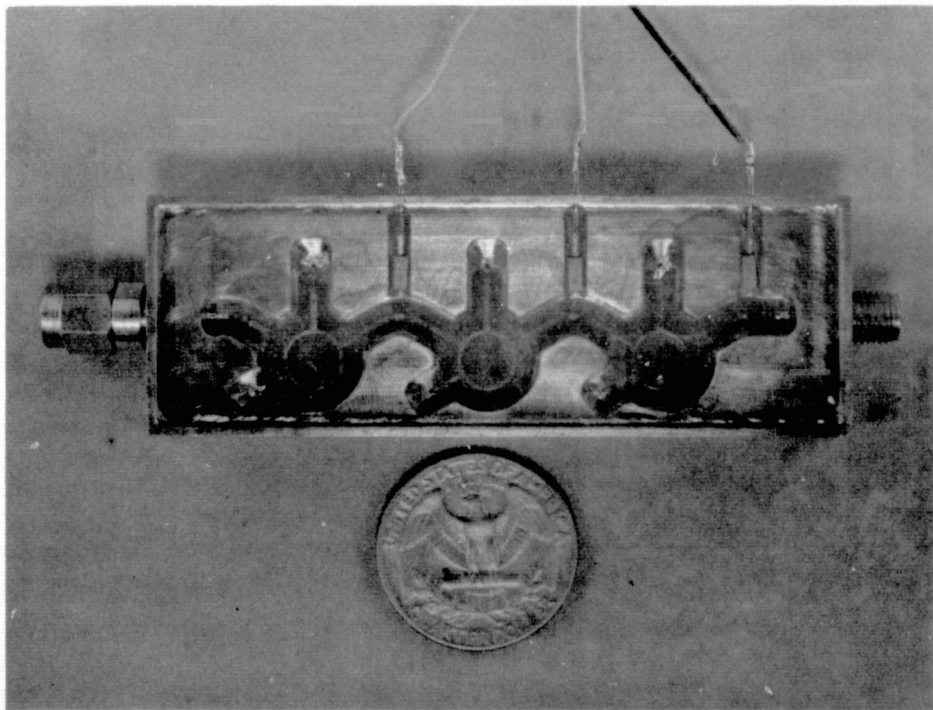Figure 3-15. Microstrip Phase Shifter Substrate.

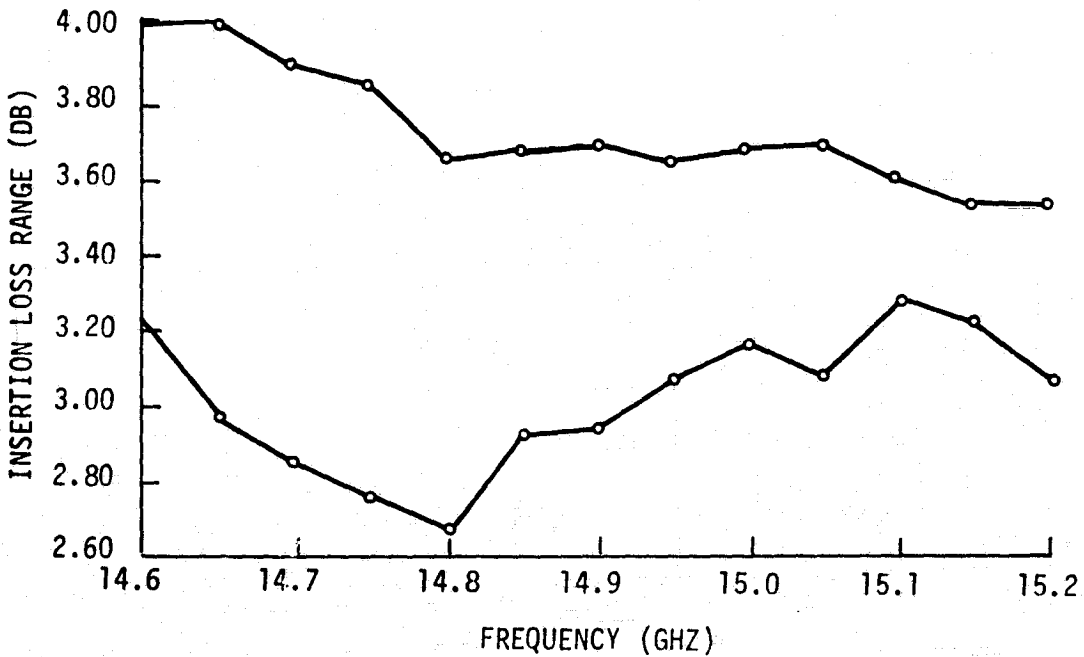

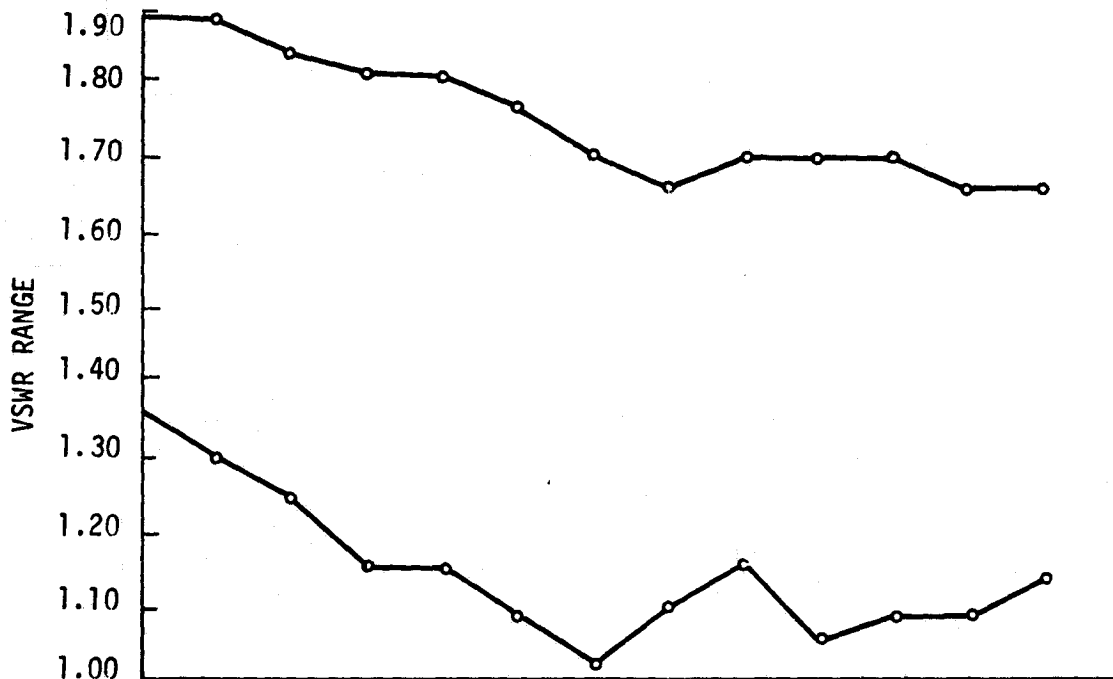Figure 3-16. Experimental Microstrip Phase Shifter.

Figure 3-17. Ku-Band Microstrip Phase Shifter VSWR and Insertion Loss Characteristics.
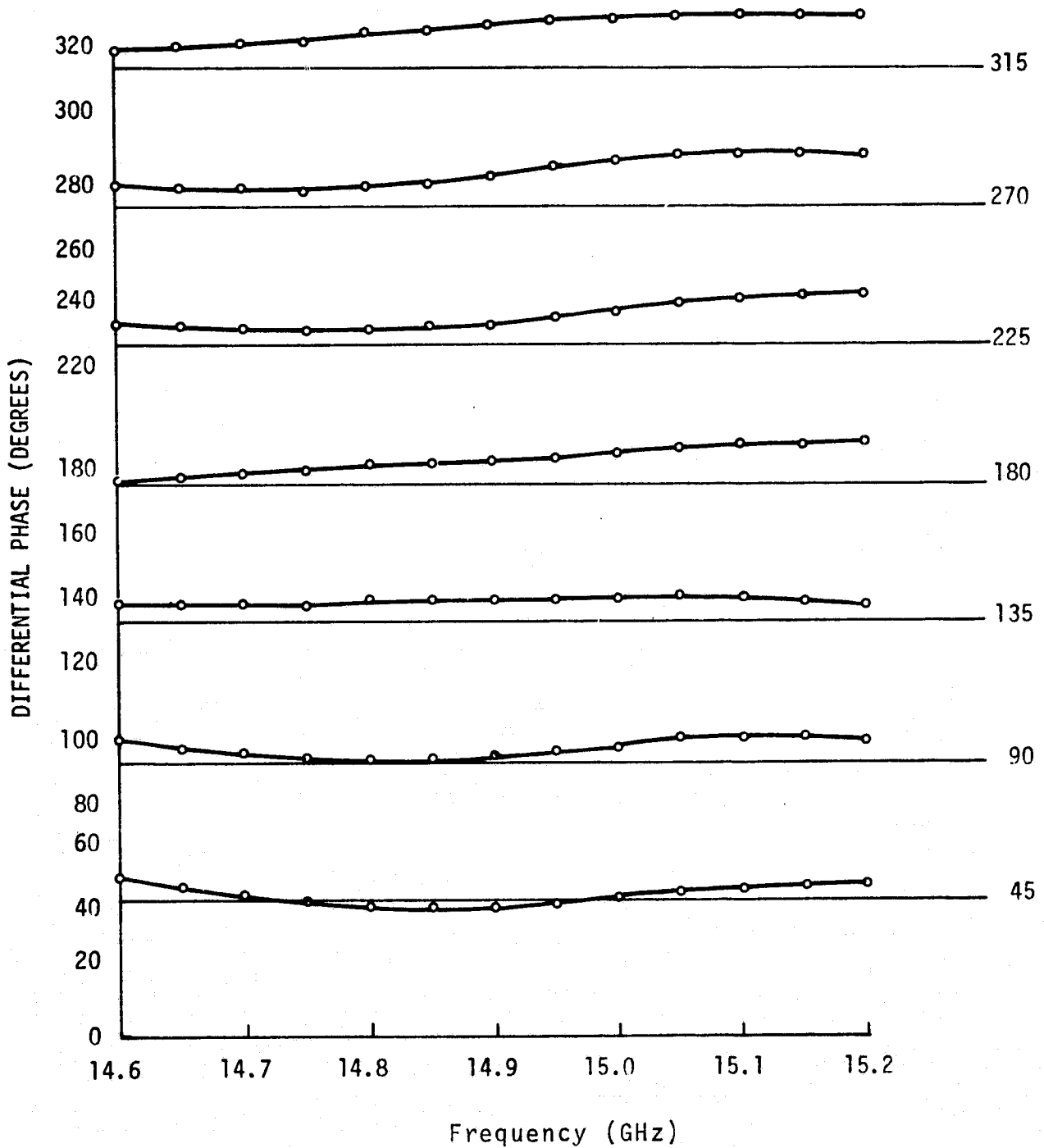
Figure 3-18. Ku-Band 3-Bit Microstrip Phase Shifter
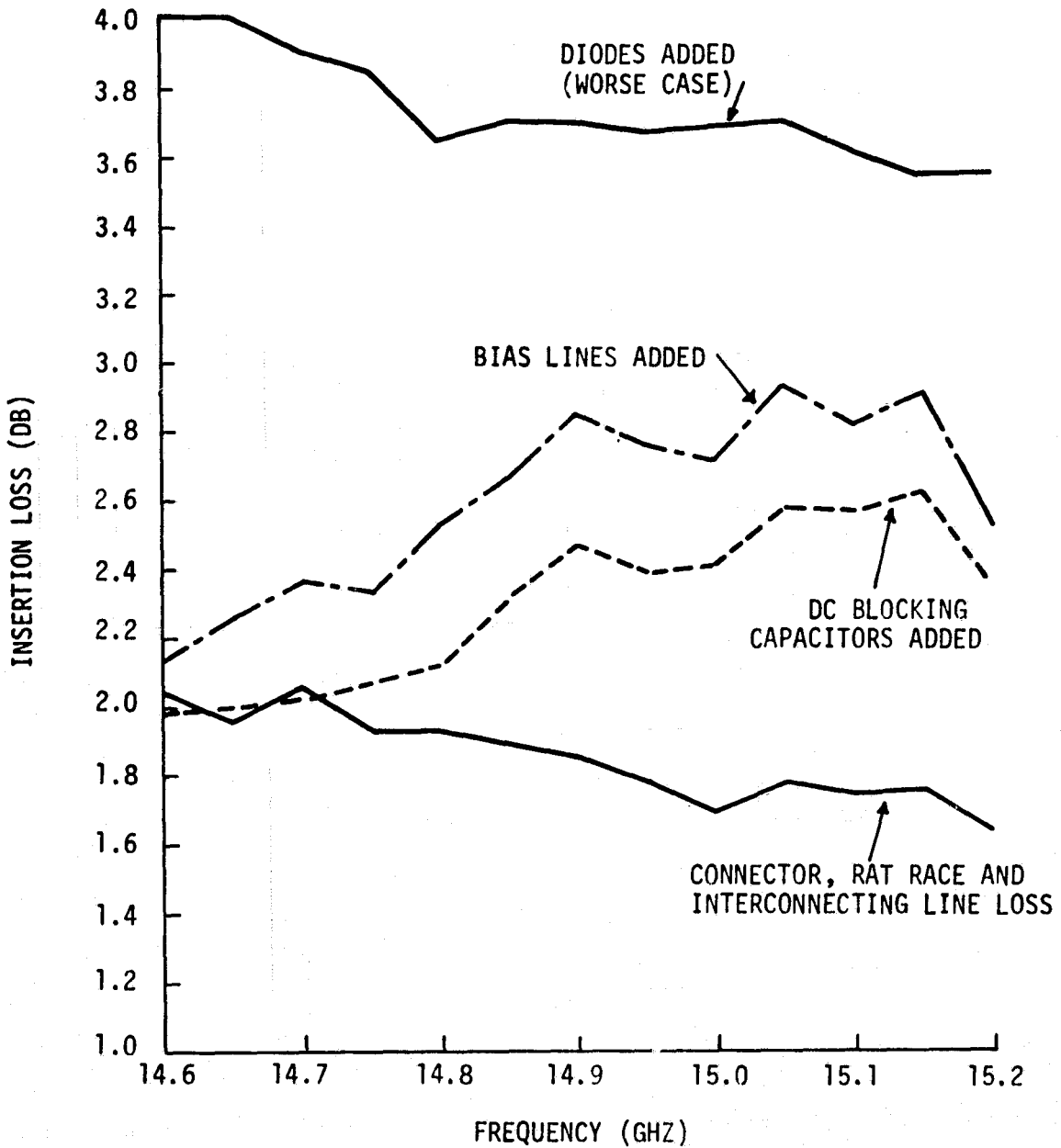Characteristics.

Figure 3-19. Measured Losses for Microstrip Ku-Band
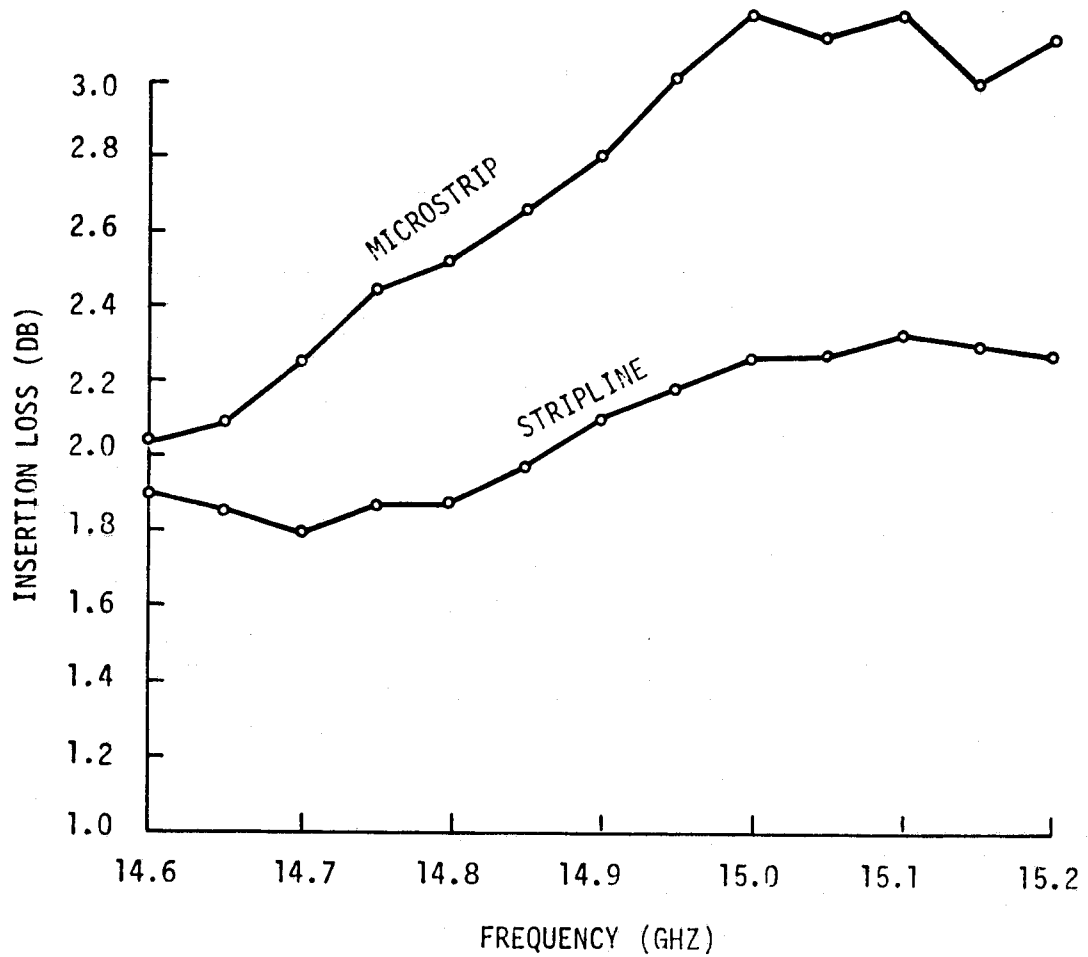3-Bit Phase Shifters.

Figure 3-20. Measured Cold Circuit Losses For Microstrip and Stripline
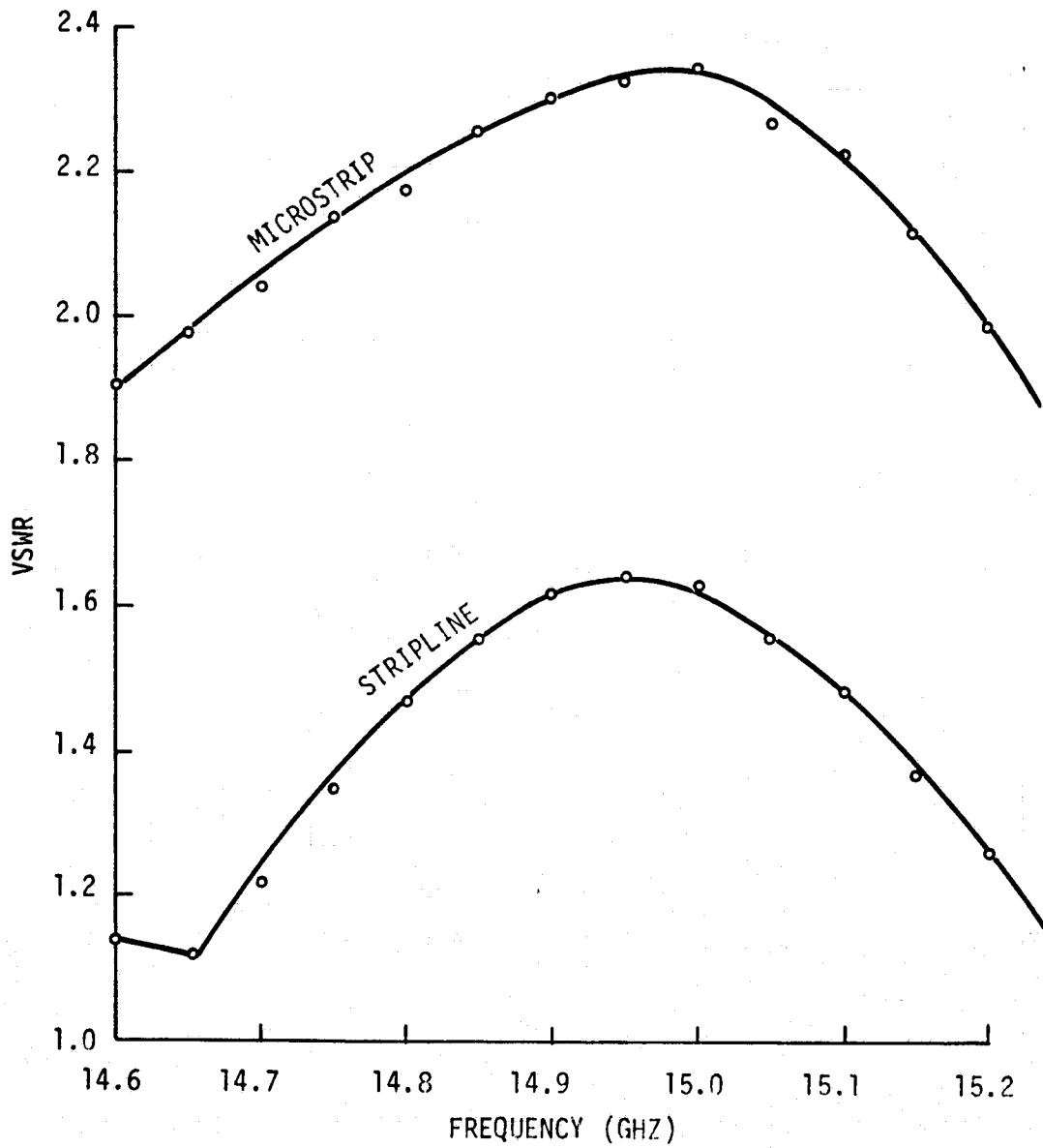Ku-Band 3-Bit Phase Shifters

Figure 3-21. Measured Cold Circuit VSWR For Microstrip And
Stripline Ku-Band 3-Bit Phase Shifters

SECTION IV

S-BAND ARRAY INTEGRATION AND EVALUATION

A.   ANTENNA SYSTEM INTEGRATION

Figure 4-1 shows the AESPA V S-band array configuration. All
elements shown in this figure were available from the last program phase except
the receiver monopulse comparator and the transmitter sum network. These
circuits were constructed using stripline rat-race hybrid couplers photo-
etched on 3M Company K-6098 copper clad laminate 1/16 inch thick. A single
sum beam is provided by the transmit combiner; while the receiver combiner
provides a sum beam, and both azimuth and elevation difference beams. The
hybrids used in these networks were evaluated and found to have a maximum
VSWR of 1.15, minimum isolation of 30 dB, and maximum coupling unbalance of
.15 dB in their required operating bands. The configuration of each network
is shown in Figures 4-2 and 4-3.

The biggest problem associated with the integration of the antenna
system was that of effecting the proper interface between the steering computer
and the remaining array elements. Evaluation of the system at the antenna
range facility was begun in January. The receive Σ pattern obtained at
boresight beam pointing direction was in good agreement with computer
predicted results, however attempts to steer the beam were not successful.
Troubleshooting of the array was accomplished by use of an open module that
was moved to various locations to determine if proper phase settings were
achieved. The measured phase settings were compared to the calculated
values for a given beam pointing direction that were supplied by an IBM 360
array analysis program (PLϕ1). The results of these tests that were made
after all interface problems were solved are shown in Figures 4-4 through
4-8. Figures 4-4 and 4-5 show calculated and measured transmit phase
settings for an azimuth scan angle of 60°. Figure 4-6 shows measure receive
settings for this angle. Figures 4-7 and 4-8 show measured receive
and transmit settings for an elevation scan angle of 60°. Most of the
problems encountered in this series of tests were found in the computer
software. With the software problems solved, a major hardware problem was
identified. Improper module phase settings were found to occur because of
cross-talk between clock lines connecting the array driver board and logic
manifolds. This problem was solved by shielding the clock lines. The
software developed for the system permits proper beam scanning in one quad-
rant (positive angles). This program is given in hexidecimal form in Table
4-1. An alternate form that permits scanning in four quadrants has not
been used to date and is shown in Table 4-2. A photograph of the complete
array system evaluated during this phase of the program is shown in Figure
4-9.

B.   ANTENNA SYSTEM EVALUATION
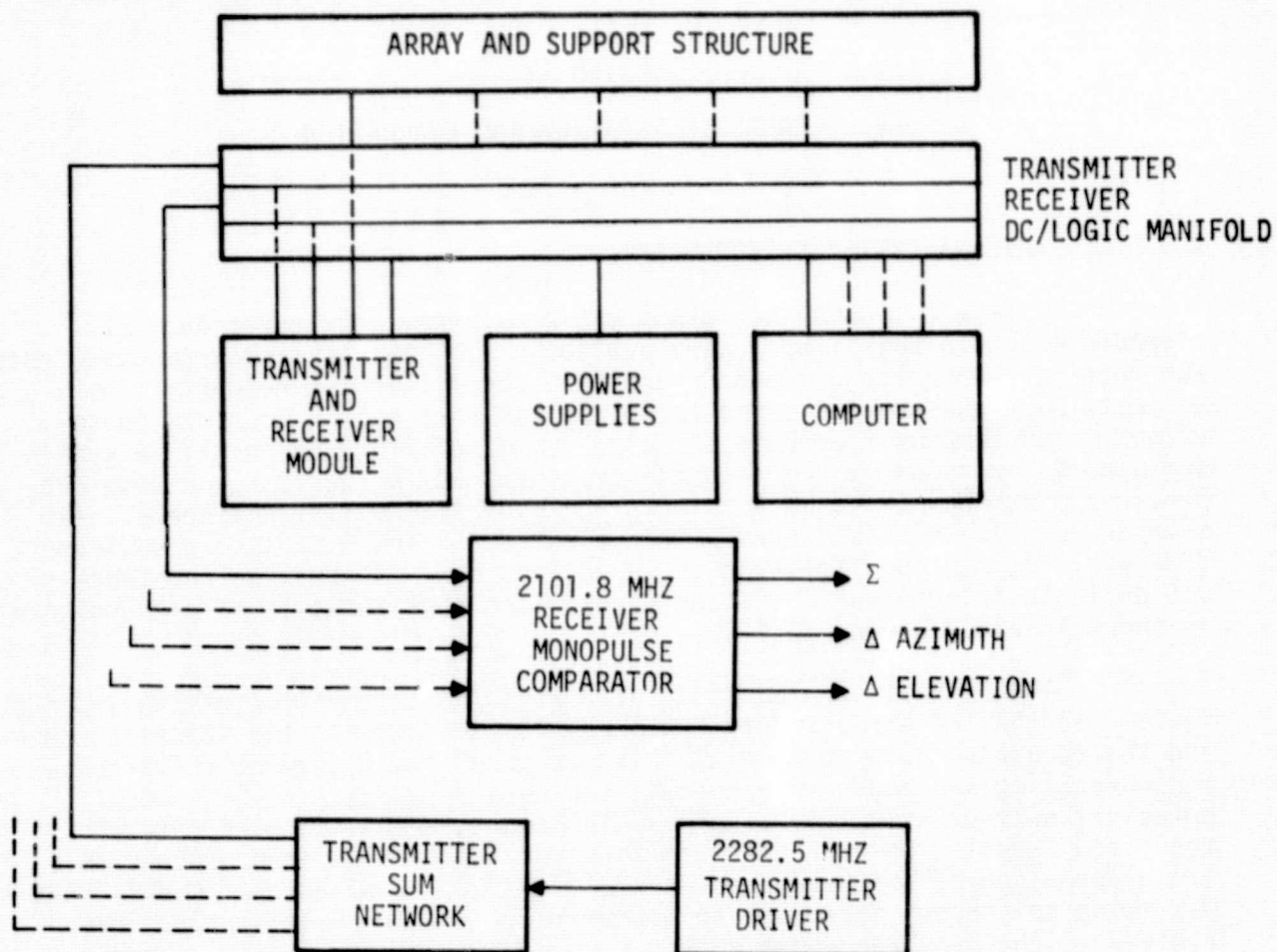
1.   Radiation Patterns

Equipment Group

4-1

Figure 4-1. AESPA V S-Band Array Configuration

ARRAY MANIFOLDS
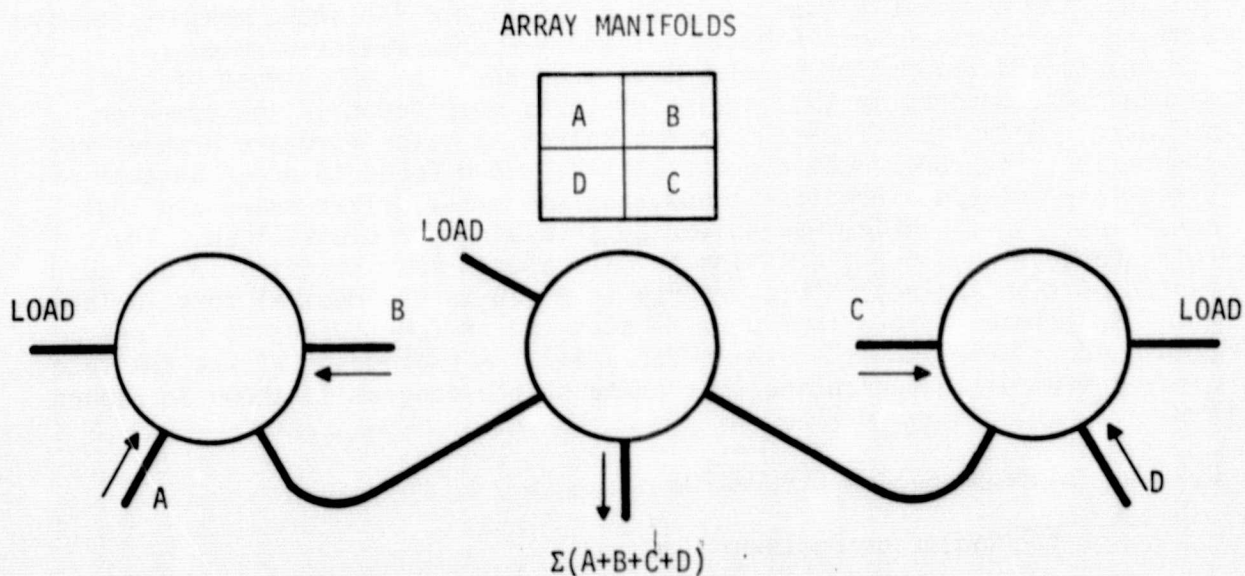
Figure 4-2. Transmitter Sum Network.

ARRAY MANIFOLDS

A	B
D	C

$\Delta(A-B)+(C-D)$

D

C

B

(A)

$\Delta(A+B)-(C+D)$

$\Sigma(A+B+C+D)$
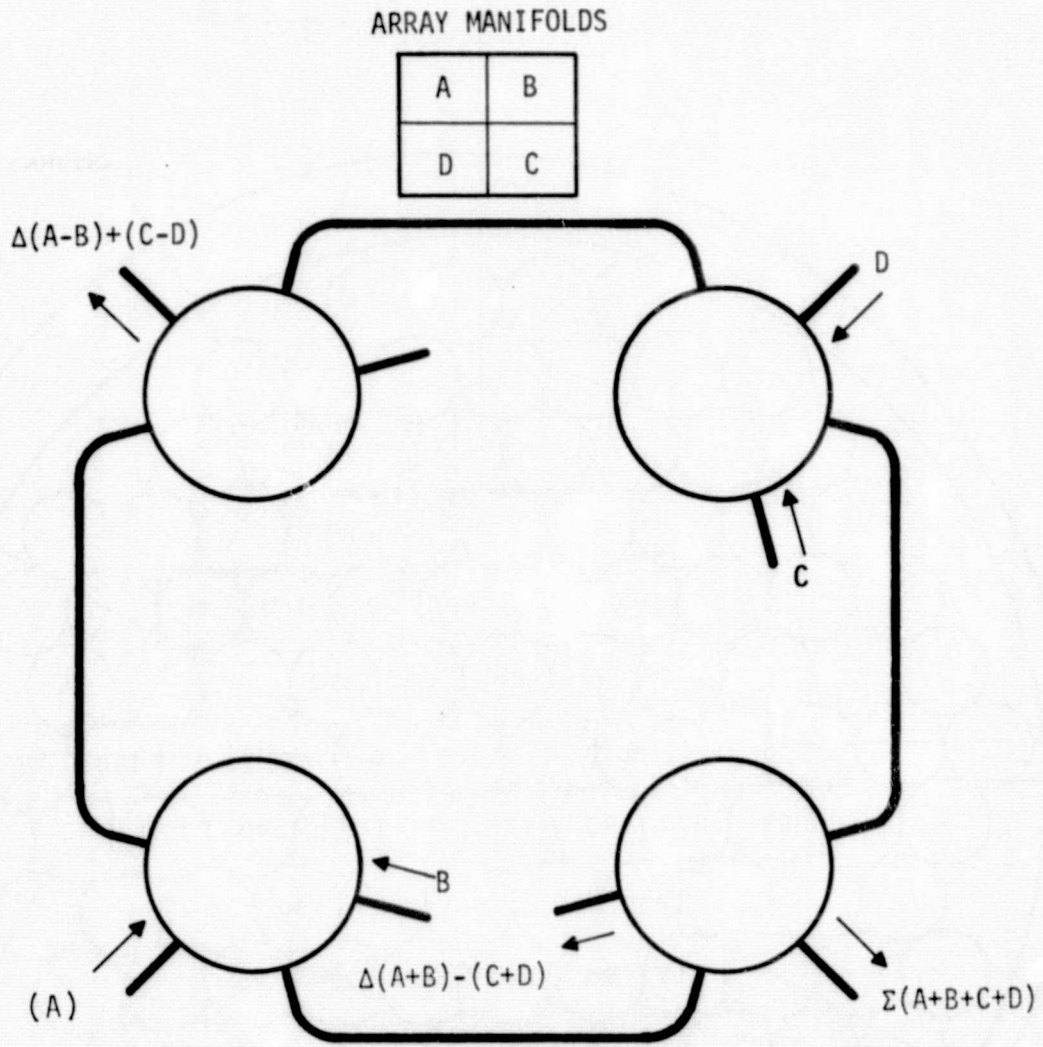
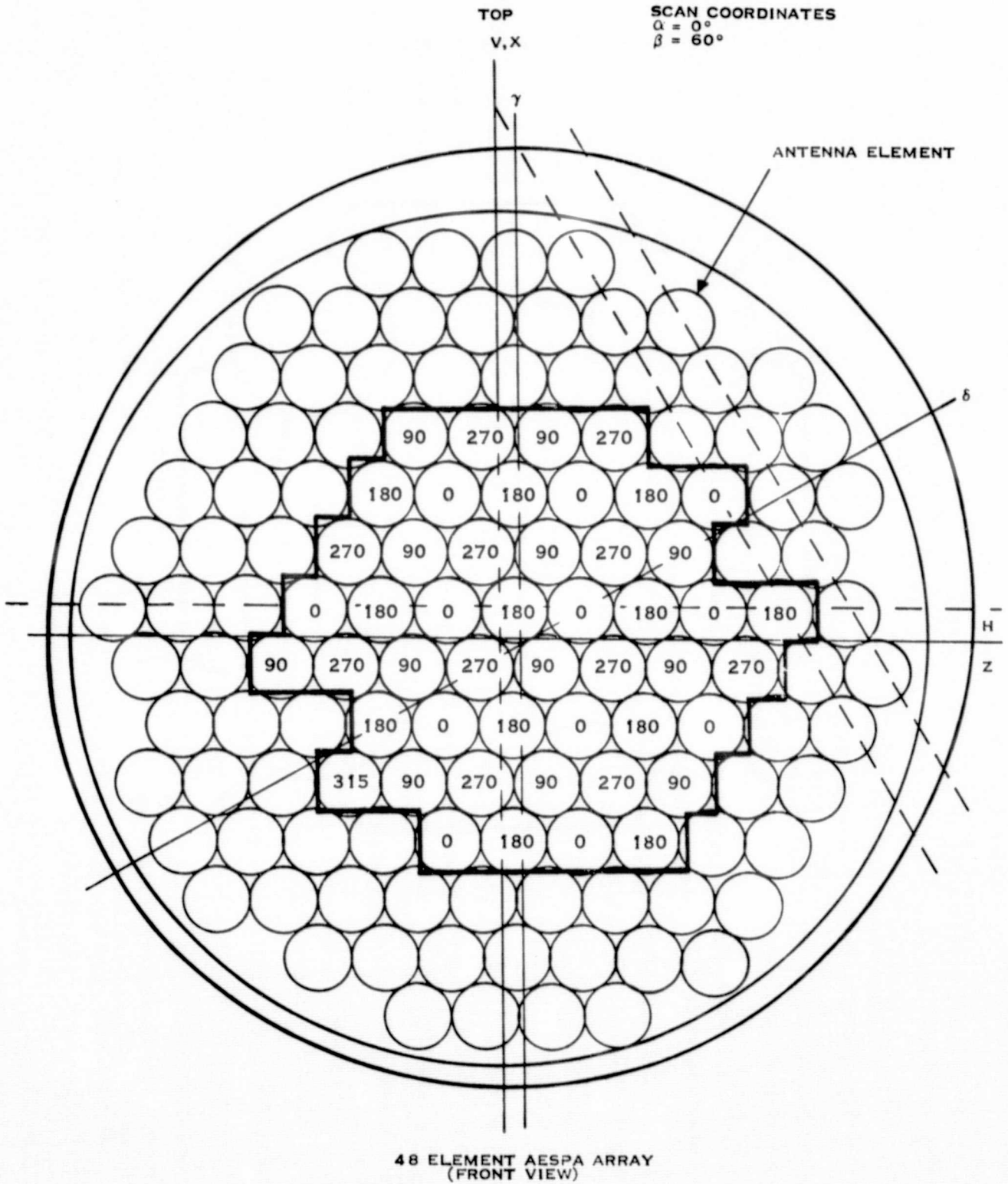Figure 4-3.   Receiver Monopulse Combiner.

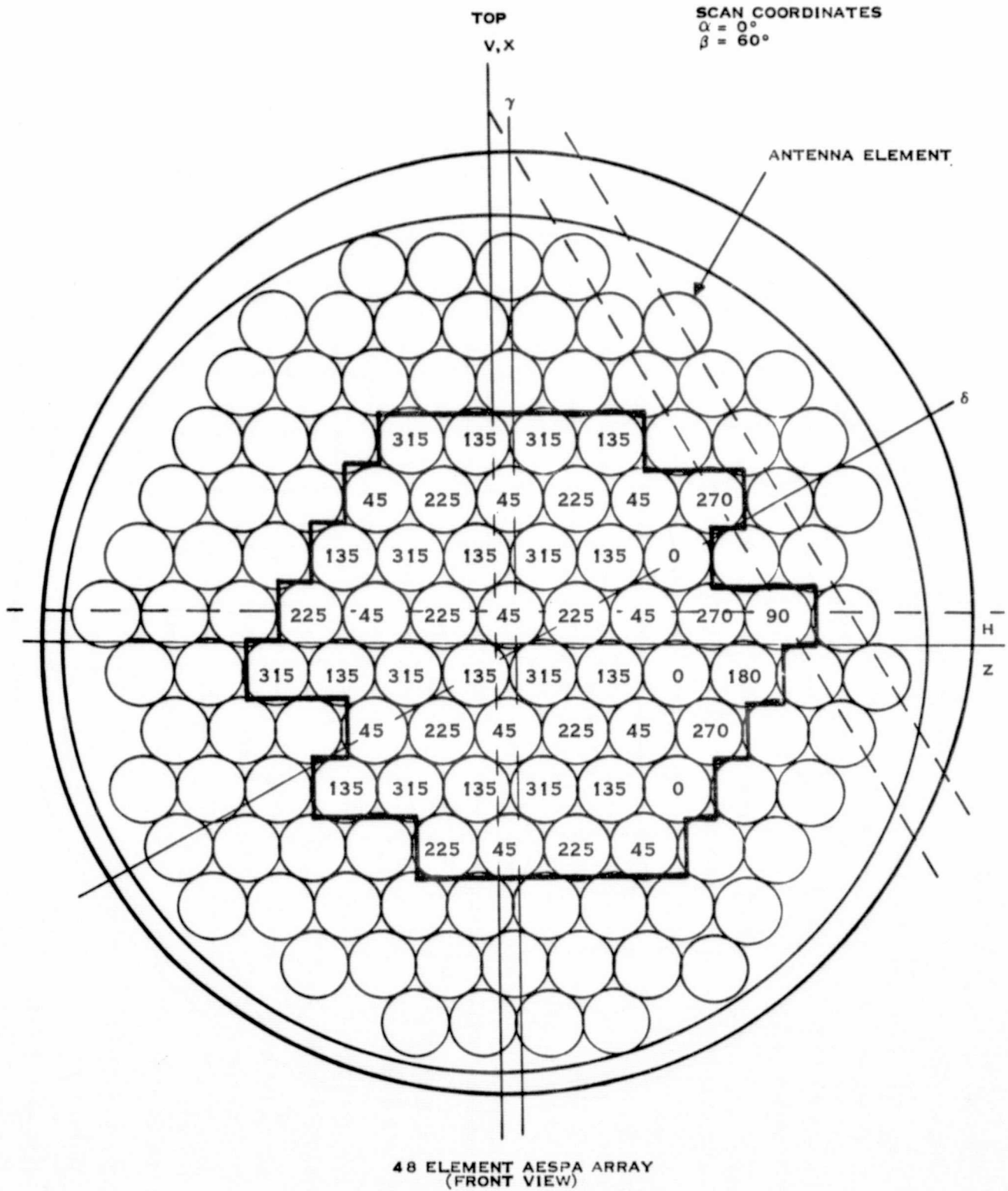Figure 4-4.   Calculated Transmitter Phase Shifter Settings.

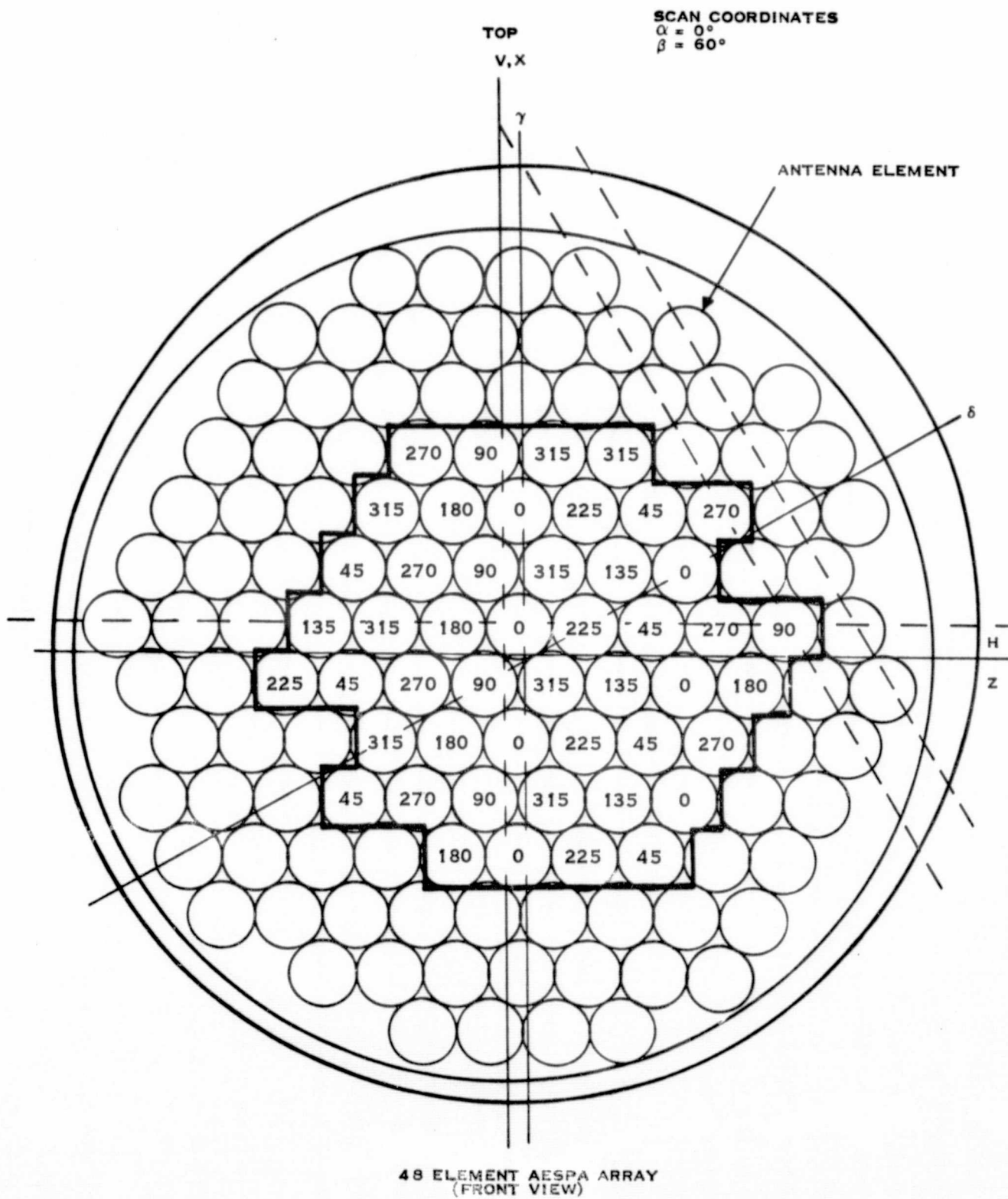Figure 4-5.   Measured Transmitter Phase Shifter Settings.

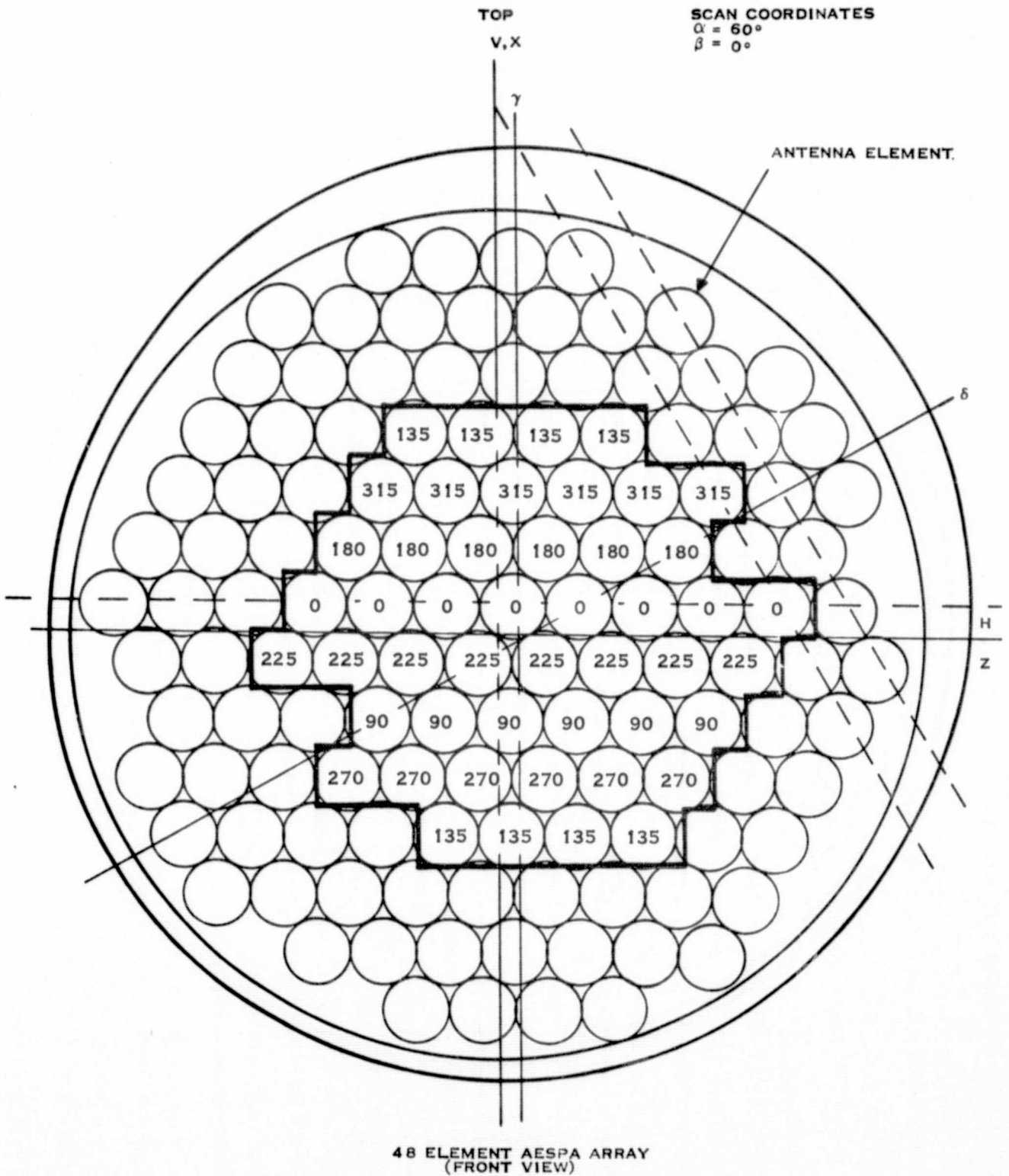Figure 4-6.   Measured Receiver Phase Shifter Settings.

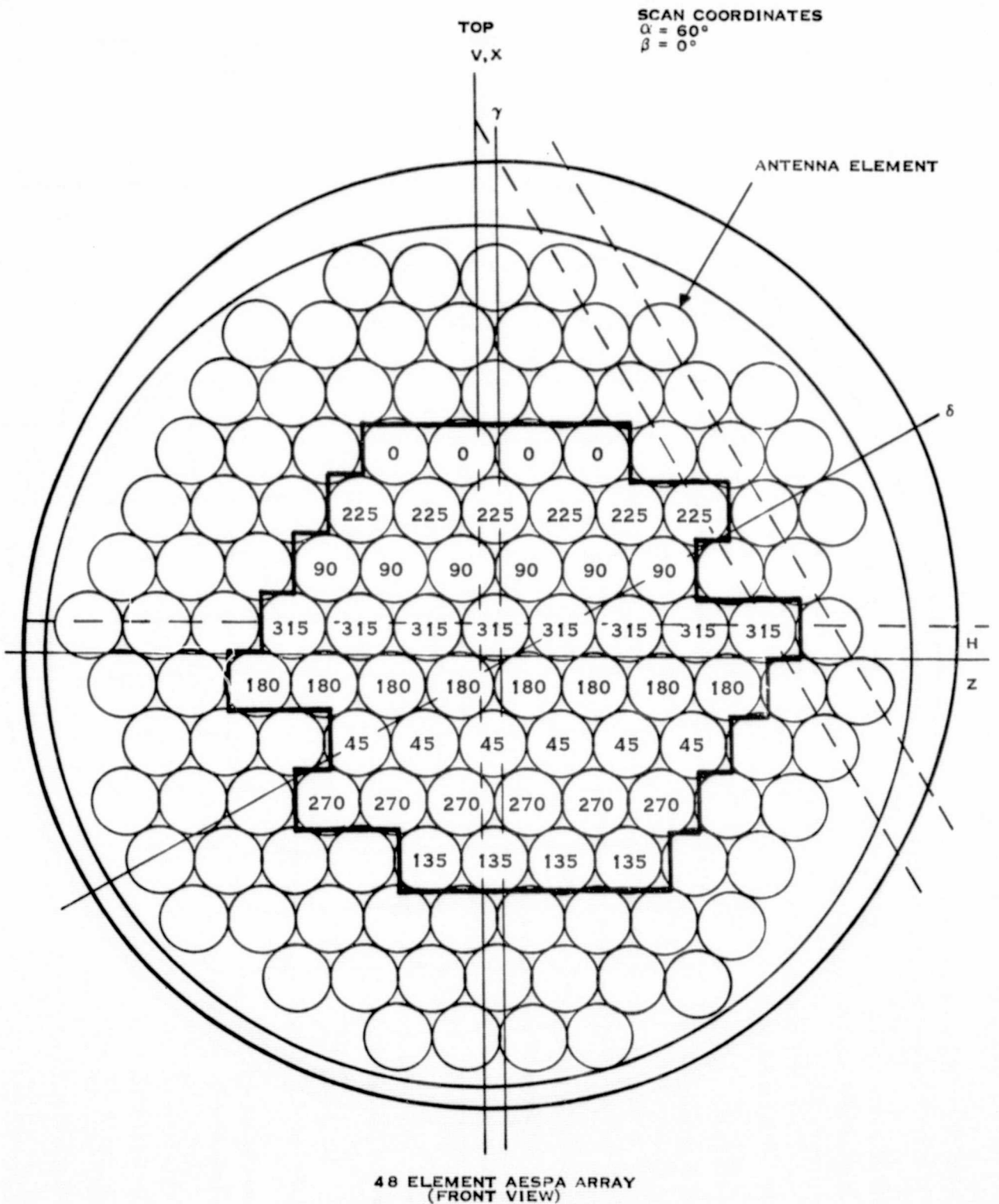Figure 4-7. Measured Transmitter Phase Shifter Settings.

Figure 4-8. Measured Receiver Phase Shifter Settings.

The coordinate systems used in the array evaluation are
shown in Figure 4-10. The plane of the array is shown in the X-Y plane,
with its top along the X-axis, and its boresight along the Z axis. A
beam pointing vector is shown with its projections in the three rectangular
coordinate planes indicated by the dotted vector representations. The
spherical coordinates θ and ϕ define beam pointing directions achieved by
mechanical positioning of the antenna. The coordinates α and β, measured
from the Z axis to the projections of the vector into the X-Z and Y-Z
planes respectively, define the electronic beam scanning coordinates. The
mathematical relationship between the two coordinate systems is given in
equations (1) and (2) below.

$$\beta = \sin^{-1} (\sin\theta \sin\phi) \tag{1}$$
$$\alpha = \cos^{-1} (\cos\theta /\cos\beta) \tag{2}$$

A simplified two dimensional representation of the array coordinate system
as viewed from the antenna rear is shown in Figure 4-11. Elevation beam
scanning is accomplished by varying the α coordinate, and azimuth beam
scanning is accomplished by varying the β coordinate. Angular values
are available over the 0-90° range in steps of 2.8° from the computer
table lookup memory. The desired values are entered in computer memory
location 26 for β and location 3F for α. The lookup table showing the
hexidecimal representation of the angular values is shown in Table 4-3.

Calculated radiation patterns were obtained at the transmit
frequency (2282.5 MHz) by use of a mathematical model of the array
constructed using IBM 360 Program PLØ1. These calculated patterns were
made using an assumed elemental power pattern distribution proportional
to cosine$^{3.7}$(θ). Amplitude and phase errors in the manifolds .nd modules
were assumed zero. Measured transmit azimuth patterns are shown compared
with this calculated pattern data in Figure 4-12. Shown are the unscanned
beam, and beams scanned to β angles of 20, 40, and 60 degrees. All re-
maining radiation patterns for the array are presented in Appendix A.
Table 4-4 provides a description of patterns presented therein. All
patterns were measured with a rotating linearly polarized source antenna
to provide an indication of axial ratio over the complete angular measurement
range.

2. Receiver Gain

A block diagram of the test set-up used to measure AESPA
receiver radiation patterns and gain is shown in Figure 4-13. The gain of
interest is that available at the AESPA array Σ-channel receiver terminals.
This gain was measured over the receiver frequency band for a beam steered
to mechanical boresight, and at a frequency of 2101.8 MHz for beams
steered to 20, 40, and 60 degrees in azimuth. The gain was measured by
comparing the AESPA output energy available at the peak of the beam, to
that available from a standard gain horn. A plot of measured gain
available from the antenna when steered to boresight is shown in Figure
4-14. Table 4-5 shows measured gain values obtained when the beam is
scanned in azimuth.

The coordinate systems used in the array evaluation are shown in Figure 4-10. The plane of the array is shown in the X-Y plane, with its top along the X-axis, and its boresight along the Z axis. A beam pointing vector is shown with its projections in the three rectangular coordinate planes indicated by the dotted vector representations. The spherical coordinates θ and ϕ define beam pointing directions achieved by mechanical positioning of the antenna. The coordinates α and β, measured from the Z axis to the projections of the vector into the X-Z and Y-Z planes respectively, define the electronic beam scanning coordinates. The mathematical relationship between the two coordinate systems is given in equations (1) and (2) below.

$$\beta = \sin^{-1} (\sin\theta \sin\phi) \tag{1}$$
$$\alpha = \cos^{-1} (\cos\theta /\cos\beta) \tag{2}$$

A simplified two dimensional representation of the array coordinate system as viewed from the antenna rear is shown in Figure 4-11. Elevation beam scanning is accomplished by varying the α coordinate, and azimuth beam scanning is accomplished by varying the β coordinate. Angular values are available over the 0-90° range in steps of 2.8° from the computer table lookup memory. The desired values are entered in computer memory location 26 for β and location 3F for α. The lookup table showing the hexidecimal representation of the angular values is shown in Table 4-3.

Calculated radiation patterns were obtained at the transmit frequency (2282.5 MHz) by use of a mathematical model of the array constructed using IBM 360 Program PLϕ1. These calculated patterns were made using an assumed elemental power pattern distribution proportional to cosine$^{3.7}$(θ). Amplitude and phase errors in the manifolds and modules were assumed zero. Measured transmit azimuth patterns are shown compared with this calculated pattern data in Figure 4-12. Shown are the unscanned beam, and beams scanned to β angles of 20, 40, and 60 degrees. All remaining radiation patterns for the array are presented in Appendix A. Table 4-4 provides a description of patterns presented therein. All patterns were measured with a rotating linearly polarized source antenna to provide an indication of axial ratio over the complete angular measurement range.

2.   Receiver Gain

A block diagram of the test set-up used to measure AESPA receiver radiation patterns and gain is shown in Figure 4-13. The gain of interest is that available at the AESPA array Σ-channel receiver terminals. This gain was measured over the receiver frequency band for a beam steered to mechanical boresight, and at a frequency of 2101.8 MHz for beams steered to 20, 40, and 60 degrees in azimuth. The gain was measured by comparing the AESPA output energy available at the peak of the beam, to that available from a standard gain horn. A plot of measured gain available from the antenna when steered to boresight is shown in Figure 4-14. Table 4-5 shows measured gain values obtained when the beam is scanned in azimuth.

TABLE 4-1

AESPA COMPUTER SOFTWARE FOR (+) ANGLES ONLY

DISTRIBUTE		PROGRAM		TX			
000	737	016	726	030	425	060	520
1	401	017	480	31	62A	61	561
2	622	018	563	32	440	62	B40
3	400	019	C40	33	628	63	621
4	624	1A	21E	34	402	64	520
5	524	1B	E50	35	627	65	A00
6	SE0	1C	663	36	4XX(β)	66	620
7	A30	1D	10D	37	600	67	100
8	6E4	1E	480	38	570		
9	401	1F	562	39	5AA		
A	623	020	C40	3A	D60	RX	
B	400	21	225	3B	6A0	050	422
C	625	22	E50	3C	800	51	62A
D	525	23	662	3D	600	52	43B
E	561	24	105	3E	570	53	62B
F	A10	25	400	3F	4XX(α)	54	401
10	665	26	622	040	600	55	627
11	AD0	27	623	41	530	56	136
12	E50	28	702	42	D10		
13	666	29	713	43	528		
14	702	02A	000	44	D10		
15	713			45	661		
				46	160		

TABLE 4-2

AESPA COMPUTER SOFTWARE FOR (±) ANGLES

DISTRIBUTE		PROGRAM		TX					
000	737	016	726	030	425	047	6A0	060	520
1	401	17	480	31	62A	48	800	61	561
2	622	18	563	32	440	49	600	62	B40
3	400	19	C40	33	62B	4A	570	63	621
4	624	1A	21E	34	402	4B	4XX(α)	64	520
5	524	1B	E50	35	627	4C	629	65	A00
6	5E0	1C	663	36	401	4D	251	66	620
7	A30	1D	10D	37	930	4E	351	67	100
8	6E4	1E	480	38	4XX(β)	4F	800		
9	401	1F	562	39	628	050	AC0		
A	623	020	C40	3A	23E	51	600	RX	
B	400	21	225	3B	33E	52	530	070	422
C	562	22	E50	3C	800	53	D10	71	62A
D	525	23	662	3D	AC0	54	52B	72	43B
E	561	24	105	3E	600	55	D10	73	62B
F	A10	25	400	3F	570	56	529	74	401
10	665	26	622	040	5AA	57	25B	75	627
11	AD0	27	623	41	D60	58	35B	76	136
12	E50	28	702	42	568	59	850		
13	666	29	713	43	247	5A	AD0		
14	702	02A	000	44	347	5B	661		
15	713			45	8A0	5C	160		
				46	AE0				
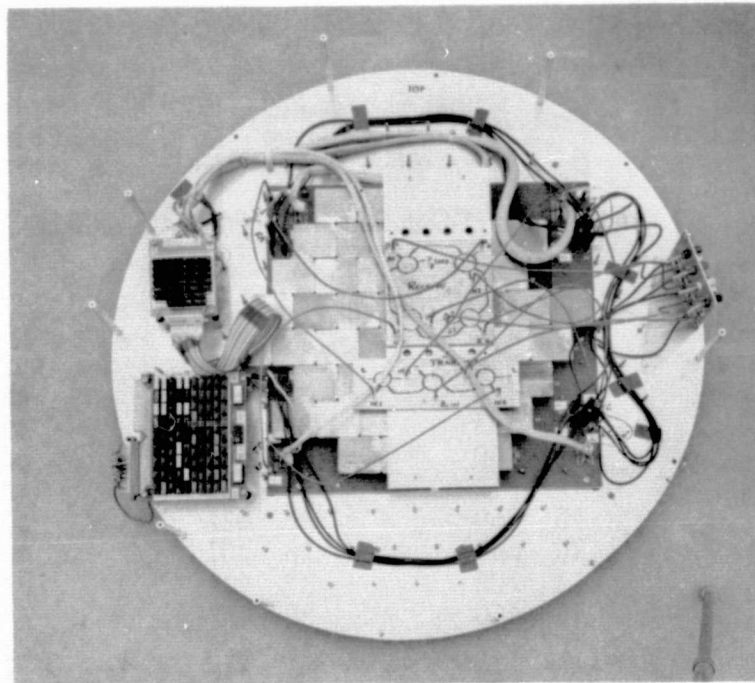
Figure 4-9.   AESPA V Antenna Array Assembly.
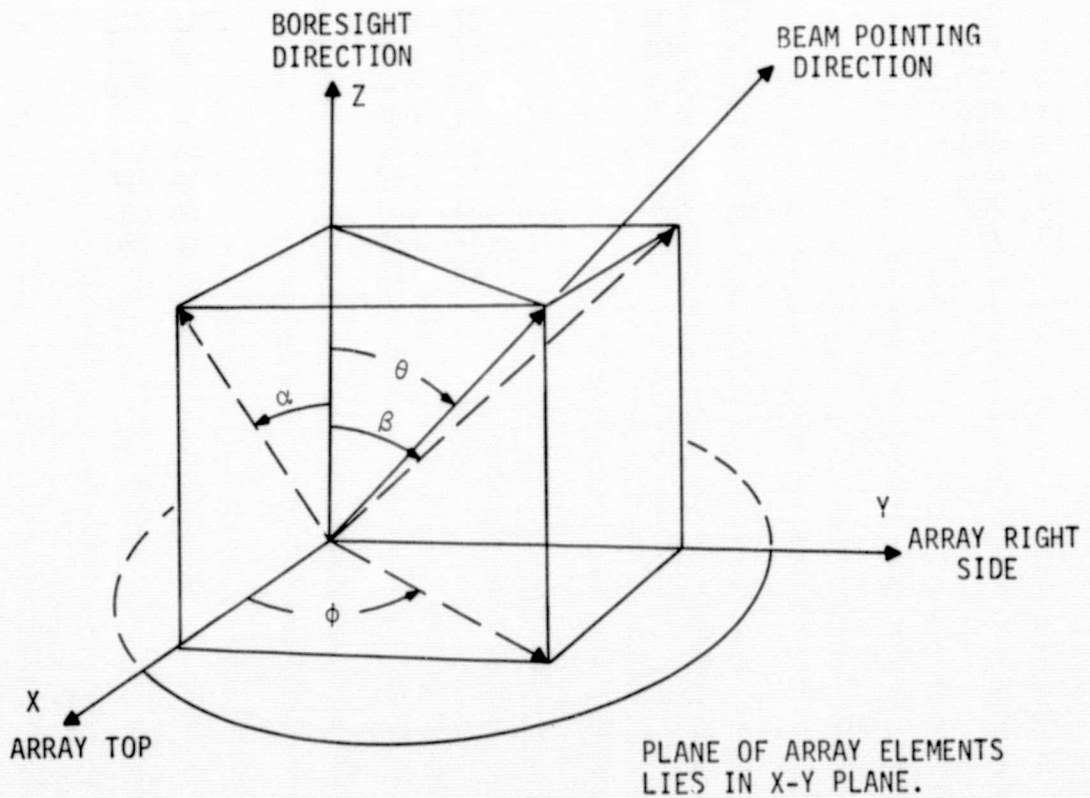
Figure 4-10.   Coordinates Utilized for AESPA
Antenna System Evaluation.

TABLE 4-3.

ELECTRONIC SCAN ANGLES AVAILABLE AND THEIR
HEXIDECIMAL COMPUTER ENTRY REPRESENTATIONS

Hexidecimal Computer Entry	Scan Angle	Hexidecimal Computer Entry	Scan Angle
00	0	13	53.4
01	2.81	14	56.3
2	5.63	15	59.1
3	8.44	16	61.9
4	11.25	17	64.7
5	14.06	18	67.5
6	16.88	19	70.3
7	19.69	1A	73.1
8	22.5	1B	75.9
9	25.3	1C	78.8
A	28.1	1D	81.6
B	30.9	1E	84.4
C	33.8	1F	87.2
D	36.6		
E	39.4		
F	42.2		
10	45.0		
11	47.8		
12	50.6		

ARRAY TOP

X-Y PLANE, ARRAY REAR VIEW
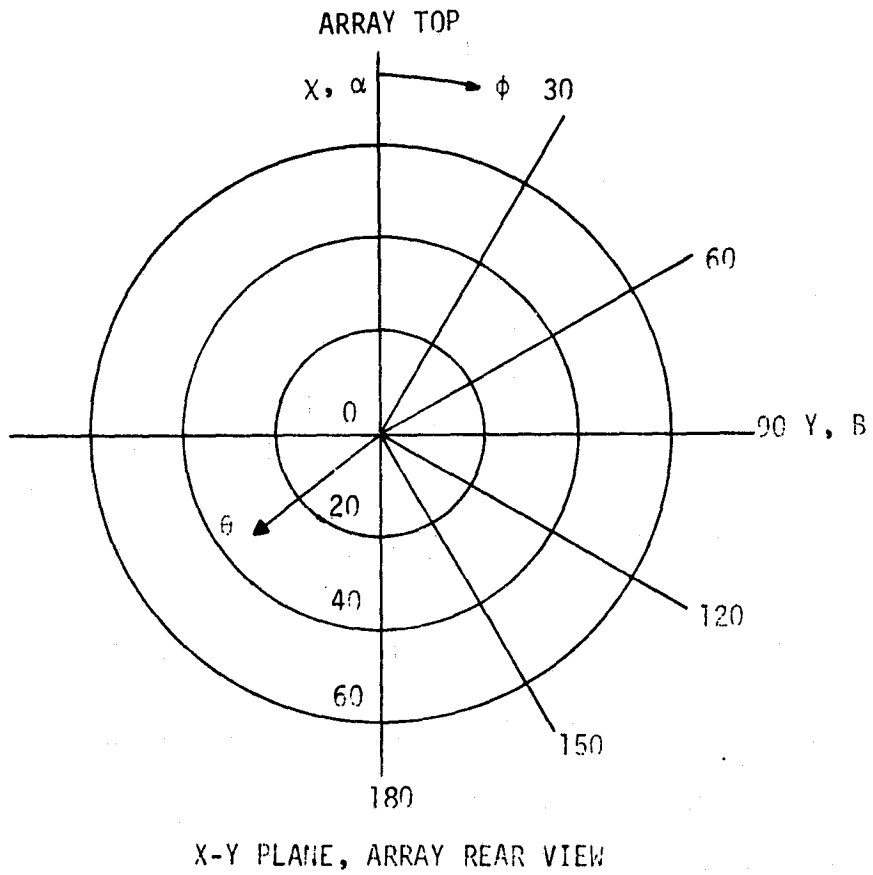
Figure 4-11. Two Dimensional Representation of Array Coordinate System.
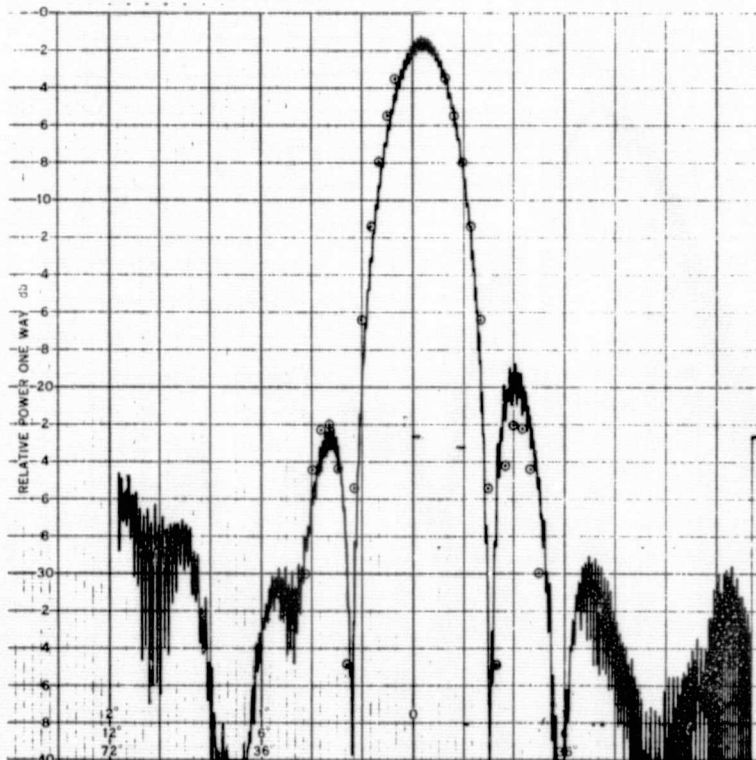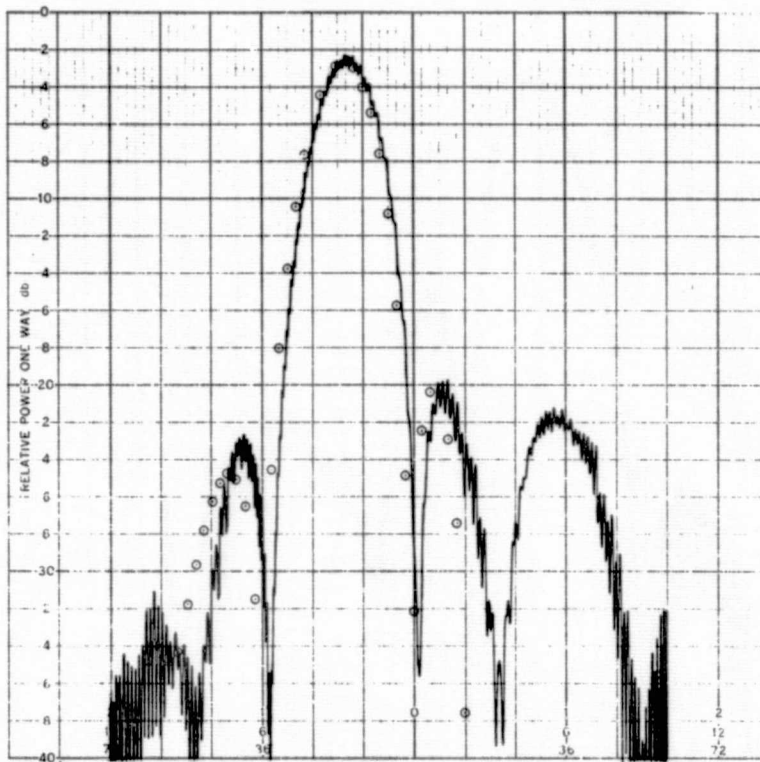
Figure 12.   AESPA Array Transmitter Azimuth Radiation Patterns For Scan
Angles of 0°, 20°, 40°, and 60°
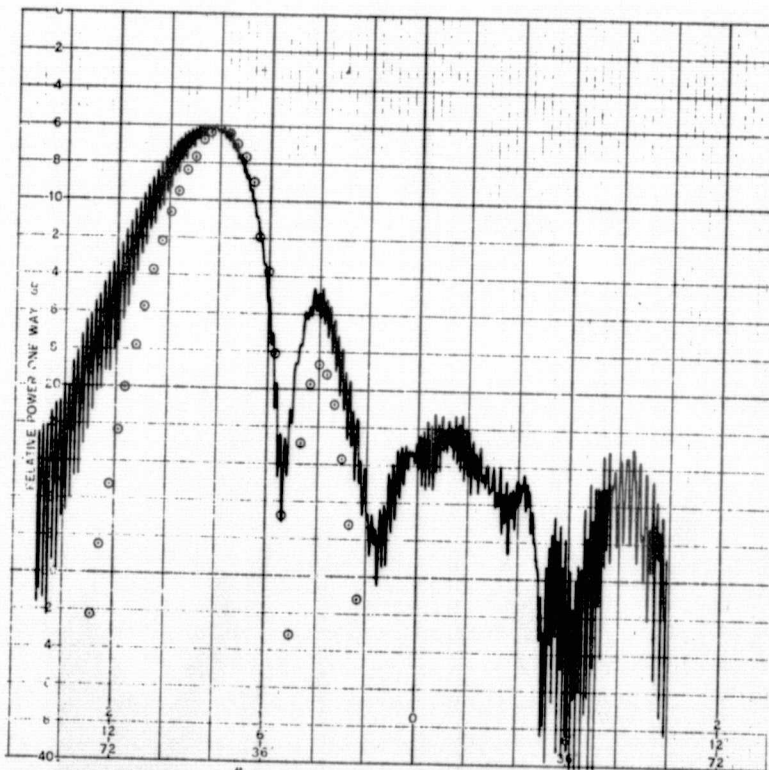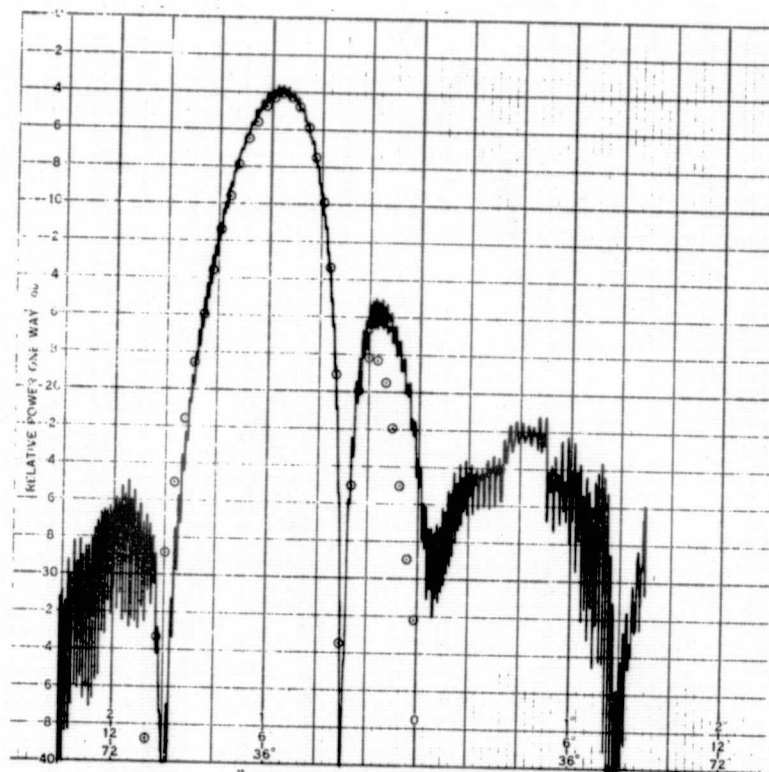
Figure 12. Continued

Table 4-4. Array Pattern Data
Shown in Appendix-A

Figure	Θ	φ	α	β	Description
A-1	Variable	0	0 20 40 60	0	Σ Transmitter Elevation
A-2		90	0	0 20 40 60	Σ Receiver Azimuth
A-3		0	0 20 40 60	0	Σ Receiver Elevation
A-4		30 60	17.5 36 56.3 11.25 22.5 40.9	9.85 18.7 25.7 16.88 33.8 48.6	Σ Receiver Scan Angles Not Coincident With Azimuth Or Elevation Axis.
A-5		90	0	0 40	Receive Σ and Δ in Azimuth
		0	0 40	0 0	Receive Σ and Δ in Elevation
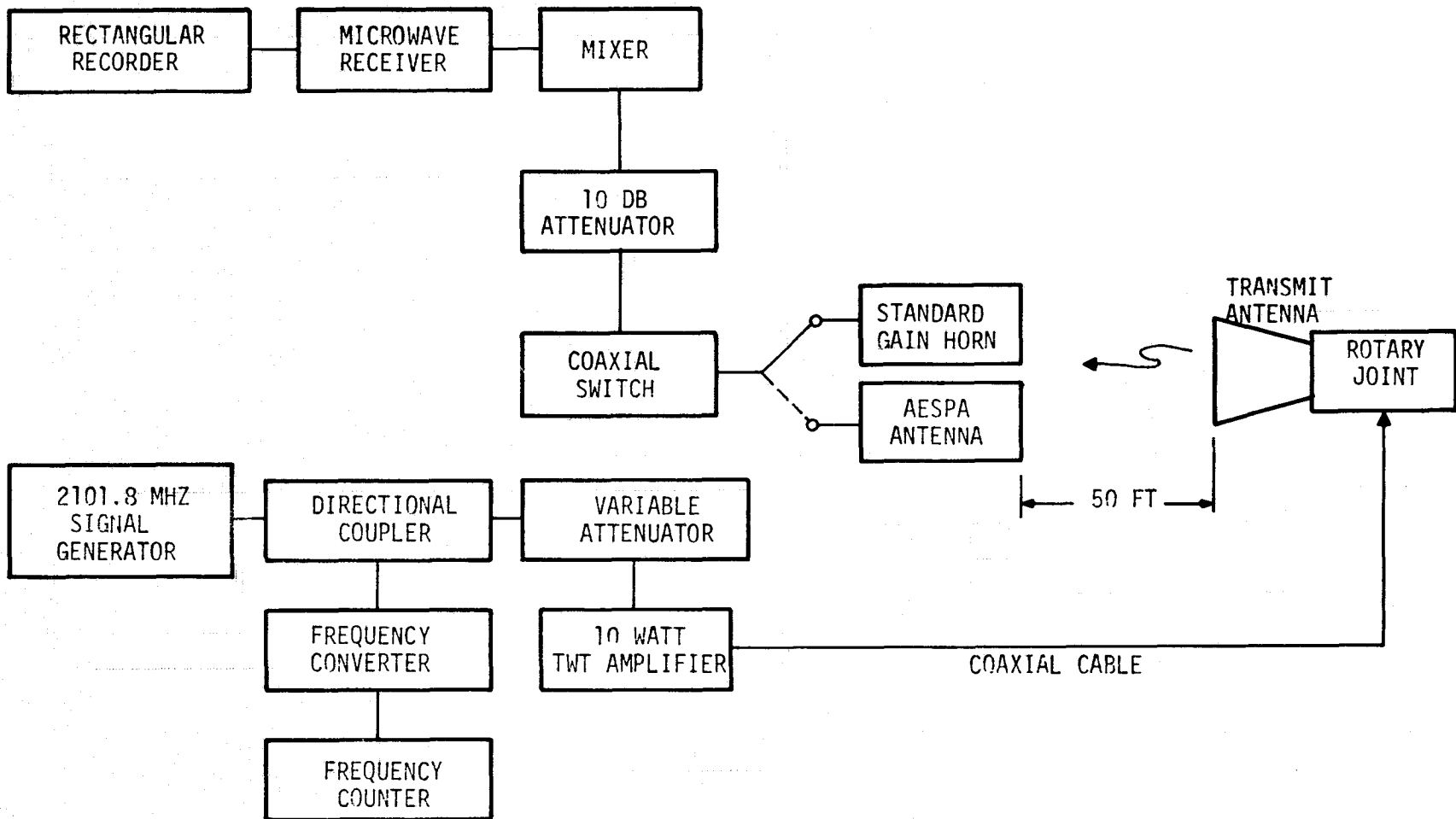
Figure 4-13. Block Diagrams of Receiver Radiation Pattern
And Gain Test Set-Up.

RECEIVER Σ CHANNEL STEERED TO
MECHANICAL BORESIGHT
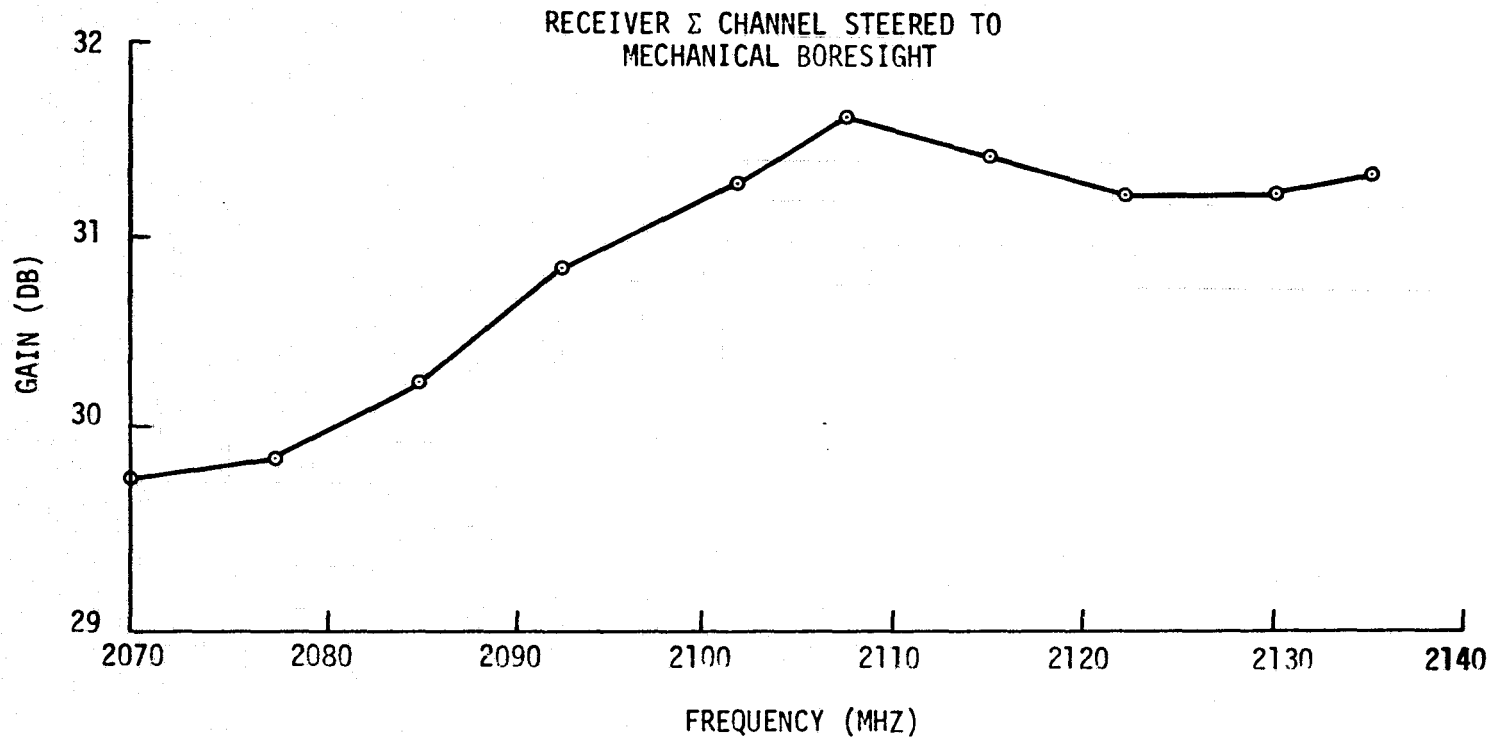
Figure 4-14. AESPA Antenna System Gain Relative to
Circular Isotropic Radiator

TABLE 4-5. MEASURED RECEIVER Σ CHANNEL GAIN AT 2101.8 MHz AS A FUNCTION OF AZIMUTH ELECTRONIC SCAN ANGLE

GAIN (dB)	β (AZIMUTH SCAN ANGLE)
31.35	0
30.35	20
28.55	40
26.35	60

A calculated value of the gain at 2101.8 GHz is obtained for comparison with the measured value below. The elements contributing to the gain are the array factor, T/R module gain, and array element gain (See Table 4-6). The array factor was computed by the PLφ1 Program, the module gain was determined from results of the last program phase, and the spiral element gain was determined during the array evaluation program. The elements contributing to array losses include the monopulse combiner, the manifolds, and the connecting cables and connectors. The combiner and manifold losses were measured, and the cable and connector losses were estimated.

TABLE 4-6. CALCULATED AESPA RECEIVER GAIN

GAIN (dB)	CONTRIBUTOR
16.8	Array Factor
18.9	T/R Module
1.4	Spiral Array Element
37.1	

LOSS (dB)	CONTRIBUTOR
1.4	Monopulse Comparator
1.1	Manifolds
1.0	Cables and Connectors
3.5	

Total Claculated Gain = 37.1 - 3.5 = 33.6 dB
Total Measured Gain = 31.4 dB
Gain Difference = 2.2 dB

3. Transmitter Gain and EIRP

A block diagram of the test set-up used to measure AESPA transmitter radiation patterns, gain, and EIRP is shown in Figure 4-15. The gain relative to circular isotropic was measured at 2282.5 MHz for beams steered to azimuth angles of 0, 20, 40, and 60 degrees. The measured results are listed in Table 4-7.
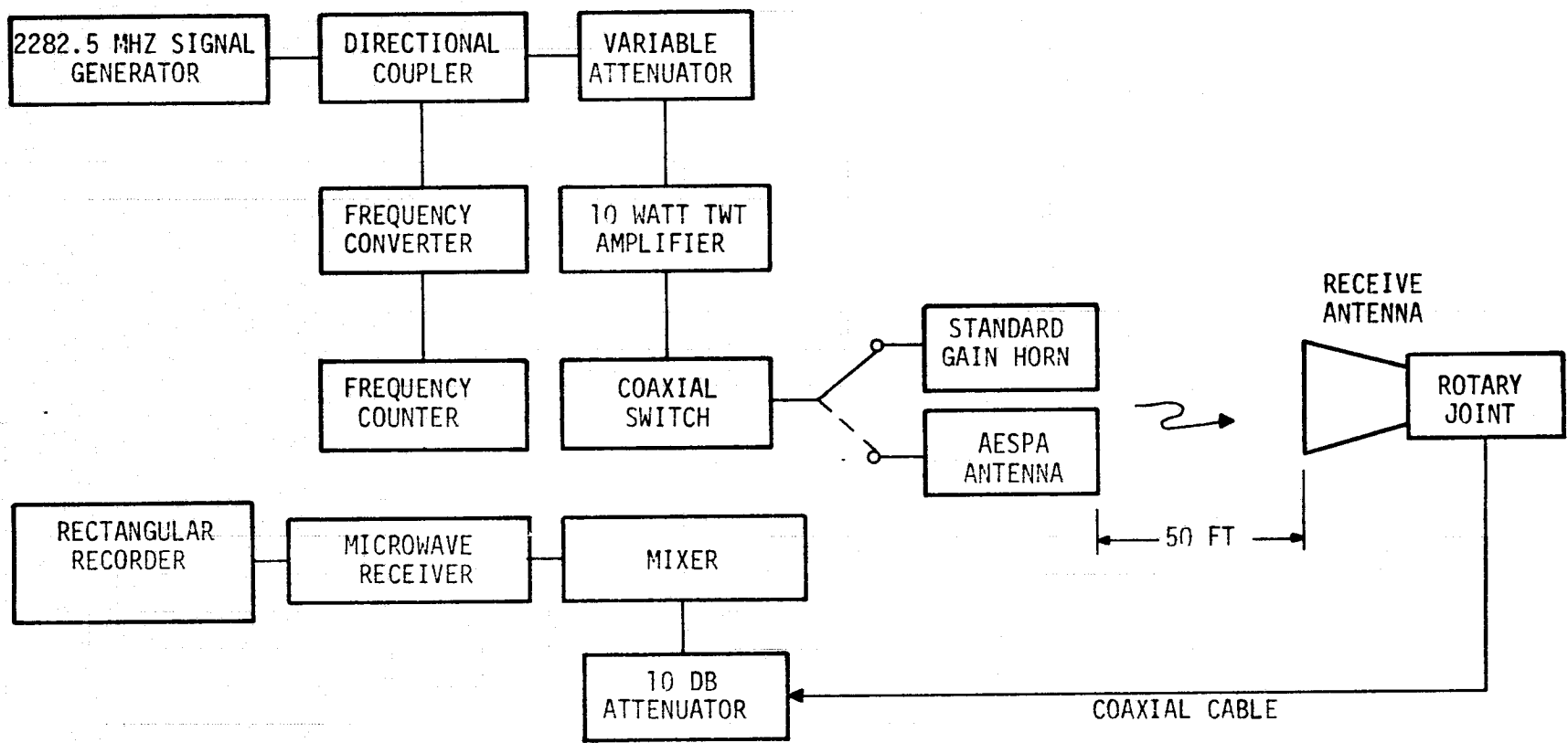
Equipment Group

```
┌──────────────────┐   ┌──────────────┐   ┌──────────────┐
│ 2282.5 MHZ SIGNAL│───│ DIRECTIONAL  │───│ VARIABLE     │
│ GENERATOR        │   │ COUPLER      │   │ ATTENUATOR   │
└──────────────────┘   └──────────────┘   └──────────────┘
                              │                   │
                       ┌──────────────┐   ┌──────────────┐
                       │ FREQUENCY    │   │ 10 WATT TWT  │
                       │ CONVERTER    │   │ AMPLIFIER    │
                       └──────────────┘   └──────────────┘
                              │                   │
                       ┌──────────────┐   ┌──────────────┐      ┌──────────────┐
                       │ FREQUENCY    │   │ COAXIAL      │──────│ STANDARD     │
                       │ COUNTER      │   │ SWITCH       │      │ GAIN HORN    │
                       └──────────────┘   └──────────────┘      └──────────────┘
                                                                ┌──────────────┐
                                                                │ AESPA        │
                                                                │ ANTENNA      │
                                                                └──────────────┘
┌──────────────┐   ┌──────────────┐   ┌──────────────┐
│ RECTANGULAR  │───│ MICROWAVE    │───│ MIXER        │
│ RECORDER     │   │ RECEIVER     │   │              │
└──────────────┘   └──────────────┘   └──────────────┘
                                              │
                                       ┌──────────────┐
                                       │ 10 DB        │
                                       │ ATTENUATOR   │
                                       └──────────────┘
```

RECEIVE ANTENNA

ROTARY JOINT

|←— 50 FT —→|

COAXIAL CABLE

Figure 4-15.   Block Diagram of Transmitter Radiation Pattern,
Gain, and EIRP Test Set-up

TABLE 4-7. MEASURED TRANSMITTER GAIN AT
2282.5 MHz AS A FUNCTION OF AZIMUTH ELECTRONIC SCAN ANGLE

GAIN (dB)	β(AZIMUTH SCAN ANGLE) In Degrees
31.85	0
31.20	20
29.80	40
27.40	60

The transmitter calculated gain for 0 degree azimuth scan is determined for comparison with the measured value in Table 4-8.

TABLE 4-8. CALCULATED AESPA TRANSMITTER GAIN

GAIN (dB)	CONTRIBUTOR
16.8	Array Factor
16.0	T/R Module
1.4	Spiral Element
34.2	

LOSS (dB)	CONTRIBUTOR
0.4	Monopulse Comparator
1.1	Manifolds
1.0	Cables and Connectors
2.5	

Total Calculated Gain = 34.2 -2.5 = 31.7 dB
Total Measured Gain =   31.85 dB
Difference   .15 dB

The drive power required to "turn-on" the individual module transmitters was determined during the last program phase to be 25 milliwatts. Using the loss estimate of Table 4-8, the total RF power required to drive the array should be 2.5 dB above (25 milliwatts/module x 48 modules) or 2.13 watts. An actual power input of 2.5 watts was found to be satisfactory. With this power applied, the total antenna system was found to require 7 amps from the 18 volt supply and 6 amps from the 5 volt supply.

The EIRP is then 31.85 dB above 2.5 watts or 35.85 dBW.

4. Dynamic Steering Effects

A block diagram of the test set-up used for measurement of dynamic steering effects is shown in Figure 4-16. The purpose of this test is to determine the effect on received signal amplitude and phase caused by

Equipment Group
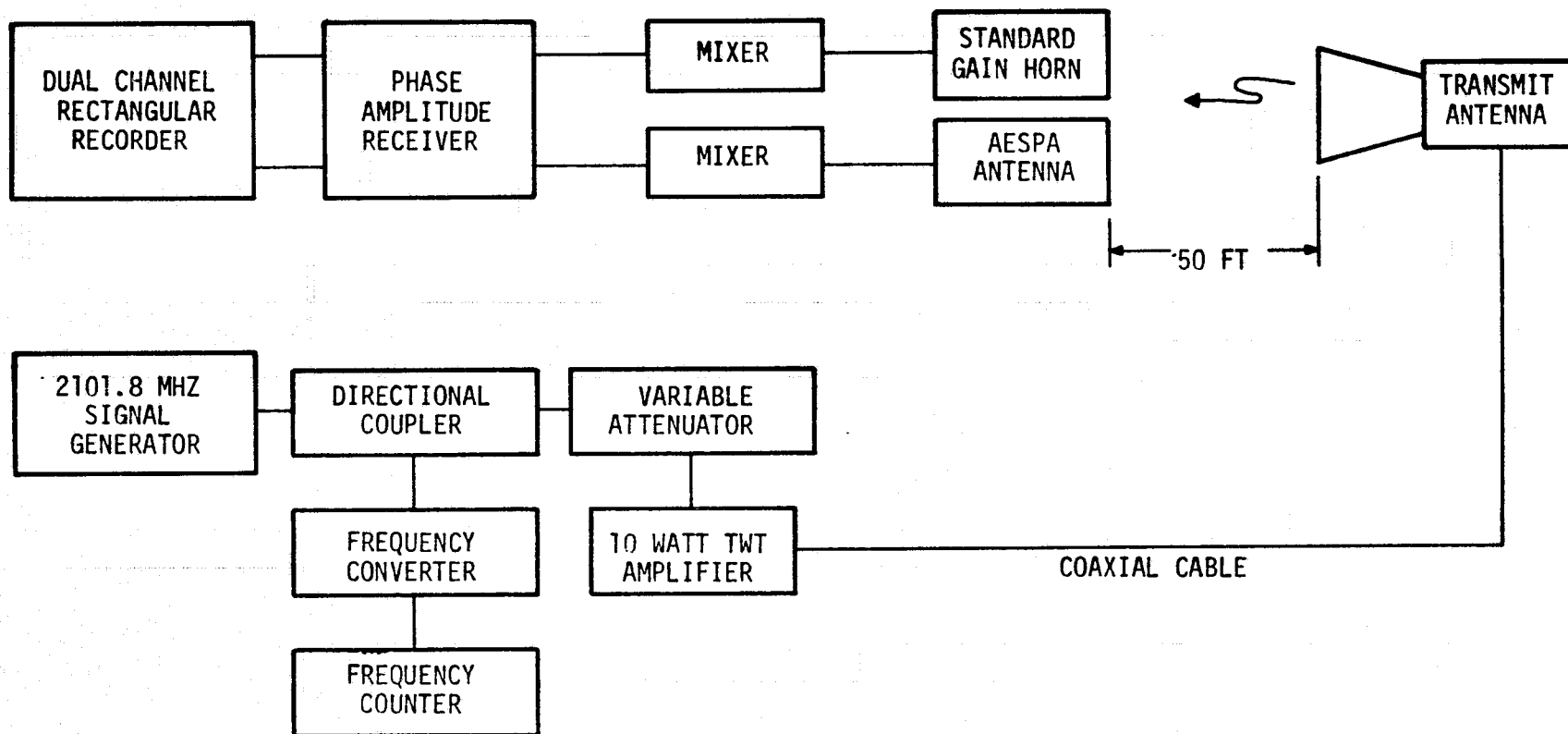
Figure 4-16. Block Diagram of Test Set-up For Determining
Beam Steering Effects

electronic steering of the beam by the minimum increment of 2.8°. The test was performed for a beam steered at mechanical boresight, and for a beam steered near an azimuth angle of 40°. A dual channel rectangular recorder and phase/amplitude receiver were utilized to permit simultaneous recording of phase and amplitude variations. Figure 4-17 shows the results obtained near boresight and Figure 4-18 shows the results near 40°. The amplitude variation is seen to reach a minimum value in both tests as beam cross-over is reached. The phase variation is seen to have a value of approximately 6° for the boresight scan case and 16° for the 40° scan case. Because the phase variation at 40° scan was greater than had been anticipated, it was felt that the nature of the variation should be more fully determined. This could best be accomplished by determining the contribution to the total phase variation made by each module phase shifter. This experiment was performed by (1) scanning the beam to 39.4° in the normal nammer (2) entering a new azimuth scan angle (β) of 42.2° in program address 36, (3) modifying the software to permit manual entry of the new phase data, and (4) recording the array phase after each module phase data entry. By use of this technique the phase variation cause by an individual module is determined as the module phases are manually set in the same sequence as they are normally set at the system clock rate. The results of this test are shown in Figure 4-19. The maximum variation caused by an individual module phase shifter is seen to be approximately 3°.

5. Noise Temperature

Figure 4-20 shows a block diagram of the test set-up used to measure antenna noise temperature. The tests were conducted on the same antenna range used for prior tests. The antenna positioner was adjusted to point the antenna vertically into the sky. The measurements are made by determining the ratio of noise powers available at the receiver output (using the precision IF attenuator) when the input termination is changed. By pre-measuring the receiver noise temperature, and using calibrated noise sources of 10,000°K and 290°K the noise temperature of the sky and the AESPA array can be determined. The first ratio (Y_R) is one that is commonly determined in receiver noise figure measurements made by "Y" factor method. For this measurement the input termination is switched between the two calibrated quantities, leaving only the receiver noise temperature (T_R) unknown.

$$Y_R = \frac{10,000 + T_R}{290 + T_R} \tag{1}$$

The second ratio (Y_A) is determined by switching the input termination between the AESPA antenna and the 10,000°K source. Since T_R is obtainable from (1), the only unknown is the array temperature (T_A).

$$Y_A = \frac{10,000 + T_R}{T_A + T_R} \tag{2}$$

The value of array temperature determined from (2) contains contributions from the sky. The magnitude of this contribution was determined using the horn antenna. The value of temperature obtained was assumed to be due to the sky along. This ratio Y_H and an alternate Y_H' were determined by switching

Equipment Group
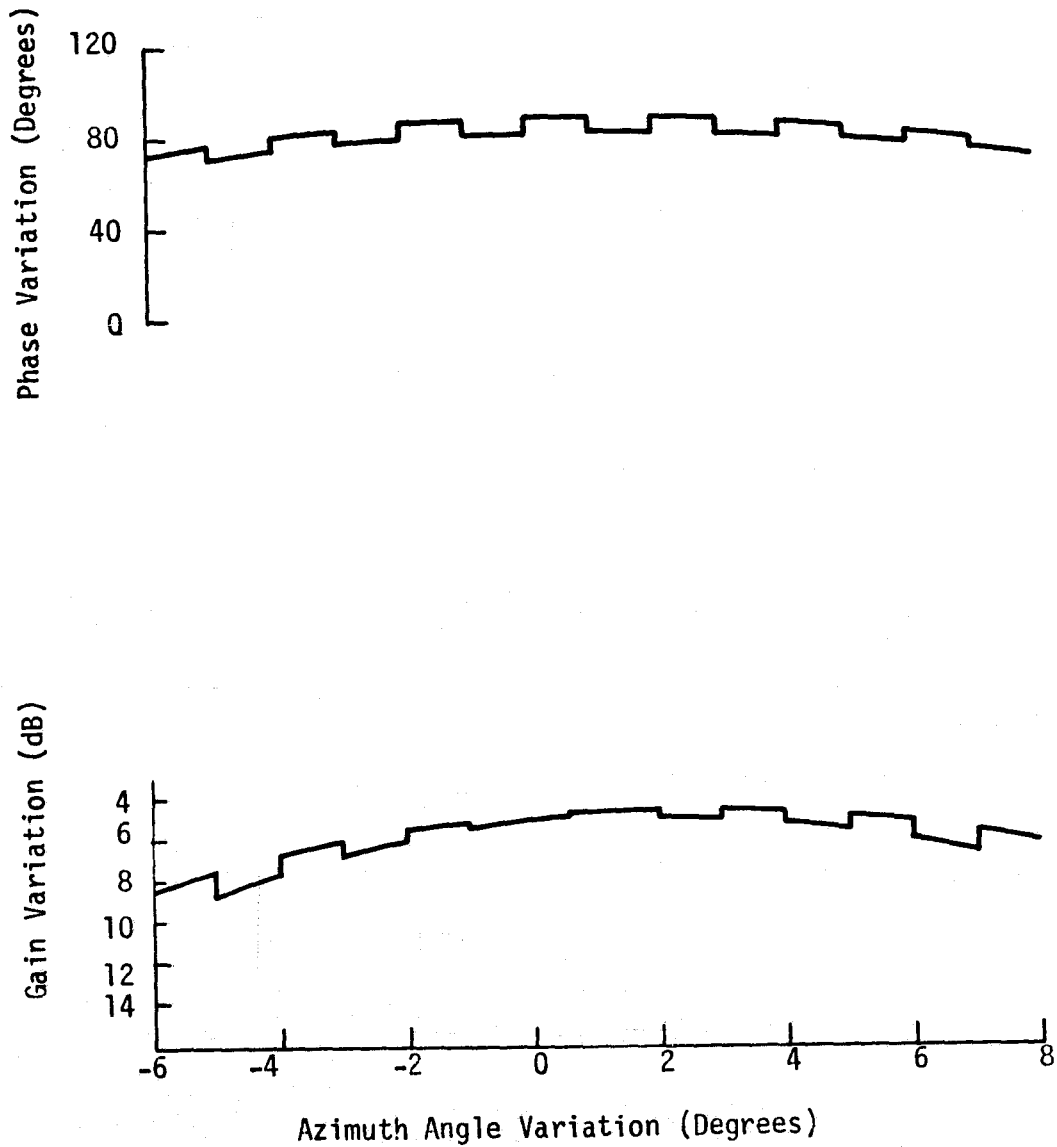
Figure 4-17. Measured Phase and Gain Variations Caused by Steering
the Array Between Azimuth Angles of 0° and 2.8°
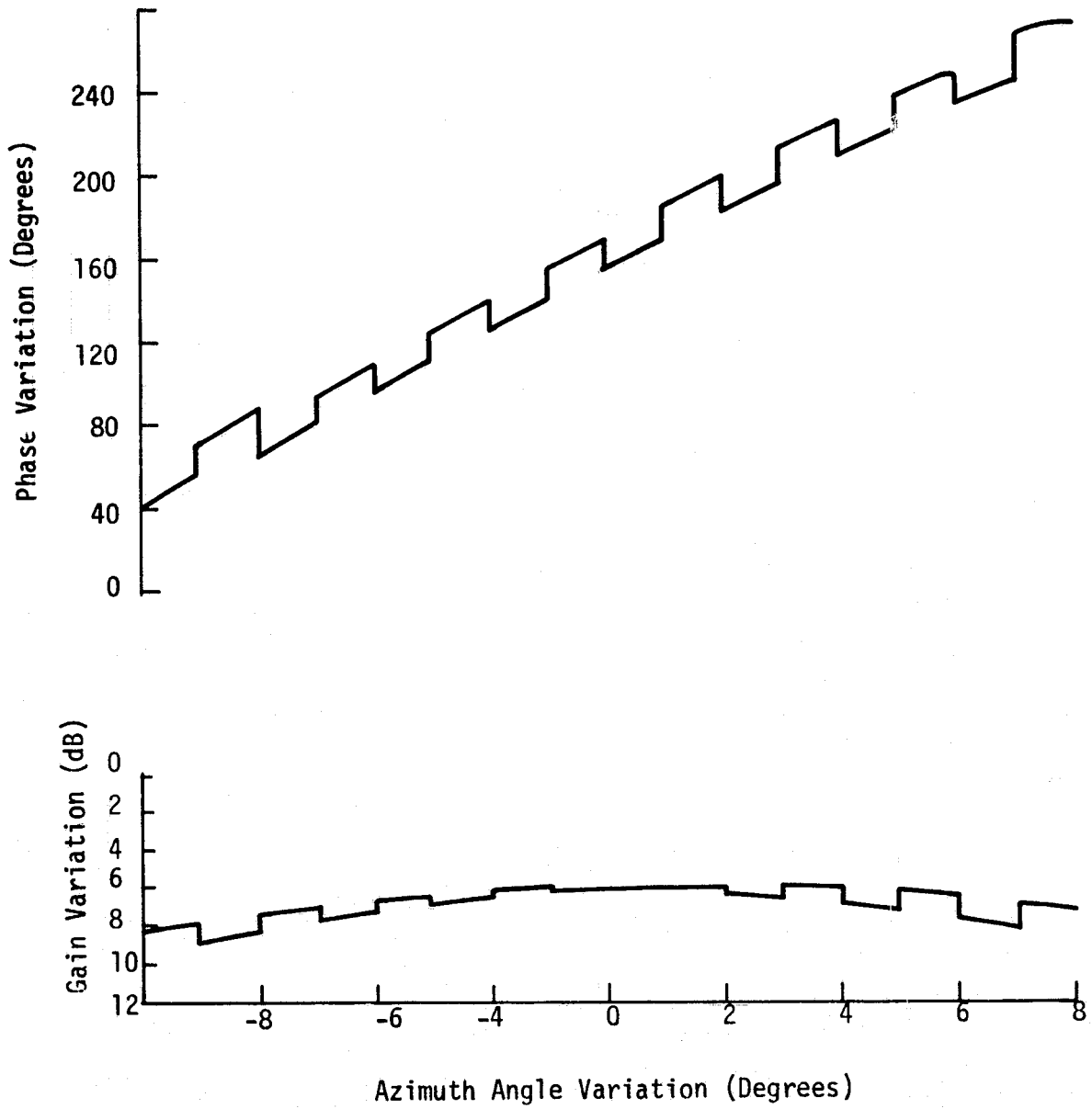
Figure 4-18. Measured Phase and Gain Variations Caused by Steering
The Array Between Azimuth Angles of 39.4° and 42.2°
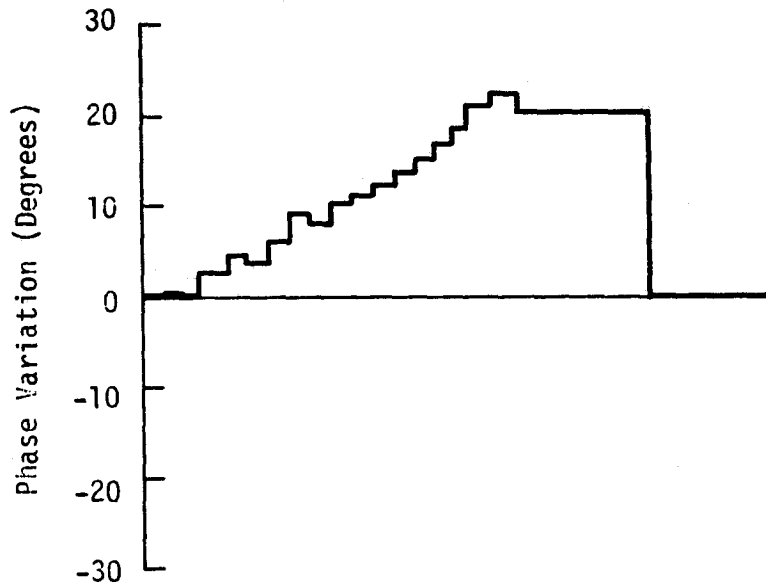
Module Phasor Manual Reset Time
(Scale Arbitrary)

Figure 4-19. Measured Phase Variation Caused by Steering the Array Between
Azimuth Angles of 39.4° and 42.2° (Showing Contribution of
Individual Module Phase Shifters)
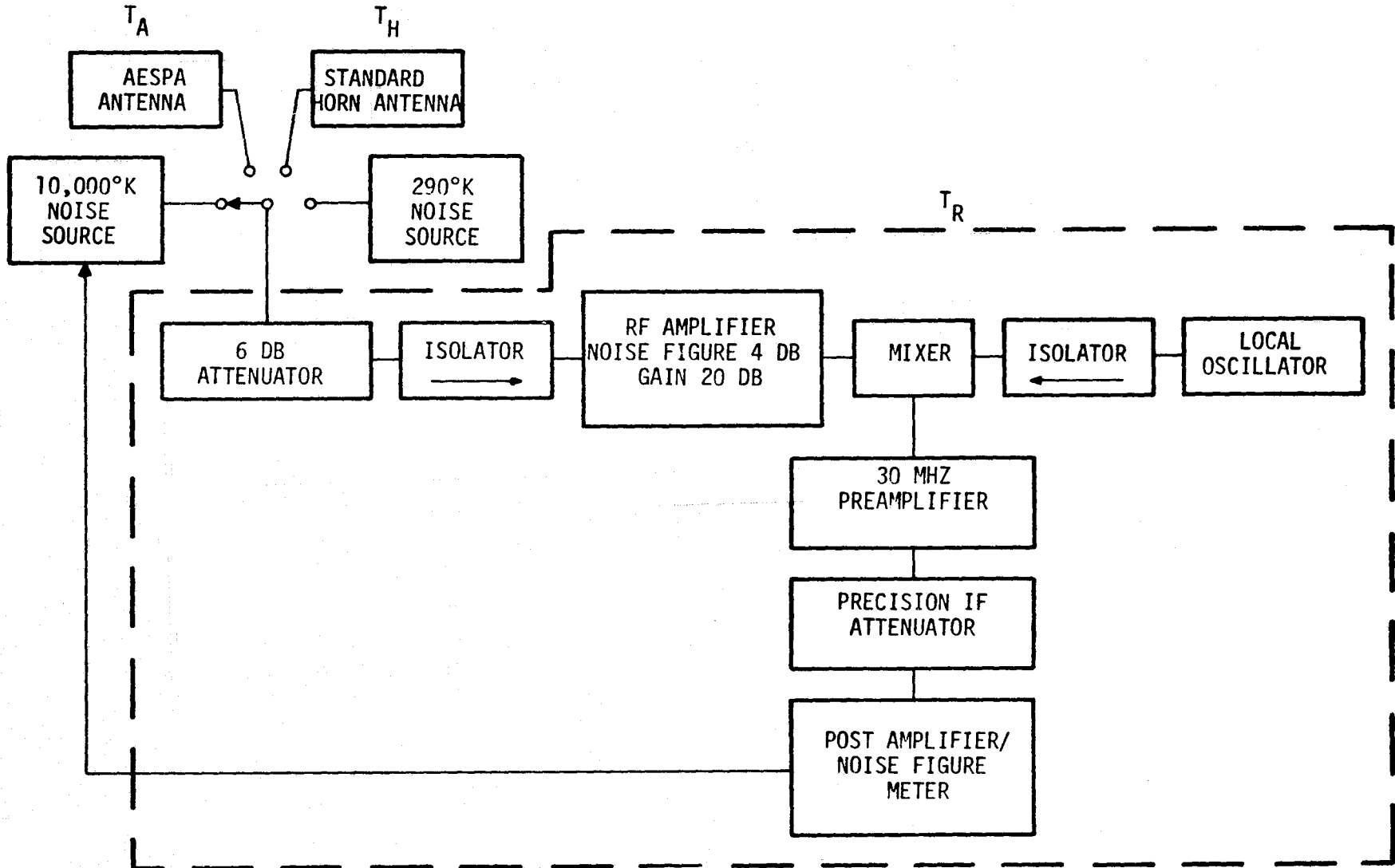
Figure 4-20. Block Diagram for Test Set-up Used to
Determine Antenna Noise Temperature

the input termination between the horn and the two calibrated noise sources.

$$Y_H = \frac{10,000 + T_R}{T_H + T_R} \tag{3}$$

$$Y_H' = \frac{290 + T_R}{T_H + T_R} \tag{4}$$

The data obtained using these measurement procedures and the corresponding calculated noise temperatures are shown in Table 4-9.

TABLE 4-9. MEASURED NOISE RATIOS AND
CORRESPONDING CALCULATED NOISE TEMPERATURES

MEASURED QTY.	RATIO (dB)	CALCULATED QTY.	NOISE TEMP°K
Y_R	6.4	T_R	2596
Y_A	3.0	T_A	22,533
Y_H	6.9	T_H	-25.4
Y_H'	0.54	T_H	-1.04

The theoretical AESPA antenna temperature corresponding to the quantity measured is given by:

$$T_A = [T_{sky} + (F-1)290]G_E \tag{5}$$

where T_{sky} is equal to T_H, F is T/R module noise figure, and G_E is antenna electronic gain. The negative values of sky temperature calculated above are believed to be caused by slight errors in the rated noise output of the argon noise source. The value will be assumed to be 0°K for computational purposes. The average module noise figure is obtained from data measured during the last program phase to be 5.64 dB. With the receiver local oscillator tuned to 2100 MHz, the electronic gain is determined from that data and array manifold losses to be approximately 14 dB. Use of these quantities in equation (5) yields a calculated array noise temperature of 21,837°K. The value determined above from measured quantities is 22,533°K.

Appendix A
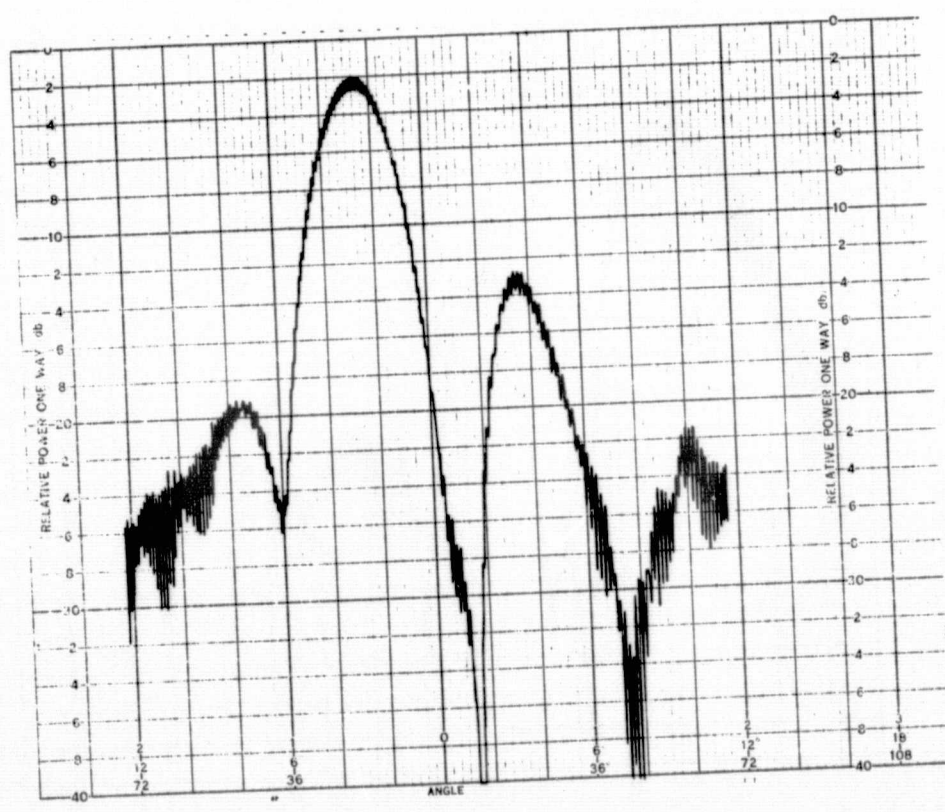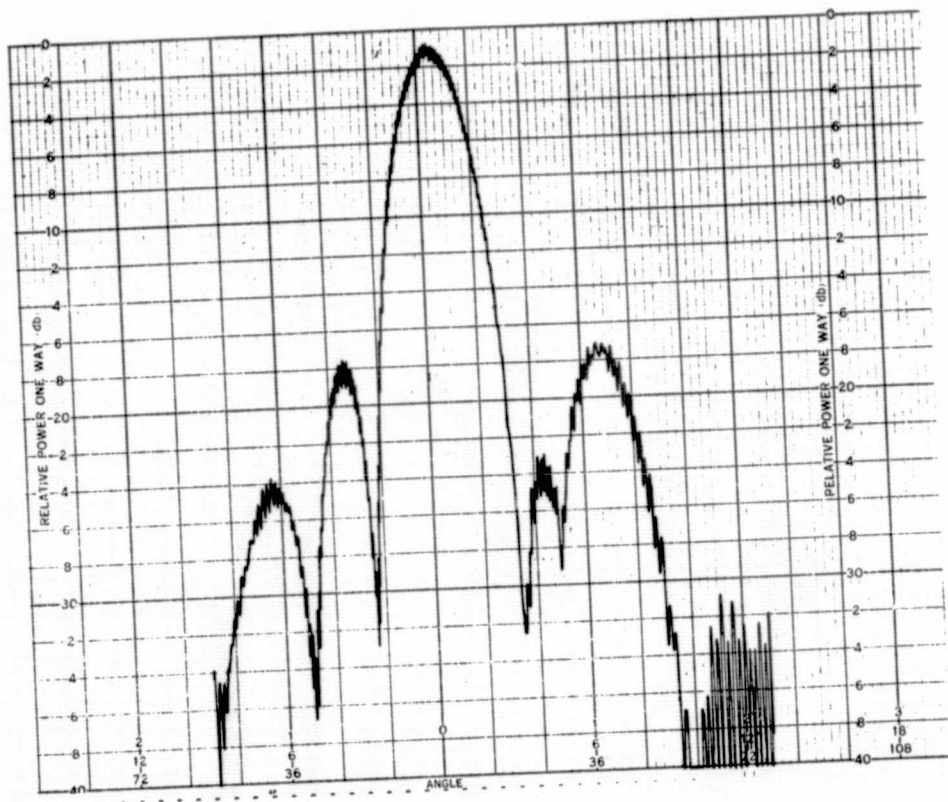
A-1(a) Transmit Elevation Patterns for Scan Angles of 0° and 20°
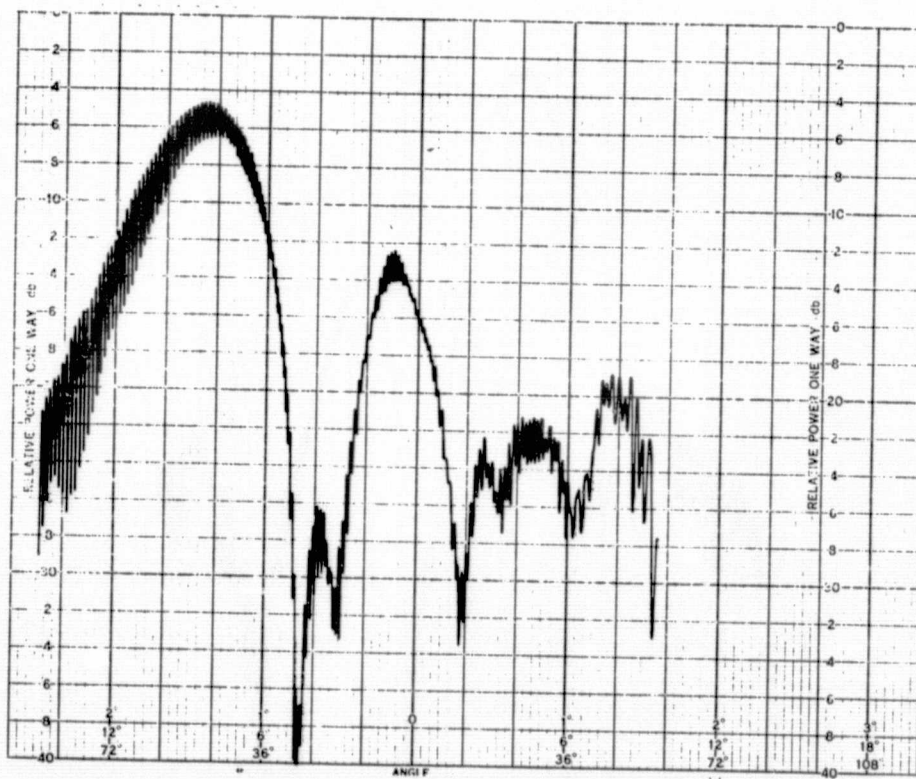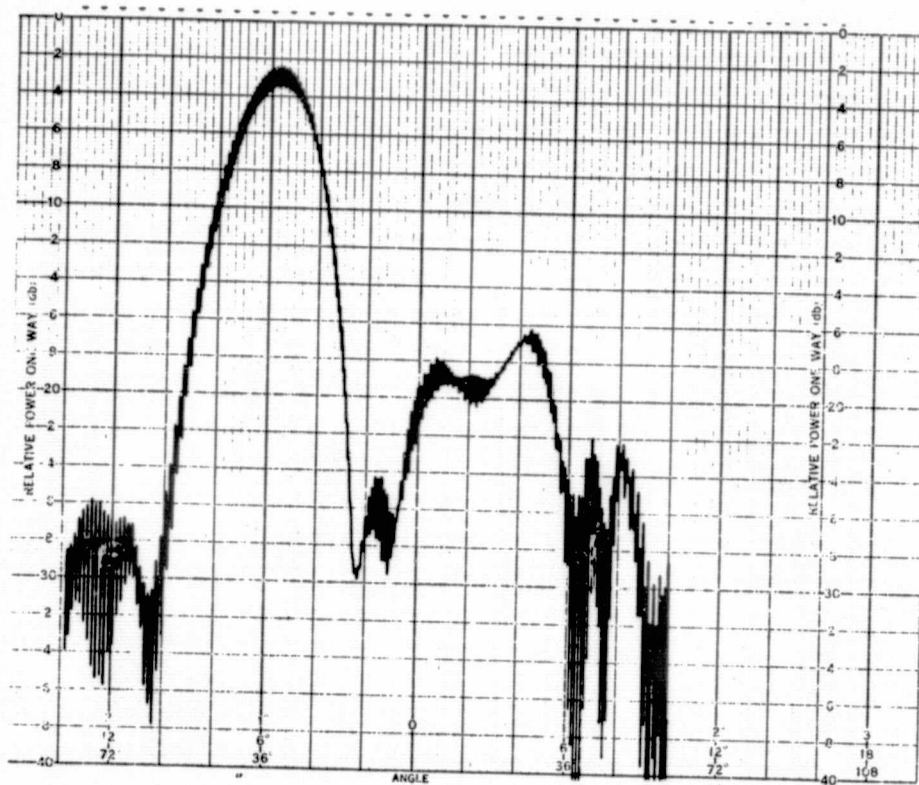
A-1(b) Transmit Elevation Patterns for Scan Angles of 40° and 60°
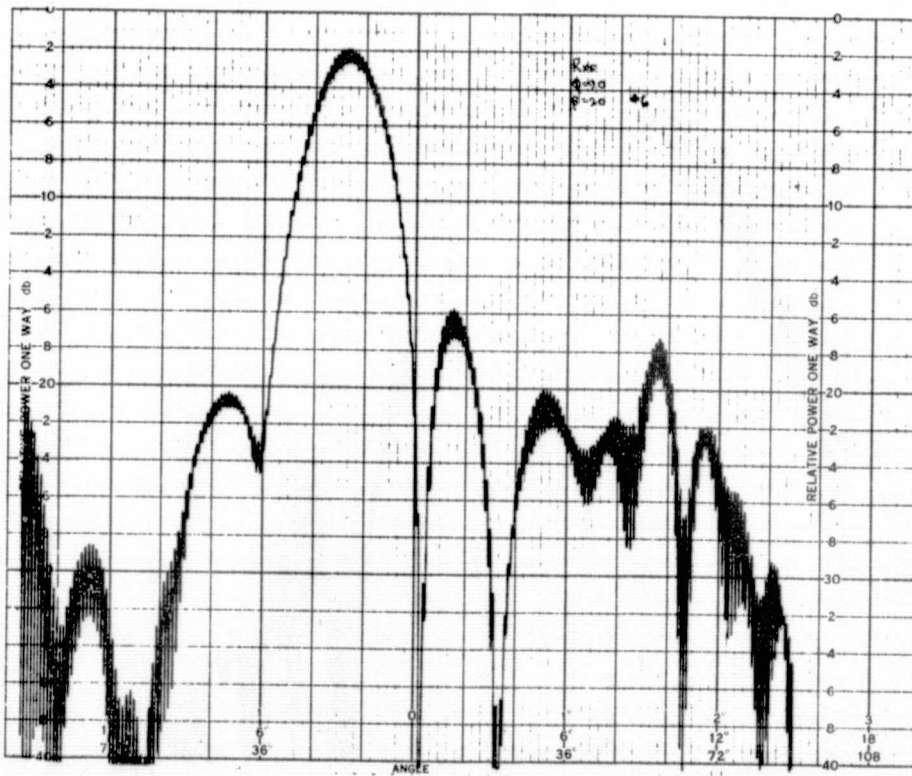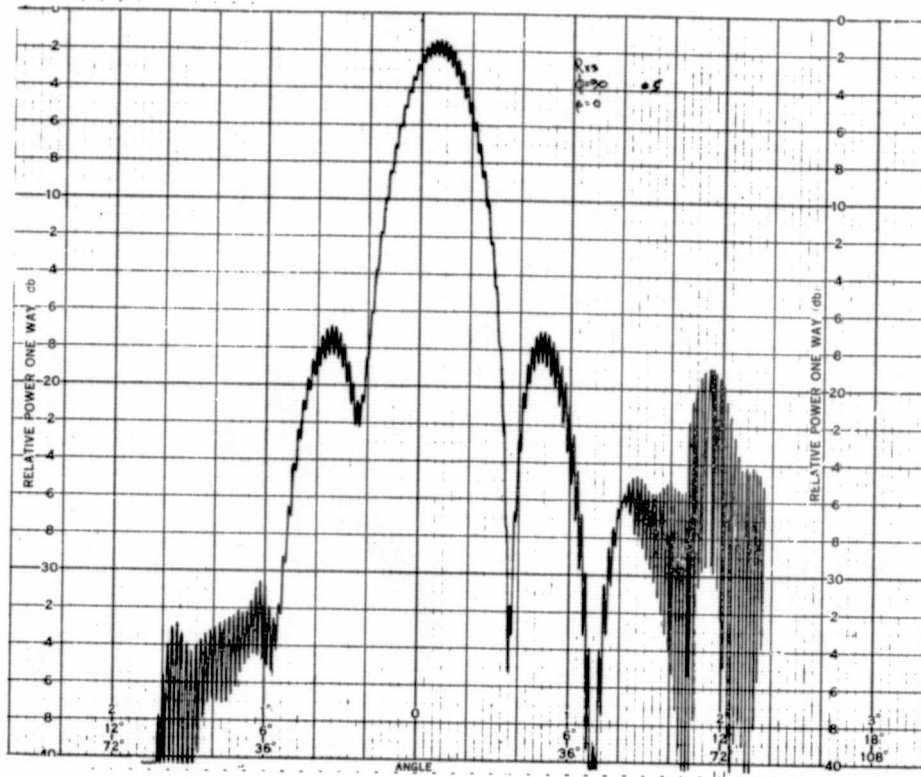
A-2(a)   Σ -Receive Azimuth Patterns for Scan Angles of 0° and 20°
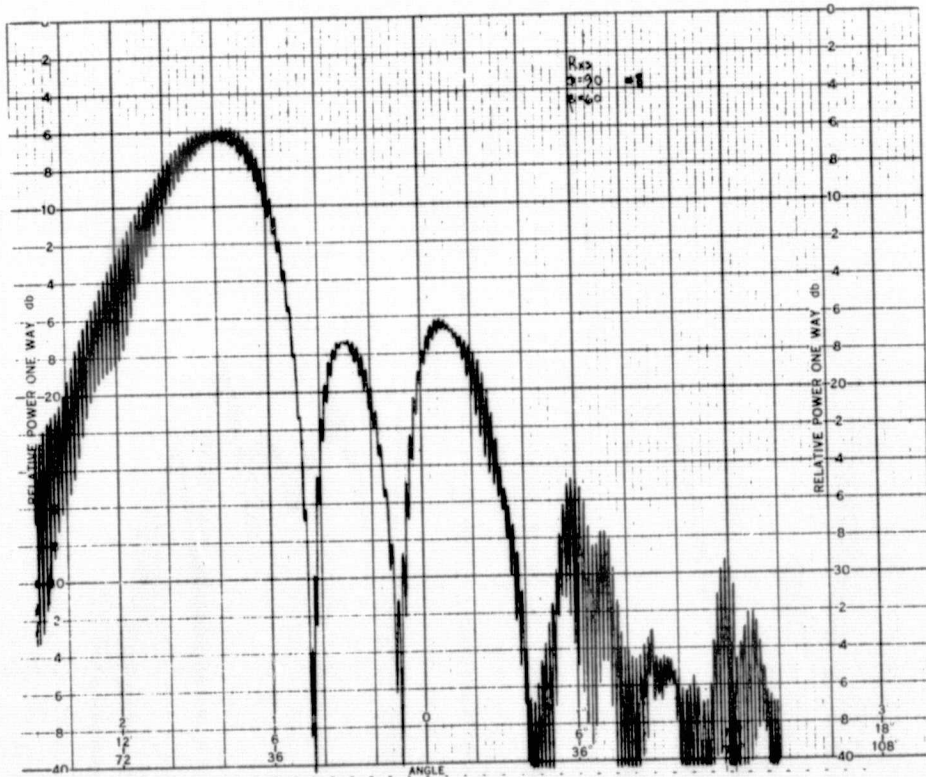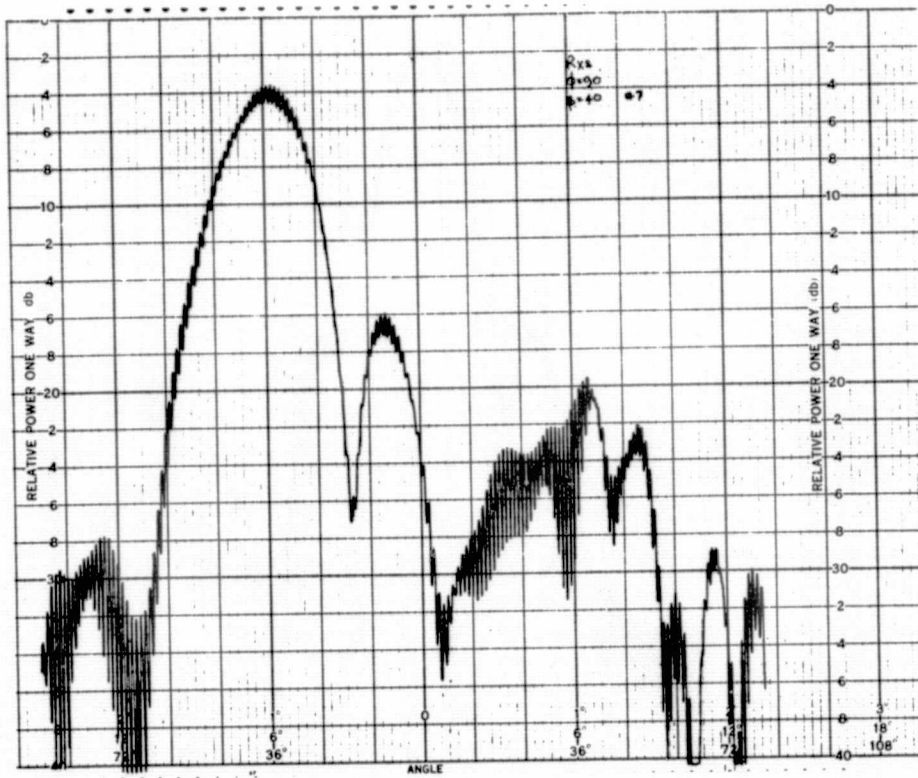
A-2(b)   Σ-Receive Azimuth Patterns for Scan Angles of 40° and 60°
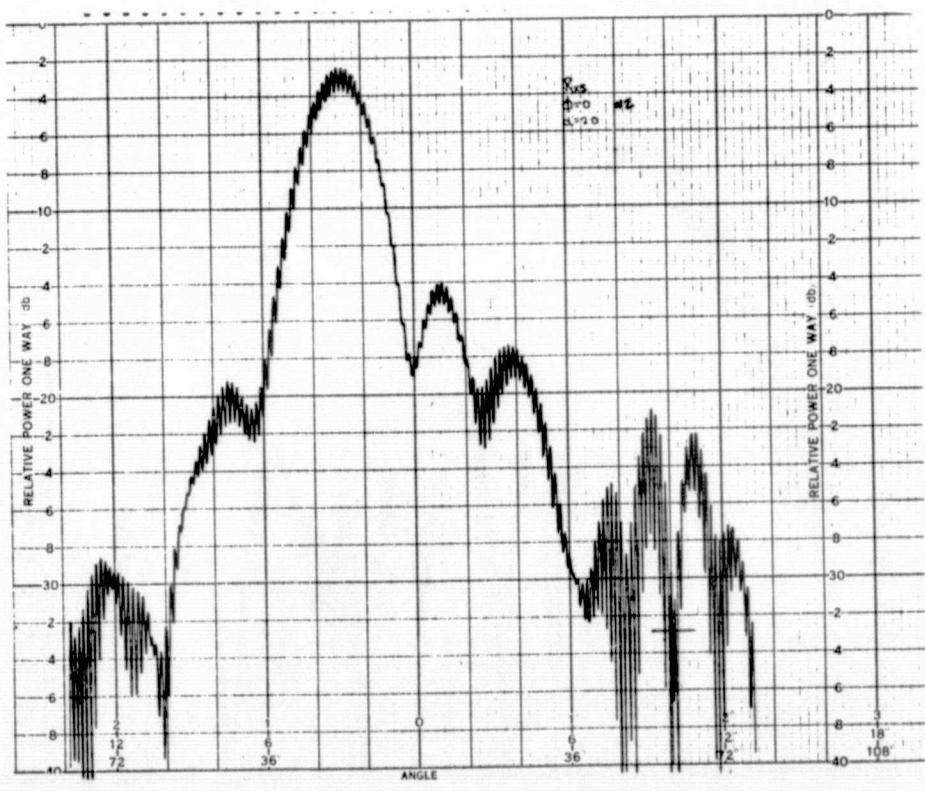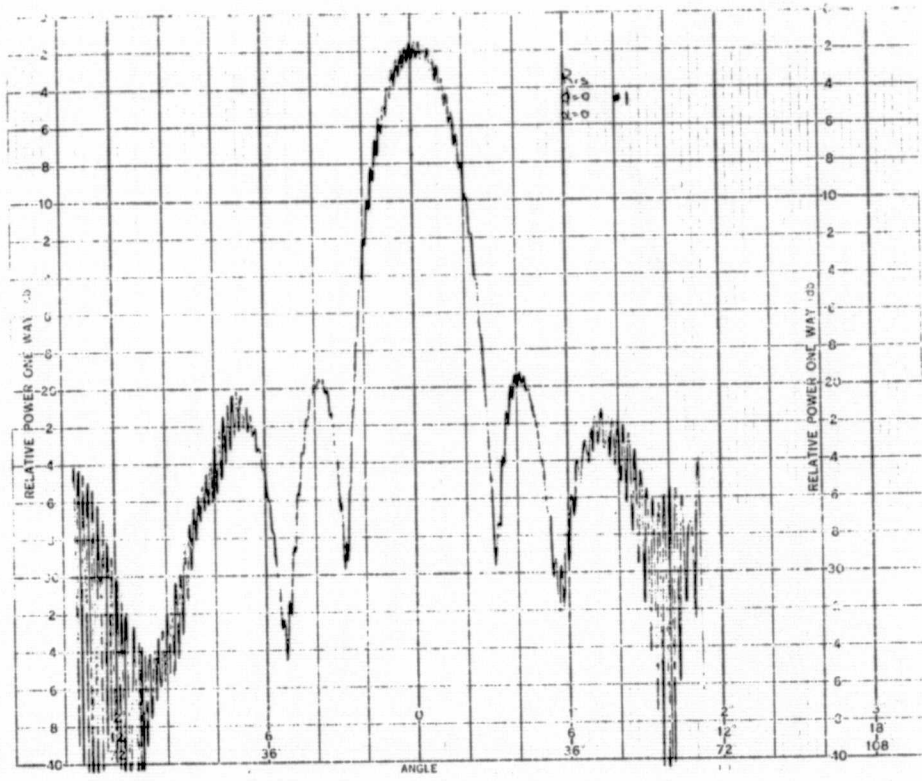
A-3(a) Σ-Receive Elevation Patterns for Scan Angles of 0° and 20°
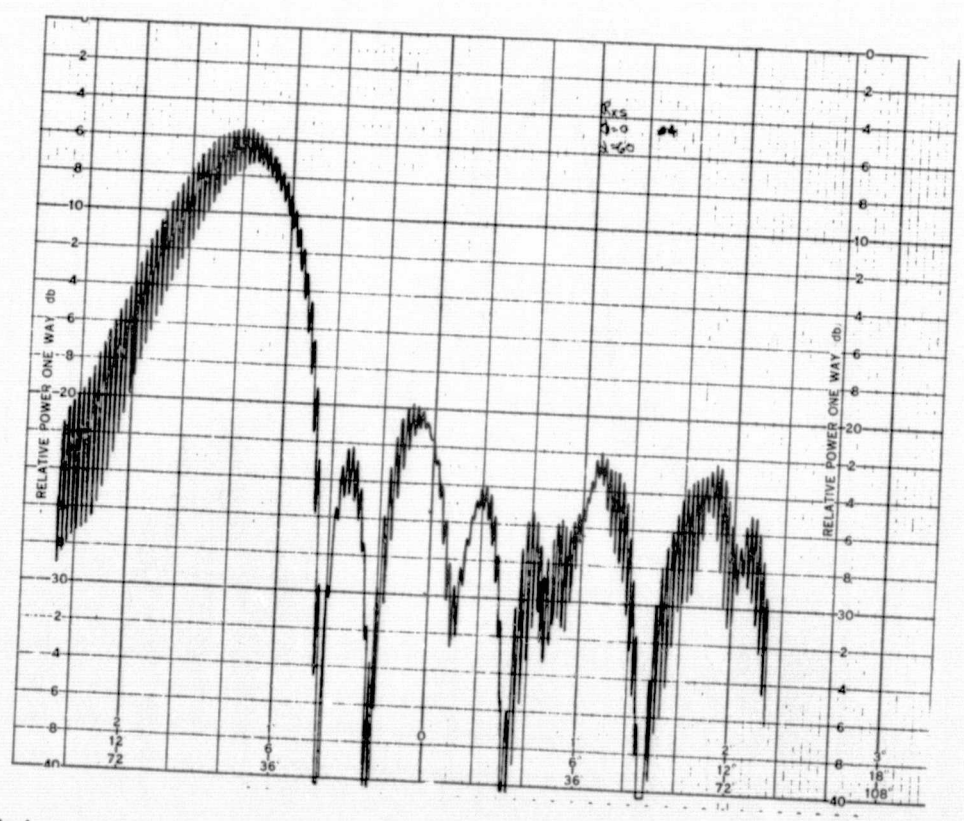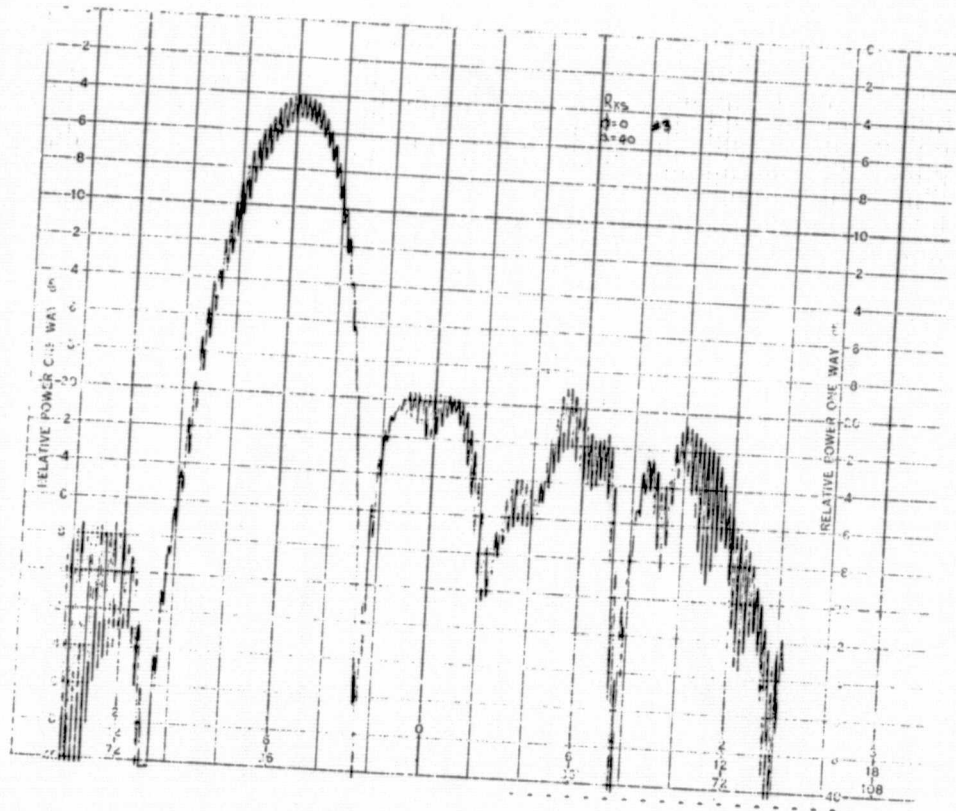
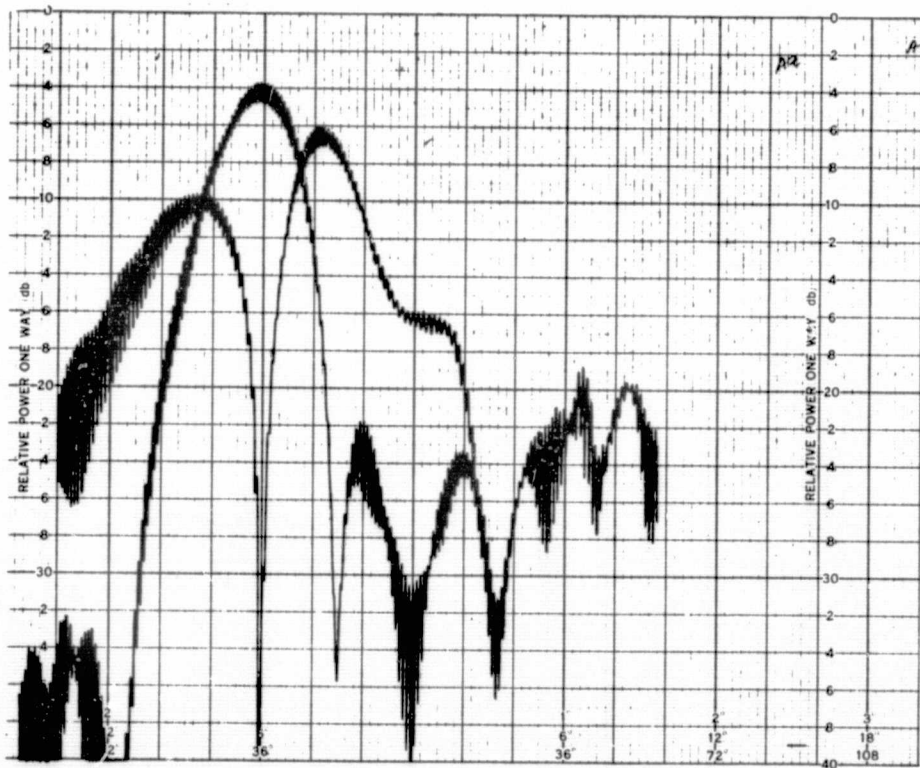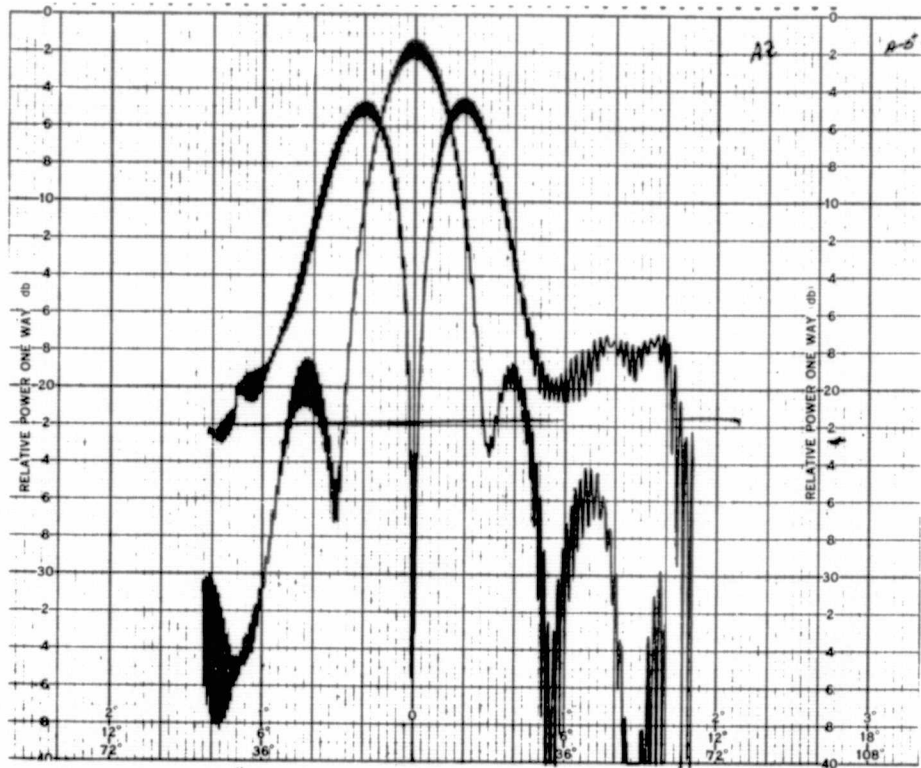A-3(b)   Σ-Receive Elevation Patterns for Scan Angles of 40° and 60°
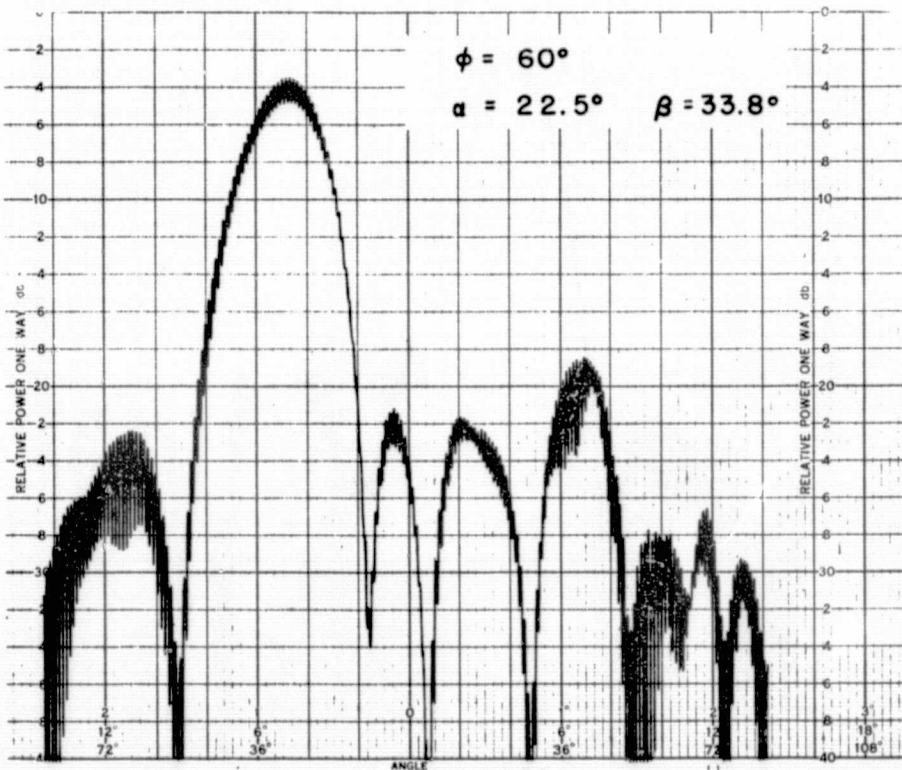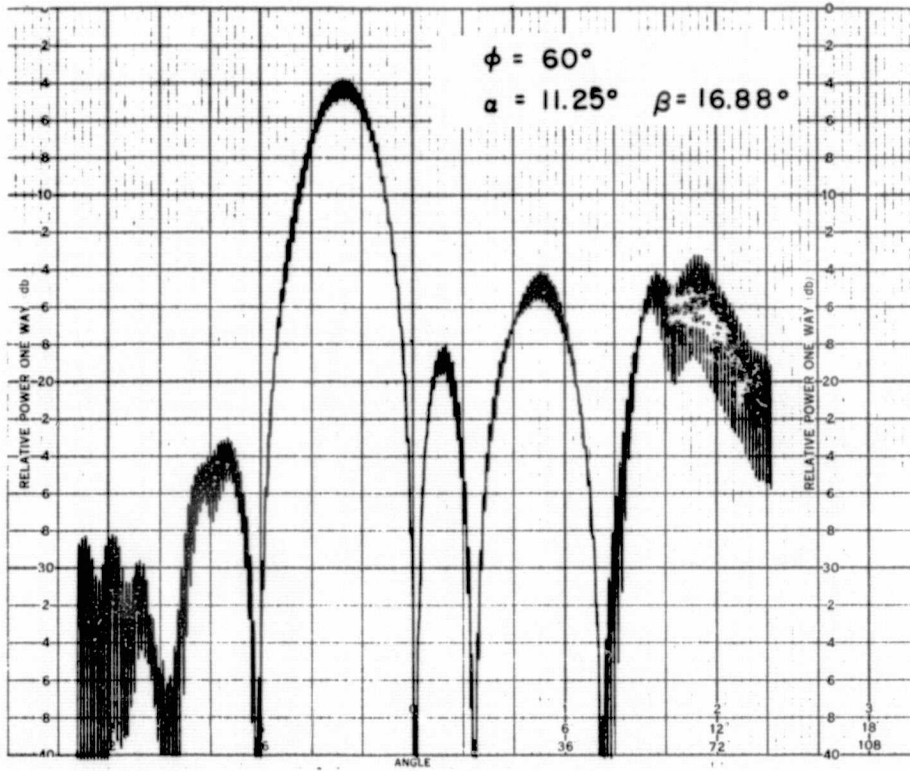
$\phi = 60°$
$\alpha = 11.25°$ $\beta = 16.88°$

$\phi = 60°$
$\alpha = 22.5°$ $\beta = 33.8°$

A-4(a) Σ -Receive Patterns for Compound Electronic Scan Angles

Equipment Group

$\phi = 60°$
$\alpha = 40.9$ $\beta = 48.6$

$\phi = 30°$
$\alpha = 17.5°$ $\beta = 9.85°$

A-4(b) Σ -Receive Patterns for Compound Electronic Scan Angles

A-8
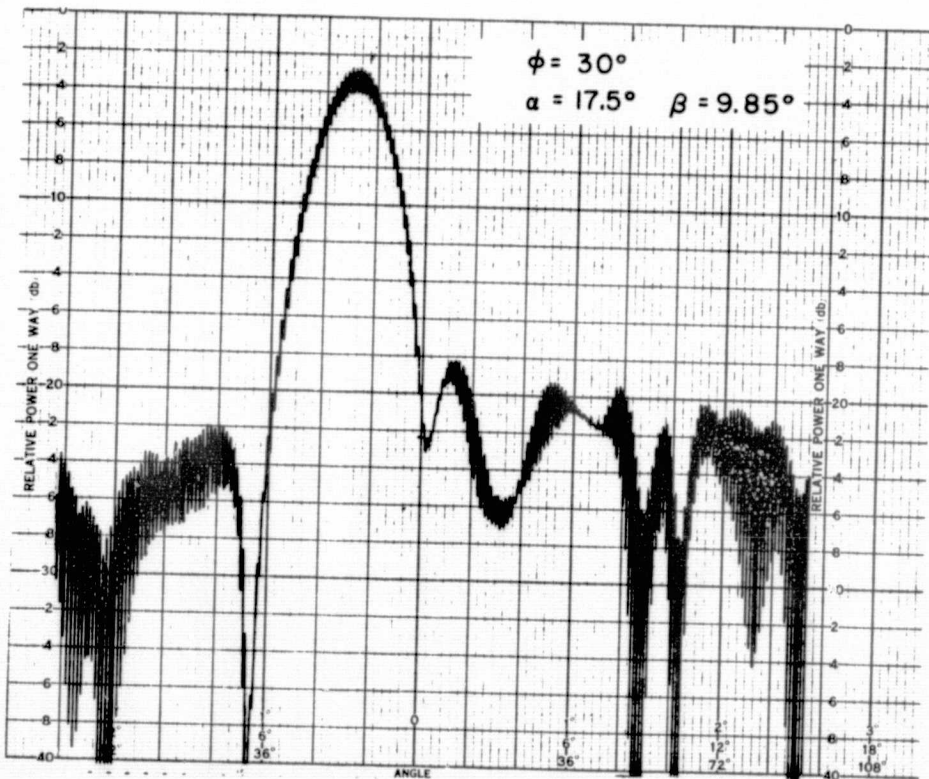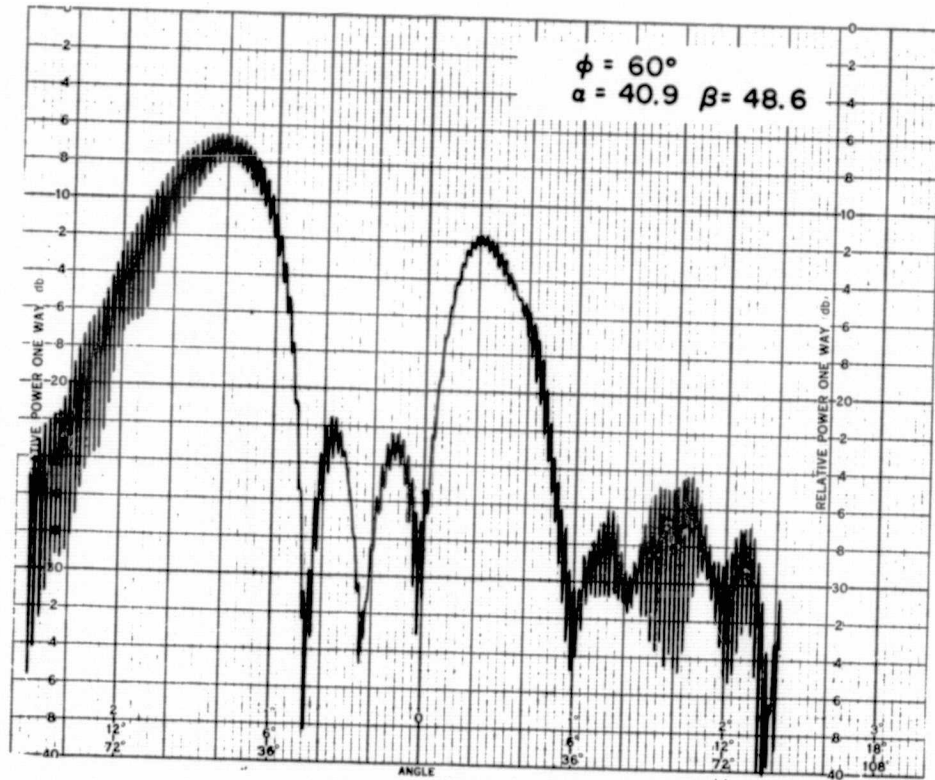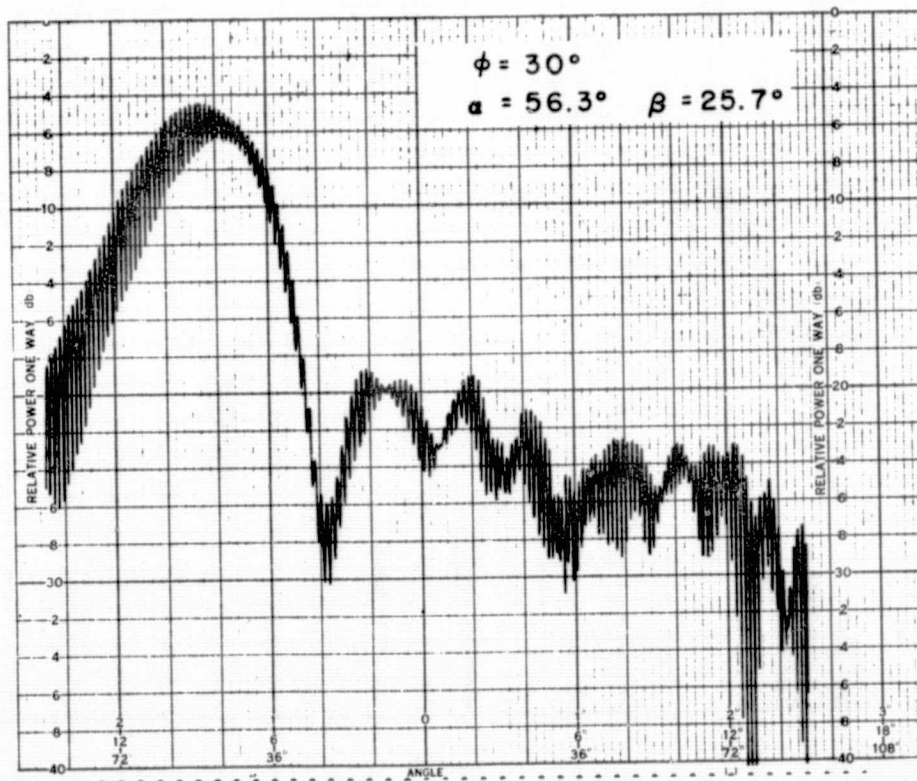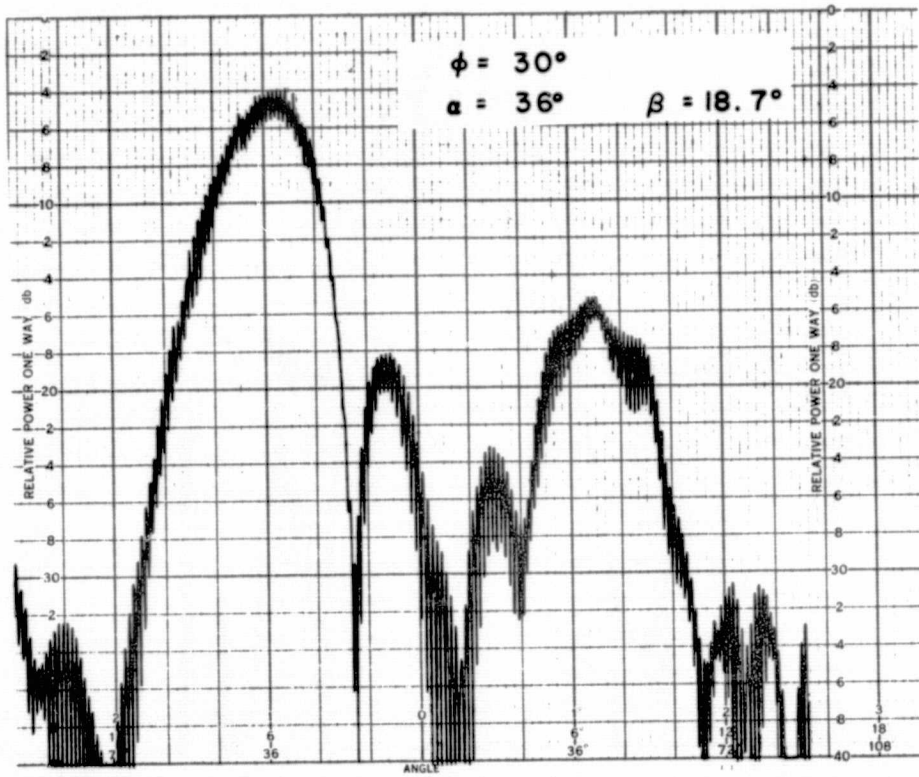
A-4(c) Σ -Receive Patterns for Compound Electronic Scan Angles

A-5(a) Receive Σ and Δ Azimuth Patterns for Scan Angles of 0° and 40°
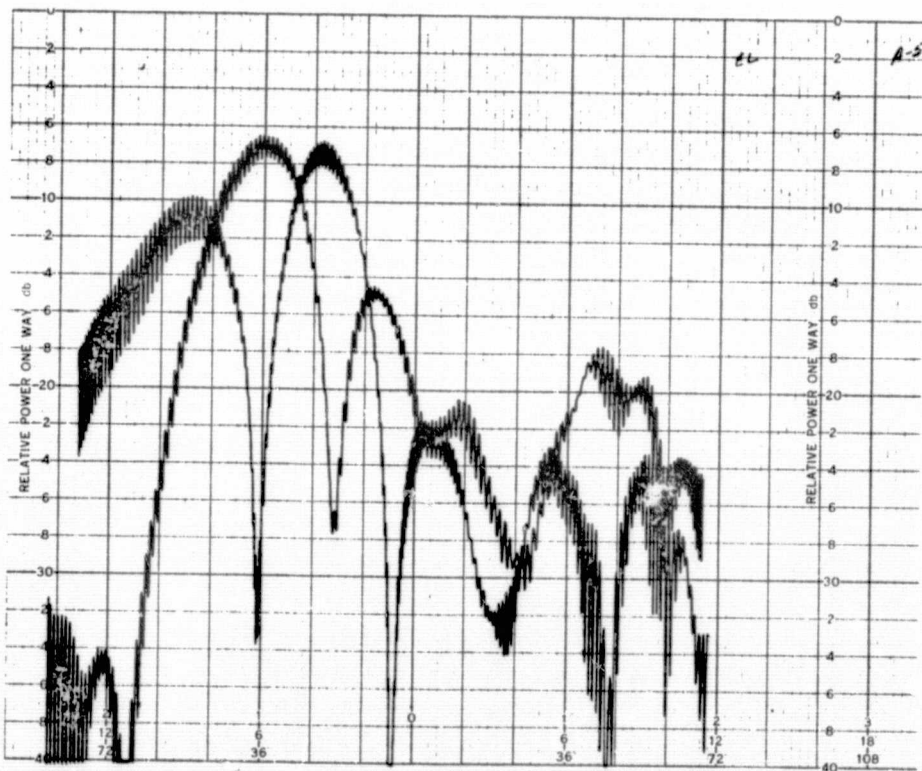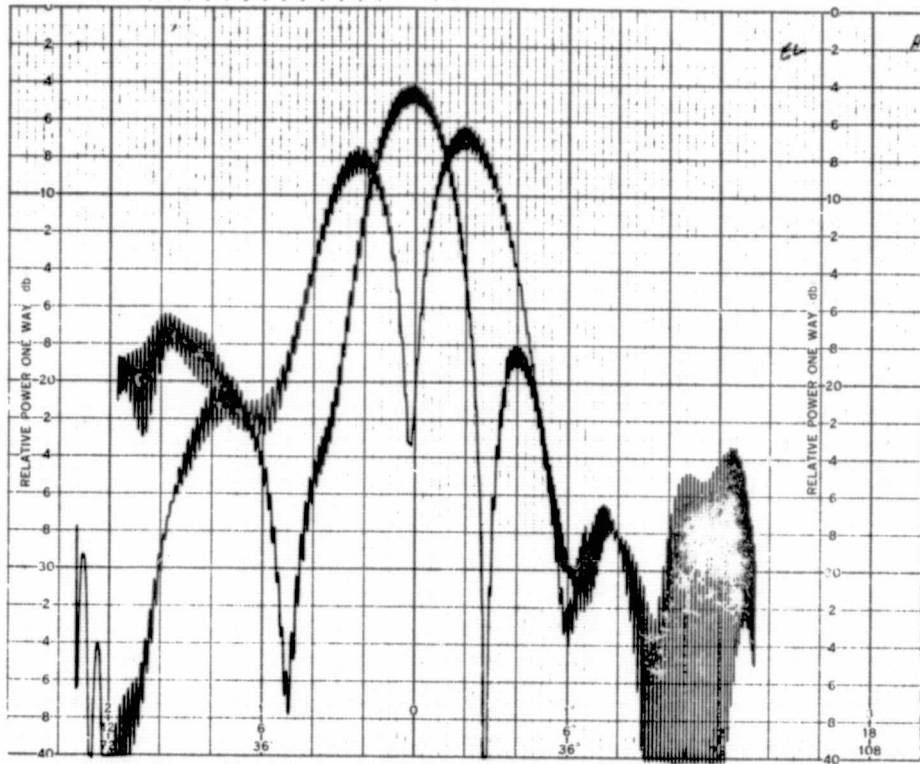
A-5(b) Receive Σ and Δ Elevation Patterns for Scan Angles of 0° and 40°

Equipment Group

Appendix B
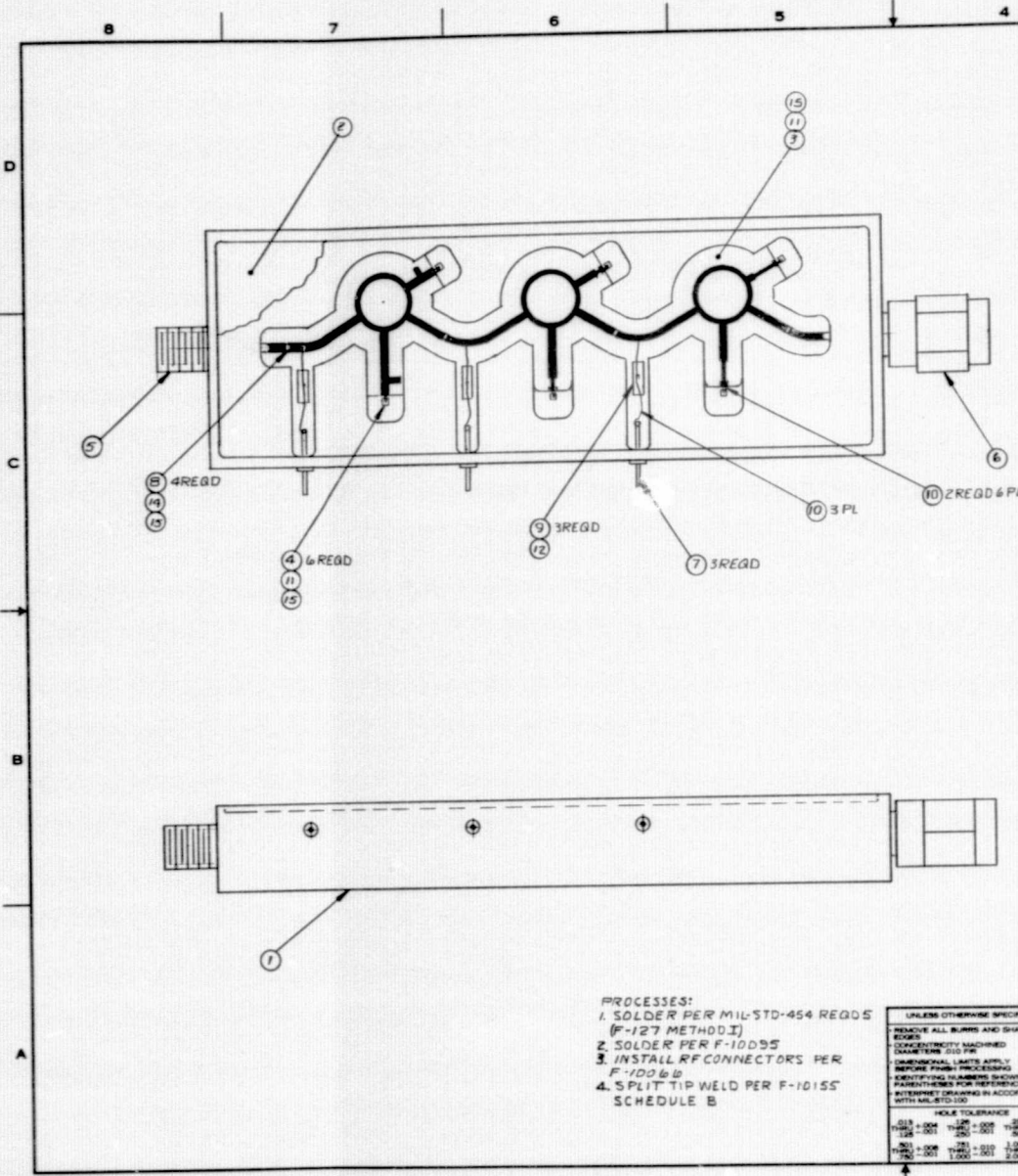
NOTES:

1. INSTALL ITEM 8 ONTO ITEM 3 USING ITEM 14 AND 15 PER PROCESS 1 PRIOR TO INSTALLING ITEM 3 INTO ITEM 1
2. INSTALL ITEM 9 ONTO ITEM 3 USING ITEM 12 PRIOR TO INSTALLING ITEM 3 INTO ITEM 1
3. INSTALL ITEM 3 AND 4 IN ITEM 1 USING ITEM 11 AND 15 PER PROCESS 2
4. INSTALL ITEMS 5 AND 6 IN ITEM 1 PER PROCESS 3
5. INSTALL ITEM 7 IN ITEM 1 USING ITEM 15 AND 11 PER PROCESS 1
6. SOLDER CONDUCTOR OF ITEM 5 TO ETCH ON ITEM 3 USING ITEM 11 PER PROCESS 1
7. ATTACH ITEM 10 PER PROCESS 4
8. INSTALL COVER ITEM 2 USING ITEM 11 PER PROCESS 1

PROCESSES:
1. SOLDER PER MIL-STD-454 REQ 5 (F-127 METHOD I)
2. SOLDER PER F-10095
3. INSTALL RF CONNECTORS PER F-10066
4. SPLIT TIP WELD PER F-10155 SCHEDULE B

PARTS LIST

QTY REQD		ITEM NO	CODE IDENT	PART OR IDENTIFYING NUMBER	NOMENCLATURE OR DESCRIPTION	PROCUREMENT SPECIFICATION
AR		15		417489-1	FLUX	
AR		13		417880-1025	SOLDER	
AR		12		410423-1	ADHSIVE	
AR		11		539934-1	SOLDER	
AR		10		539930-3	STRAP, AU, .001 X .0005	
3		9		870033-1	CHIP	
4		8		MD603K	CAPACITOR (TEXAS INST)	
3		7		802767-2	FEEDTHRU	
1		6		772030-1	CONNECTOR	
1		5		539433-1	CONNECTOR	
6		4		5082-0001	DIODE (HEWLETT PACKARD)	
1		3		870069-1	NETWORK	
1		2		870068-1	COVER	
1		1		870067-1	HOUSING	

TEXAS INSTRUMENTS
Equipment Group

KU BAND PHASE SHIFTER ASSEMBLY

SIZE	CODE IDENT NO	DRAWING NO
D	96214	SK 870030

SCALE 4/1   SHEET

NAS8-25847

D | 96214 | SK 870030

Equipment Group

PROCESSES APPLY TO THIS
SURFACE ONLY

.150

.050

.020 STK
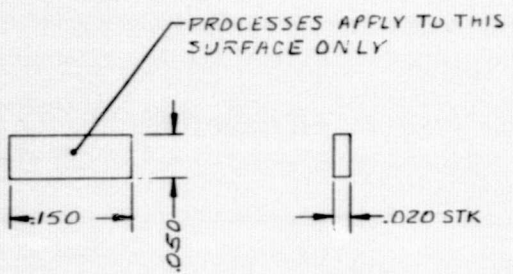
PROCESSES:
1. FILM MATALIZATION
   PRE PLATE TYPE I, F-6006
2. GOLD PLATE PER MIL-C-45204,
   TYPE III, CLASS 3 (F-39)
   (THK 250 ± 50 μ INCH)
3. NICKEL PLATE QQ-N-
   290, CLASS 2, THK 75 μ INCH
   MIN (F-42)
4. GOLD PLATE PER MIL G
   45204, TYPE III, CLASS 1,
   (F-39)(THK 100 ± 50 μ INCH)

			ZONE	LTR	DESCRIPTION	DATE	APPRO
					REVISIONS		

	AR	1		539149-2	SUBSTRATE	
-2	-1	ITEM NO	CODE IDENT	PART OR IDENTIFYING NUMBER	NOMENCLATURE OR DESCRIPTION	PROCUREMENT SPECIFICATION
QTY REQD						

PARTS LIST

UNLESS OTHERWISE SPECIFIED
- REMOVE ALL BURRS AND SHARP EDGES
- CONCENTRICITY MACHINED DIAMETERS .010 FIR
- DIMENSIONAL LIMITS APPLY BEFORE FINISH PROCESSING
- IDENTIFYING NUMBERS SHOWN IN PARENTHESES FOR REFERENCE ONLY
- INTERPRET DRAWING IN ACCORDANCE WITH MIL STD 100

UNLESS OTHERWISE SPECIFIED
- DIMENSIONS ARE IN INCHES
- TOLERANCES:
  ANGLES ± 1°
  3 PLACE DECIMALS ± .010
  2 PLACE DECIMALS ± .02

TEXAS INSTRUMENTS
INCORPORATED
Equipment Group   Dallas, Texas

CHIP, SUBSTRATE

		DATE	
DWN	Revell	5-21-75	
CHK	Per Pila	5-23-75	
ENGR	R Coats	5/23/75	
QA	J Sandli	5-23-75	
APVD	K Allison	5/23/75	

CONTR NO NAS8-25847
DESIGN ACTIVITY RELEASE

HOLE TOLERANCE
| .013 THRU .125 | + .004 - .001 | .126 THRU .250 | + .005 - .001 | .251 THRU .500 | + .006 - .001 |
| .501 THRU .750 | + .008 - .001 | .751 THRU 1.000 | + .010 - .001 | 1.001 THRU 2.000 | + .012 - .001 |

870030	1163
NEXT ASSY	USED ON

APPLICATION

SIZE C	CODE IDENT NO 96214	DRAWING NO 870033
SCALE 10/1		SHEET

20

SECTION A-A

HOUSING, KU BAND PHASE SHIFTER

TEXAS INSTRUMENTS
INCORPORATED
Equipment Group   Dallas, Texas

SIZE	CODE IDENT NO	DRAWING NO
D	96214	SK 870067

REVISIONS

ZONE	LTR	DESCRIPTION	DATE	APPROVED

3.100 +.000/-.010

1.000 +.000/-.010

.03R 4PL

.032

REVISIONS

ZONE	LTR	DESCRIPTION	DATE	APPROVED

PARTS LIST

QTY REQD	ITEM NO	CODE IDENT	PART OR IDENTIFYING NUMBER	NOMENCLATURE OR DESCRIPTION	PROCUREMENT SPECIFICATION
1	1		415164-1036	.032 BRASS SHEET H2 H SNF	

UNLESS OTHERWISE SPECIFIED
- REMOVE ALL BURRS AND SHARP EDGES
- CONCENTRICITY MACHINED DIAMETERS .010 FIR
- DIMENSIONAL LIMITS APPLY BEFORE FINISH PROCESSING
- IDENTIFYING NUMBERS SHOWN IN PARENTHESES FOR REFERENCE ONLY
- INTERPRET DRAWING IN ACCORDANCE WITH MIL-STD-100

HOLE TOLERANCE

UNLESS OTHERWISE SPECIFIED
- DIMENSIONS ARE IN INCHES
- TOLERANCES
  ANGLES ±1°
  3 PLACE DECIMALS ±.010
  2 PLACE DECIMALS ±.02

TEXAS INSTRUMENTS
INCORPORATED
Equipment Group　Dallas, Texas

COAX TUTE, KU BAND PHASE SHIFTER

SIZE	CODE IDENT NO	DRAWING NO
D	96214	SK E 70C68

SCALE 4/1　　SHEET

NEXT ASSY　USED ON
APPLICATION

Equipment Group

2.800

1.000

.200

.100

3.000

REVISIONS				
ZONE	LTR	DESCRIPTION	DATE	APPROVED

	AR	1		417946-41		.010 THK, PLASTIC SHEET, DUROID	
2	1	ITEM NO	CODE IDENT	PART OR IDENTIFYING NUMBER		NOMENCLATURE OR DESCRIPTION	PROCUREMENT SPECIFICATION
QTY REQD							

PARTS LIST

UNLESS OTHERWISE SPECIFIED
- REMOVE ALL BURRS AND SHARP EDGES
- CONCENTRICITY MACHINED DIAMETERS .010 FIR
- DIMENSIONAL LIMITS APPLY BEFORE FINISH PROCESSING
- IDENTIFYING NUMBERS SHOWN IN PARENTHESES FOR REFERENCE ONLY
- INTERPRET DRAWING IN ACCORDANCE WITH MIL STD 100

HOLE TOLERANCE

.013 THRU .125	+ .04 − .01	.126 THRU .250	+ .005 − .001	.251 THRU .500	+ .006 − .001
.501 THRU .750	+ .008 − .001	.751 THRU 1.000	+ .010 − .001	1.001 THRU 2.000	+ .012 − .001

870070	1163
NEXT ASSY	USED ON
APPLICATION	

UNLESS OTHERWISE SPECIFIED
- DIMENSIONS ARE IN INCHES
- TOLERANCES:
  ANGLES ± 1°
  3 PLACE DECIMALS ± .010
  2 PLACE DECIMALS ± .02

DWN		DATE 3-31-75
CHK		3-31-75
ENGR	R Coats	5-16-75
QA		5-20-75
APVD	R Olson	
CONTR NO	NASB-25847	
DESIGN ACTIVITY RELEASE 5-20-75		

TEXAS INSTRUMENTS
INCORPORATED
Equipment Group   Dallas, Texas

NETWORK, KU BAND
Ø SHIFTER

SIZE	CODE IDENT NO	DRAWING NO
C	96214	870069
SCALE 2.5/1		SHEET

22

AW

REVISIONS

ZONE	LTR	DESCRIPTION	DATE	APPROVED

Dimensions shown: 1.600, .645, .200, .152, 1.952

PARTS LIST

QTY REQD 2	QTY REQD 1	ITEM NO	CODE IDENT	PART OR IDENTIFYING NUMBER	NOMENCLATURE OR DESCRIPTION	PROCUREMENT SPECIFICATION
AR	1			417946-41	.010 THK, PLASTIC SHEET, DUROID	

UNLESS OTHERWISE SPECIFIED
- REMOVE ALL BURRS AND SHARP EDGES
- CONCENTRICITY MACHINED DIAMETERS .010 FIR
- DIMENSIONAL LIMITS APPLY BEFORE FINISH PROCESSING
- IDENTIFYING NUMBERS SHOWN IN PARENTHESES FOR REFERENCE ONLY
- INTERPRET DRAWING IN ACCORDANCE WITH MIL STD 100

HOLE TOLERANCE

| .013 THRU .125 | ± .004 | .126 THRU .250 | ± .005 | .251 THRU .500 | ± .006 |
| .501 THRU .750 | ± .008 | .751 THRU 1.000 | ± .010 | 1.001 THRU 2.000 | ± .012 |

UNLESS OTHERWISE SPECIFIED
- DIMENSIONS ARE IN INCHES
- TOLERANCES:
  ANGLES ± 1°
  3 PLACE DECIMALS ± .010
  2 PLACE DECIMALS ± .02

DRN	Edw D. Sem	DATE 3-31-75
CHK	J. Pence	3-31-75
ENGR	R Coats	5-16-75
QA	J Sandl	5-20-75
APVD	R Allison	
CONTR NO	NAS8-25847	
DESIGN ACTIVITY RELEASE	5-21-75	

TEXAS INSTRUMENTS
INCORPORATED
Equipment Group   Dallas, Texas

NETWORK, KU-BAND
PHASE SHIFTER

| SIZE C | CODE IDENT NO 96214 | DRAWING NO 889833 |
| SCALE 5/1 | | SHEET |

B70070 1163
NEXT ASSY   USED ON
APPLICATION

22

AW